NASA-CR-195523

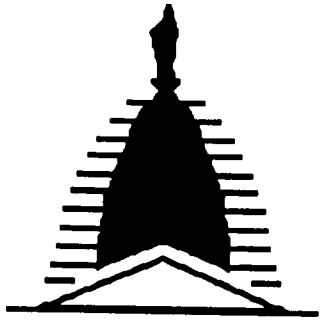

NASW-4435

NASA/USRA UNIVERSITY ADVANCED DESIGN PROGRAM 1992-1993

PROJECT CENTER MENTOR: NASA-AMES DRYDEN FLIGHT RESEARCH FACILITY

FINAL DESIGN PROPOSAL

The Diamondback

A Simulated Commercial Air Transportation Study

April 1993

Department of Aerospace and Mechanical Engineering
University of Notre Dame
Notre Dame, IN 46556

NASA/USRA UNIVERSITY
ADVANCED DESIGN PROGRAM
1992-1993

UNIVERSITY SPONSOR
BOEING COMMERCIAL AIRPLANE COMPANY

DESIGN PROPOSAL

GREEN GROUP - THE *DIAMONDBACK*

A proposal in response to a Commercial Air Transportation Study

April 8, 1993

Department of Aerospace and Mechanical Engineering
University of Notre Dame
Notre Dame, IN 46556

GREEN GROUP
Joel Faust
Peter Hoar
Jason Lubanski
Sean Ryan
Todd Surritte
Tony Yang

TABLE OF CONTENTS

1. Executive Summary

The *Diamondback* is a 100-passenger aircraft designed to cruise at 28 ft/s and compete against the 40-passenger HB-40 in the Aeroworld commercial transport market. Initially designed to service the shorter but more heavily traveled routes, the *Diamondback*'s effective range has increased from an initial 10000 ft to 15000 ft. The take-off length for the design is 25.4 ft and the minimum turn radius is 25 ft.

Unlike conventional aircraft, the *Diamondback* utilizes an innovative configuration known as the joined wing. Such a design connects the wing and tail forming a diamond in both the front and plan views. For the *Diamondback*, the wing and tail have the same span and chord with the wing sweep equaling the tail's negative sweep. Breaking new ground, the *Diamondback* is the first joined wing to be designed in Aeroworld.

The cost of operating the flight system was the consideration which ultimately guided many of the design considerations. Its influence was not a direct one but manifested itself in goals such as minimizing the drag and optimizing the propulsion system efficiency. The critical factors which had the most influence on the design were the runway length, the dihedral needed to roll the aircraft to execute a turn, and the airfoil moment about the aerodynamic center. The runway length was a significant driver of the design, requiring a high coefficient of lift to reduce the take-off speed and a high thrust to accelerate the aircraft and reduce the ground roll. The dihedral and the airfoil C_{M_0}, however, had a special significance for a joined-wing design.

Because the configuration utilized rudder and dihedral to turn, a large dihedral angle of 8° was needed. Unlike conventional designs, the wing and tail are physically and geometrically coupled such that a change in one geometry leads to a change in the other. Thus the need to obtain an effective dihedral of 8° for the *Diamondback* greatly determined the geometry of the wing and tail combination. Also unique to the joined wing is the sensitivity of the aircraft's efficiency to the moment about the aerodynamic

center of the airfoil section. Like all aircraft, as C_{M_0} becomes increasingly nose down the tail must balance the moment by increasing its incidence with respect to the wing, thus decreasing the tail's lift. Unlike conventional designs, however, the joined wing utilizes both the wing and tail to contribute to the lift. An increase in tail incidence decreases the lifting capacity of the tail and decreases the tail's usefulness in the design. Such a decrease in the tail's lifting contribution negates the advantages of the joined-wing concept which relies on the tail to do a significant portion of the lift. Ideally, no moment would exist about the section aerodynamic center.

Additionally, due to the preliminary nature of the joined wing and the lack of adequate data from which to base a baseline design, several design decisions were made to simplify the configuration. The wing and tail sweeps were set equal and opposite and both the chord and span of the wing and tail were made equal. These decisions were made to reduce the complexity of analyzing the geometry, though they also significantly limited the design space in which the configuration developed.

The most telling strength of the design is its cost per seat per 1000 ft (CPSPK). The best estimate of the *Diamondback*'s operating cost reveals that at the design payload of 100 passengers the CPSPK is 0.006 $/seat/1000 ft, less than 67% that of the HB-40 for a comparable range.

The *Diamondback* also provides other gains over conventional aircraft. Structurally, the configuration has the benefits of increased stiffness and a possible reduction in weight of the wing due to the additional support of the tail. Because of the diamond geometry of the wing and tail and the lifting contribution of the tail, the aircraft's neutral point and thus the center of gravity is located near the middle of the fuselage. This placement can reduce the sensitivity of the center of gravity to changes in the payload weight distribution since the distance to the payload from the empty weight center of gravity is reduced by the central location of the c.g..

Most importantly, the *Diamondback* exhibits an exceptionally low induced drag. With an Oswald Efficiency Factor (e) of 1.2, the design has a 25% decrease in induced drag when compared to a plane with a more conventional value of 0.9 with the same aspect ratio and lift [$C_{Di} = C_L^2/(\pi e AR)$]. For a typical jet transport the induced drag is roughly 30% of the total drag and a 25% decrease in induced drag yields nearly an 8% decrease in overall drag.

The weaknesses of the design are two-fold. First, the performance of the current aircraft exceeds that required by the Design Requirements and Objectives. To a great extent, this is due to the unique nature of the *Diamondback* and the lack of a database of similar aircraft from which to base an initial design. Because the relative lifting capacities of the wing and tail were unknown, the initial wing sizing was done conservatively as if the aircraft was of a conventional design. The design decisions which followed were guided by calculations which used these conservative performance estimates and the aircraft which emerged was over-designed. The *Diamondback* currently has an overabundance of lifting surface resulting in an increase in take-off and turning performance. This also indirectly led to a range which is considerably greater than the design range. To meet the runway length requirements, a large voltage was required to power the engine and provide a high thrust to quickly accelerate the aircraft. Achieving this voltage with the batteries available in Aeroworld, however, results in a battery capacity which greatly exceeds that required in the design, thus increasing the range beyond that required.

One of the primary objectives of the design team was to explore the intricacies of the joined-wing configuration and discover the significant variables and important considerations associated with the concept. This objective was achieved as the design progressed, but because the initial sizing was off, the design currently surpasses the targeted performance criteria.

The second weakness of the design, like the first, is a products of the unique nature of the *Diamondback*. Much of the empirical data used in conventional designs was not applicable to the joined-wing configuration and the design relied heavily on aerodynamic modeling with LinAir. Due to the close proximity of the wing and tail, significant aerodynamic interference is present between these surfaces. Moreover, this aerodynamic coupling appears to introduce non-linearity into the aircraft's aerodynamic characteristics which is difficult to model. These factors combine to greatly increase the complexity of the aerodynamic and stability and control calculations, and point to a high degree of uncertainty in the accuracy of the modeling. Without access to better tools such as LinAir-Pro to accurately model interference and asymmetric flight conditions, the unique configuration of the *Diamondback* poses a risk in the uncertainty inherent in the performance estimates.

Overall, however, the promising characteristics of the joined wing (which can be refined with another design iteration and better modeling tools) make the *Diamondback* a strong candidate for future competition against the HB-40 in the Aeroworld passenger aircraft market. The aircraft has not yet been optimized, and re-sizing the wing and tail with the data and insight acquired in the design process will increase the overall efficiency of the *Diamondback*. The validation of the concept in the flight-test will also provide invaluable data into the joined-wing concept and the accuracy of the modeling techniques utilized in the design. By blazing the path for future joined-wing designs, the *Diamondback* is a valuable addition to the Aeroworld aviation industry.

Specification Summary

Fuselage:		
	length	5.58 ft
	finess ratio	0.13
	payload volume	9.86 ft^2
	cross sectional area	.148 ft^2
Wing:		
	aspect ratio	9.65
	span	9.65 ft
	root chord	1 ft
	dihedral	9.9 deg
	sweep	18.2 deg
	incedence angle	2.24 deg
	airfoil section	Clark-Y
Tail:		
	aspect ratio	9.65
	span	9,65 ft
	root chord	1 ft
	dihedral	-1.89
	sweep	-18.2 deg
	incedence angle	-1.62
	airfoil section	NACA 0012
Vertical tail:		
	area	1.08 ft^2
	aspect ratio	3.1
	root chord	.83 ft
	taper ratio	1.0
	airfoil section	flat plate
Propulsion:		
	motor	Astro 15
	placement	front
	propeller	Zinger 11-7
	number of blades	2
Weights:		
	total	87.52 oz
	engine	11.05 oz
	avionics	5.8 oz
Performance:		
	Vmin	21.7 ft/s
	Vmax	59.5 ft/s
	Vstall	17.8 ft/s
	range	25545 ft
	endurance	15.2 min

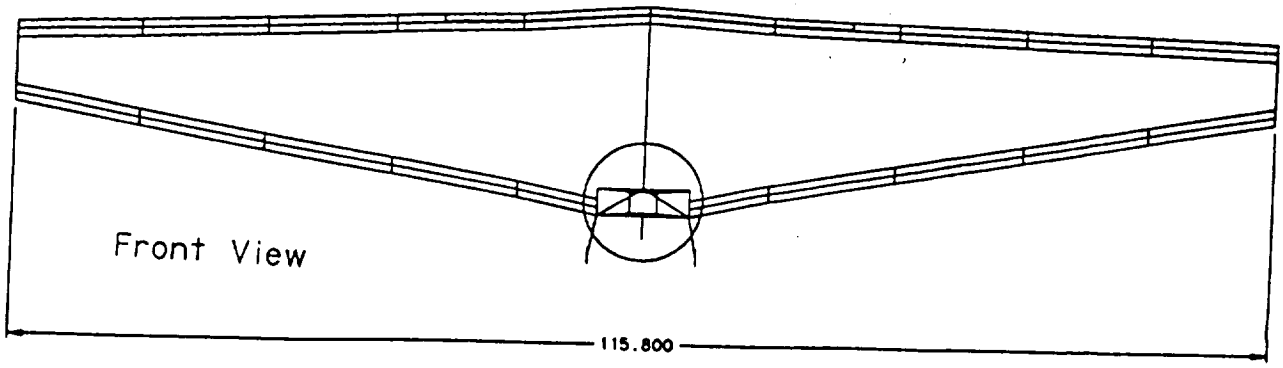

Dimensions in inches

Top View

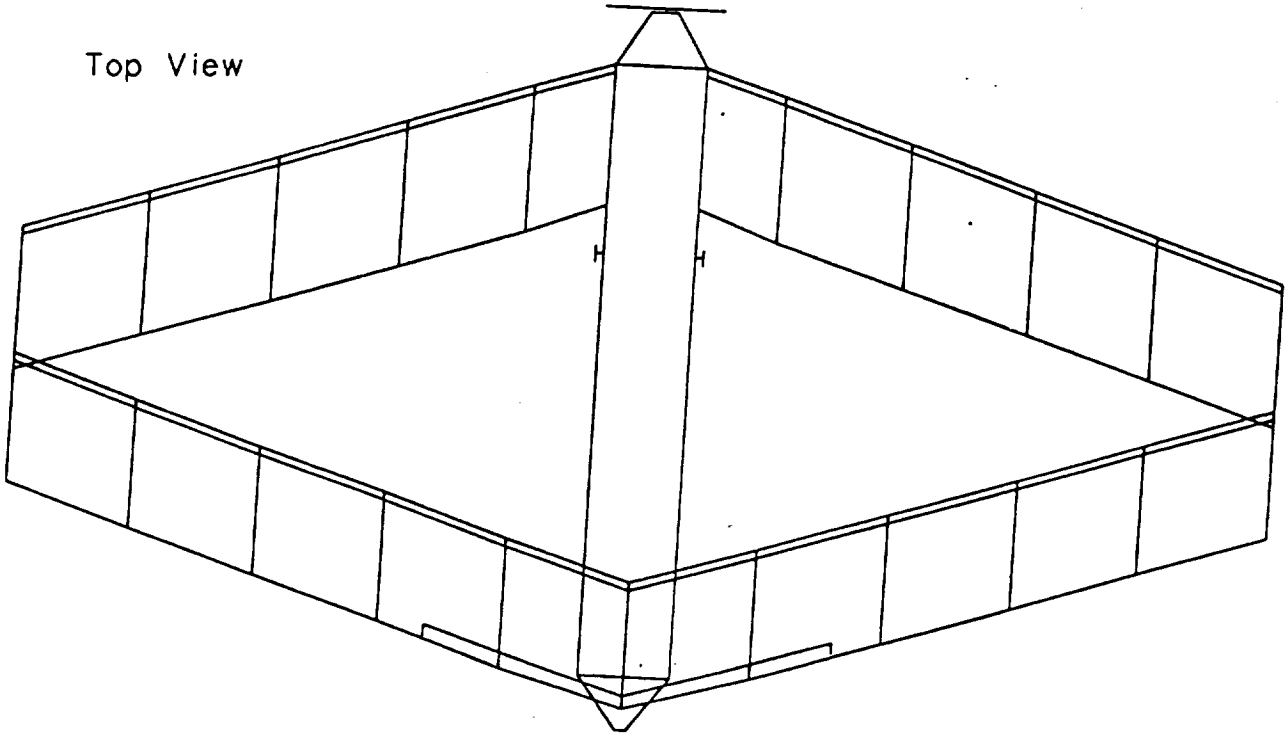

Side View

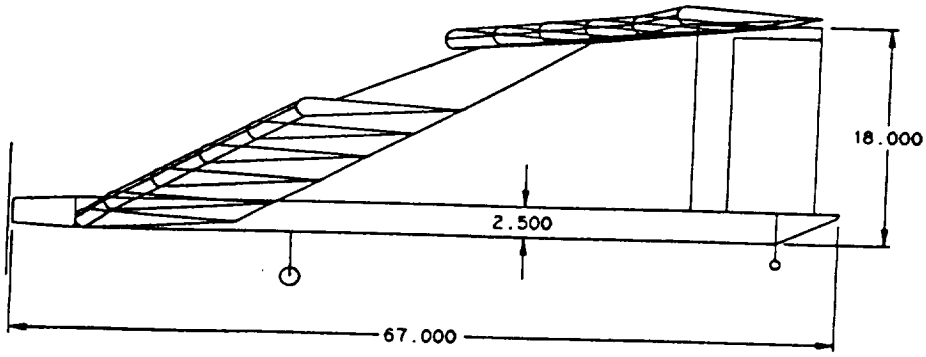

Dimensions in inches

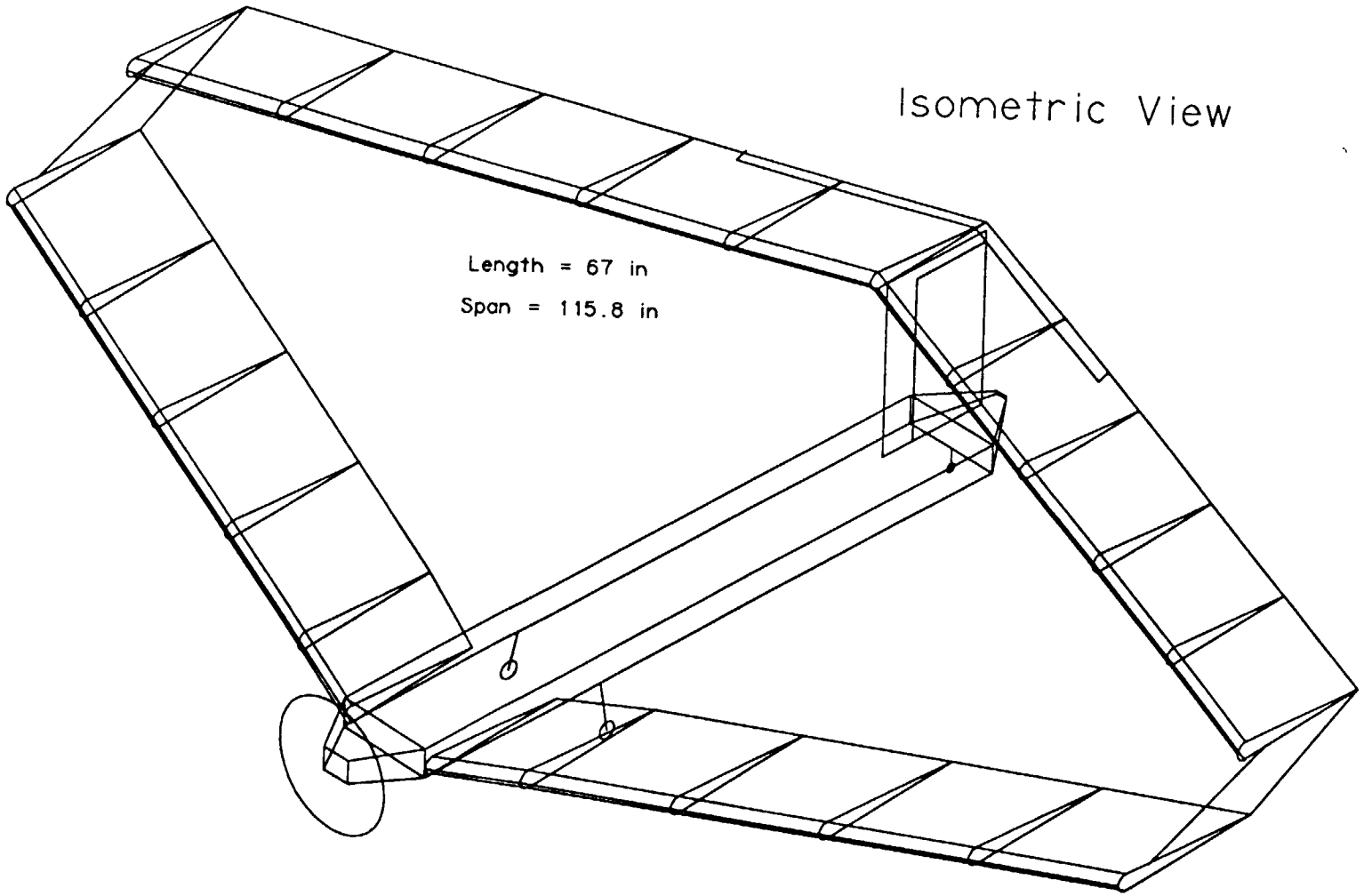
Isometric View
Length = 67 in
Span = 115.8 in

Internal Layout

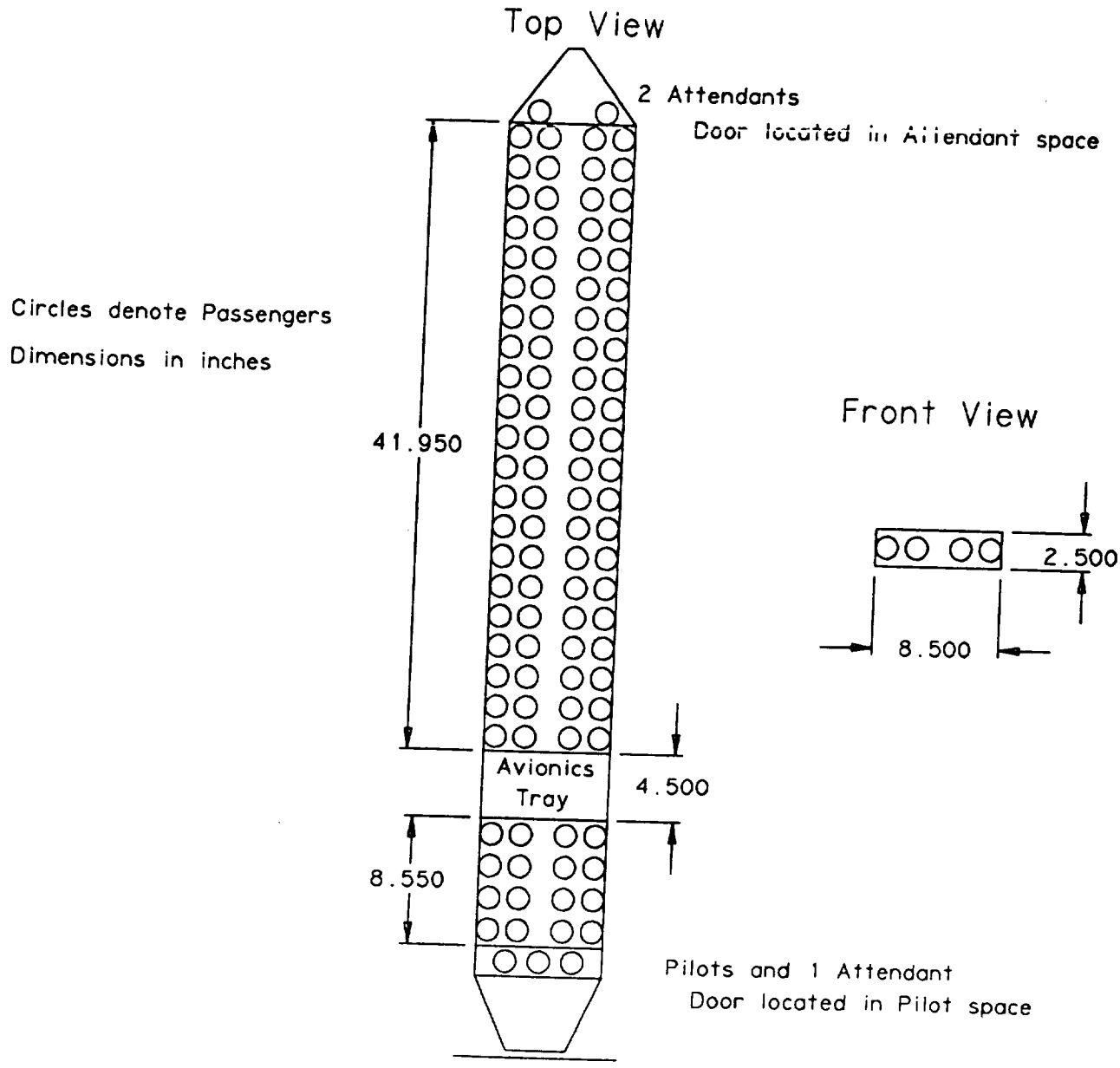

POST FLIGHT MANAGEMENT REVIEW: **Diamondback**

April 30, 1993

The following observations were made during the flight test validation for this aircraft design. This assessment is obviously quite qualitative and is based primarily upon the pilot's comments and instructor's observations.

1. For the initial flight the C.G. was at 27.8" from the nose of the fuselage.

2. First flight take-off with full down elevator and aircraft pitched up, stalled and impacted tail first. Some minor damage was done to the tail carry-through structure.

3. Second flight - moved the C.G. about 1 inch forward by moving the motor and repaired the tail structure. Still pitched up even with the elevator full down.

4. Third flight - moved the C.G. to approximately the location of the main landing gear. This required the addition of about 1 lb and the total movement was about 4.5 inches from the first flight location.

5. Still needed full down elevator to fly straight and level but then was actually a bit better in the turns when no up elevator was required to maintain altitude.

6. Rudder control was very much effected by the propwash. When the engine was throttled back for landing, there was a significant loss in rudder effectiveness.

7. Successful validation of a rather unique flight concept. Flew under control through entire closed course at approximately the required loiter speed when the C.G. was re-positioned. Landing and take-off performance was acceptable based upon the requirements.

	A	B	C	D	E	F
1	Parameter	Initials of RI:	Date: 4-8	Date:	Date:	Date:
2	*[all distances relative					
3	to aircraft nose					
4	and in common units]*					
5						
6	DESIGN GOALS:					
7	V cruise	ft/sec	28			
8	Max # of passengers		100			
9	# passenger-coach		100			
10	# passengers - 1st class		0			
11	# crew		5			
12	Max Range at Wmax		13000			
13	Altitude cruise	ft	25			
14	Minimum turn radius	ft	25			
15	Max Range at Wmin	ft	26000			
16	Maximum TO Weight-WMTO	lb	5.47			
17	Minimum TO Weight - Wmin	lb	4.89			
18	Total Cost per Aircraft	$	1994			
19	DOC	$/flight	4.61			
20	CPSPK (max design conditions)	$	0.0046			
21						
22	BASIC CONFIG.					
23	Wing Area	ft^2	9.65			
24	Maximum TO Weight - WMTO	lb	5.47			
25	Empty Flight Weight	lb	4.89			
26	Wing loading(WMTO)	lb/ft^2	0.57			
27	max length	ft	5.58			
28	max span	ft	9.65			
29	max height	ft	21.4			
30	Total Wetted Area	ft^2	52.8			
31						
32	WING					
33	Aspect Ratio		9.65			
34	Span	ft	9.65			
35	Area	ft^2	9.65			
36	Root Chord	ft	1			
37	Tip Chord	ft	1			
38	taper Ratio		1			
39	C mac - MAC		-0.09			
40	leading edge Sweep	degrees	18.16			
41	1/4 chord Sweep *	degrees	18.16			
42	Dihedral	degrees	9.9			
43	Twist (washout)		None			
44	Airfoil section		Clark-Y			
45	Design Reynolds number		178000			
46	t/c		11.72%			
47	Incidence angle (root)	degrees	2.24			
48	Hor. pos of 1/4 MAC	ft	0.67			
49	Ver. pos of 1/4 MAC	ft	0.08			
50	e- Oswald efficiency		1.2			
51	CDo -wing		0.023			
52	CLo - wing		0.442			
53	CLalpha -wing	per deg	0.084			
54						
55	FUSELAGE					
56	Length	ft	5.58			
57	Cross section shape		Rectangle			
58	Nominal Cross Section Area	ft^2	0.148			
59	Finess ratio		0.13			
60	Payload volume	ft^3	0.82			
61	Planform area	ft^2	3.96			
62	Frontal area	ft^2	0.035			
63	CDo - fuselage		0.014			
64	CLalpha - fuselage					
65						

	A	B	C	D	E	F
66	EMPENNAGE					
67	Horizontal tail					
68	Area	ft^2	9.65			
69	span	ft	9.65			
70	aspect ratio		9.65			
71	root chord	ft	1			
72	tip chord	ft	1			
73	average chord	ft	1			
74	taper ratio		1			
75	l.e. sweep	degrees	-18.17			
76	1/4 chord sweep	degrees	-18.17			
77	incidence angle	degrees	-1.62			
78	hor. pos. of 1/4 MAC	ft	4.83			
79	ver. pos. of 1/4 MAC	ft	1.56			
80	Airfoil section		NACA 0012			
81	e - Oswald efficiency		included in	wing		
82	CDo -horizontal		included in	wing		
83	CLo-horizontal		0.58			
84	CLalpha - horizontal	per degree	0.054			
85	CLde - wing-tail	per degree	0.01			
86	CM mac - horizontal		0			
87	Dihedral of tail	degrees	-1.89			
88						
89	Vertical Tail					
90	Area	ft^2	1.08			
91	Aspect Ratio		3.1			
92	root chord	ft	0.83			
93	tip chord	ft	0.83			
94	average chord	ft	0.83			
95	taper ratio		1			
96	l.e. sweep	degrees	None			
97	1/4 chord sweep	degrees	None			
98	hor. pos. of 1/4 MAC	ft	4.83			
99	vert. pos. of 1/4 MAC	ft	0.86			
100	Airfoil section		Flat plate			
101						
102	SUMMARY AERODYNAMICS					
103	Cl max (airfoil)		1.17			
104	CL max (aircraft)		1.5			
105	lift curve slope (aircraft)	per degree	0.139			
106	CDo (aircraft)		0.02			
107	efficiency - e (aircraft)		1.09			
108	Alpha stall (aircraft)	degrees	13			
109	Alpha zero lift (aircraft)	degrees	-3			
110	L/D max (aircraft)		14			
111	Alpha L/D max (aircraft)	degrees	3.5			
112						
113	WEIGHTS					
114	Weight total (empty)	lb	5.41			
115	C.G. most forward-x&y	ft	2.2	0.38		
116	C.G. most aft- x&y	ft	2.3	0.36		
117	Avionics	lb	0.36			
118	Payload-Crew and Pass-max	lb	0.58			
119	Engine & Engine Controls	lb	0.69			
120	Propeller	lb	0.04			
121	Fuel (battery)	lb	0.92			
122	Structure	lb	3.53			
123	Wing	lb	0.81			
124	Fuselage/emp.	lb	1.6			
125	Landing gear	lb	0.4			
126	lcg - max weight	lb	1.74			
127	lcg - empty	lb	1.68			
128						
129	PROPULSION					
130	Type of engines		Astro 15			

	A	B	C	D	E	F
131	number		1			
132	placement		Forward			
133	Pavil max at cruise	watts	70			
134	Preq cruise	watts	18.3			
135	max. current draw at TO	amps	9.8			
136	cruise current draw	amps	4.95			
137	Propeller type		Zinger			
138	Propeller diameter	inches	11			
139	Propeller pitch	inches	7			
140	Number of blades		2			
141	max. prop. rpm		7900			
142	cruise prop. rpm		3994			
143	max. thrust	lb	2.8			
144	cruise thrust	lb	0.48			
145	battery type		P90-SCR			
146	number		12			
147	individual capacity	milliAmps	900			
148	individual voltage	volts	1.2			
149	pack capacity	milliAmp hours	980			
150	pack voltage	volts	14.4			
151						
152	STAB AND CONTROL					
153	Neutral point		2.4c			
154	Static margin %MAC		24%			
155	Hor. tail volume ratio		2			
156	Vert. tail volume ratio		0.026			
157	Elevator area	ft^2	0.41			
158	Elevator max deflection	degrees	10 to -20			
159	Rudder Area	ft^2	0.68			
160	Rudder max deflection	degrees	20			
161	Aileron Area		-			
162	Aileron max deflection		-			
163	Cm alpha	per degree	0.14			
164	Cn beta	per degree	0.011			
165	Cl alpha tail	per degree	0.054			
166	Cl delta e tail					
167						
168	PERFORMANCE					
169	Vmin at WMTO	ft/sec	21.7			
170	Vmax at WMTO	ft/sec	49.7			
171	Vstall at WMTO	ft/sec	17.8			
172	Range max at WMTO	ft	18330			
173	Endurance @ Rmax	minutes	11.75			
174	Endurance Max at WMTO	minutes	13.2			
175	Range at @Emax	ft	17410			
176	Range max at Wmin	ft	18820			
177	ROC max at WMTO	ft/sec	7			
178	Min Glide angle	degrees	4.09			
179	T/O distance at WMTO	ft	25.4			
180						
181	SYSTEMS					
182	Landing gear type		Tail Drag			
183	Main gear position	ft	2.04			
184	Main gear length	ft	0.42			
185	Main gear tire size	ft	0.125			
186	nose/tail gear position	ft	5.08			
187	n/t gear length	ft	0.17			
188	n/t gear tire size	ft	0.063			
189	engine speed control		Yes			
190	Control surfaces		Elevator Rudder			
191						
192	TECH DEMO					
193	Max Take-Off Weight					
194	Empty Operating Weight					
195	Wing Area					

	A	B	C	D	E	F
196	Hor. Tail Area					
197	Vert Tail Area					
198	C.G. position at WMTO					
199	1/4 MAC position					
200	Static margin %MAC					
201	V takeoff					
202	Range max					
203	Airframe struct. weight					
204	Propulsion sys. weight					
205	Avionics weight					
206	Landing gear weight					
207						
208	ECONOMICS:					
209	raw materials cost	$	140			
210	propulsion system cost	$	149			
211	avionics system cost	$	245			
212	production manhours		120			
213	personnel costs	$	1200			
214	tooling costs	$	260			
215	total cost per aircraft	$	1994			
216	Flight crew costs	$	0.2			
217	maintenance costs	$	0.0496			
218	operation costs per flight	$	0.25			
219	current draw at cruise WMTO		3.55			
220	flight time - design Range max	hr	0.1			
221	DOC	$ per flight	4.61			
222	CPSPK	$	0.0046			

2. Mission Definition

2.1 Market Analysis

The commercial aviation industry in Aeroworld is now exclusively serviced by the HB-40. The current demand for passenger aircraft, however, suggests that the opportunity exists for the development and successful operation of a new regional transport. Due to the proven reliability of the HB-40 to the airline industry, it is desired to design a new class of aircraft which will not compete head to head with the HB-40. The limited number of technological advancements made since the introduction of the HB-40 are not enough to warrant the large risk involved in trying to steal the competitors market. Therefore, a market analysis is necessary to identify a new commercial market.

The market is determined by the total number of daily passengers which need to be transported between Aeroworld cities. The HB-40 services Aeroworld as a 40-passenger aircraft with a usable range of 17,000 ft. This enables the HB-40 to efficiently service less than 4% of the total Aeroworld market, as evidenced in Figure 2.1. Several criteria were placed on the development of this data. The first requirement being that in order to efficiently serve a market, the aircraft has to operate at a minimum of 70% capacity. Second, the transport can efficiently operate at any range below its maximum usable range. Third, given the current passenger demands of Aeroworld, only configurations with a capacity greater than that of the HB-40 were considered. Finally, it was determined that tying to meet the take-off requirements associated with the 20 ft and 24 ft runways of cities O and C would significantly hinder performance at cruise. Therefore cities O and C were omitted from the analysis in Figure 2.1.

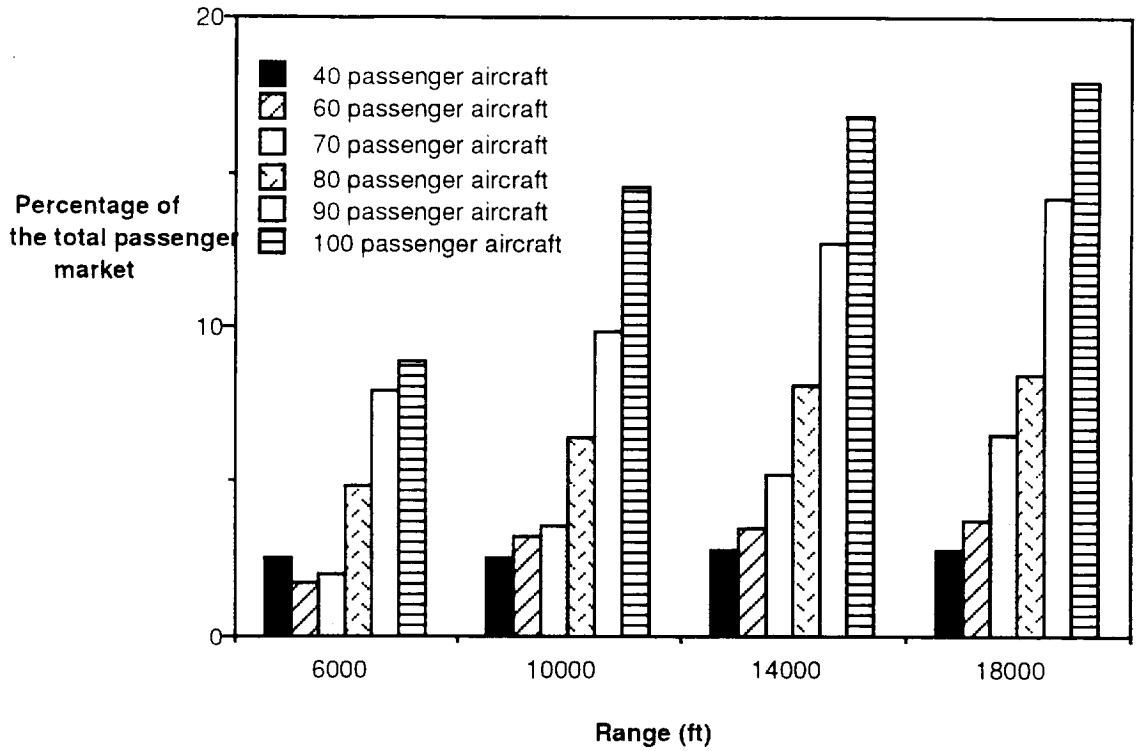

Figure 2.1 Percent of the Total Market Efficiently Captured by Various Aircraft

An analysis of the passenger transport market depicted in Figure 2.1 indicates that there is a demand for a larger, regional transport in Aeroworld. From this analysis it was decided to design an new aircraft with a usable range of 10,000 ft and a capacity of 100 passengers and 5 crew. This proposed aircraft would be able to satisfy nearly 15% of the entire Aeroworld passenger market. The target market of this proposed aircraft and that of the HB-40 are depicted in Figure 2.2. Advantages of this larger aircraft include decreasing the number of daily flights presently needed between some cities. This reduction in flights will allow the airlines to reduce crew and maintenance cost. Reducing the number of daily flights also increases the life of the airline's fleet thereby reducing the problems associated with the retirement of older aircraft. Fianally, a larger aircraft will also reduce the number of take-offs and landings at each airport, which serves to reduce the air-traffic density. Each of these advantages are factored into the direct operating costs of the aircraft and make a better investment for the airline.

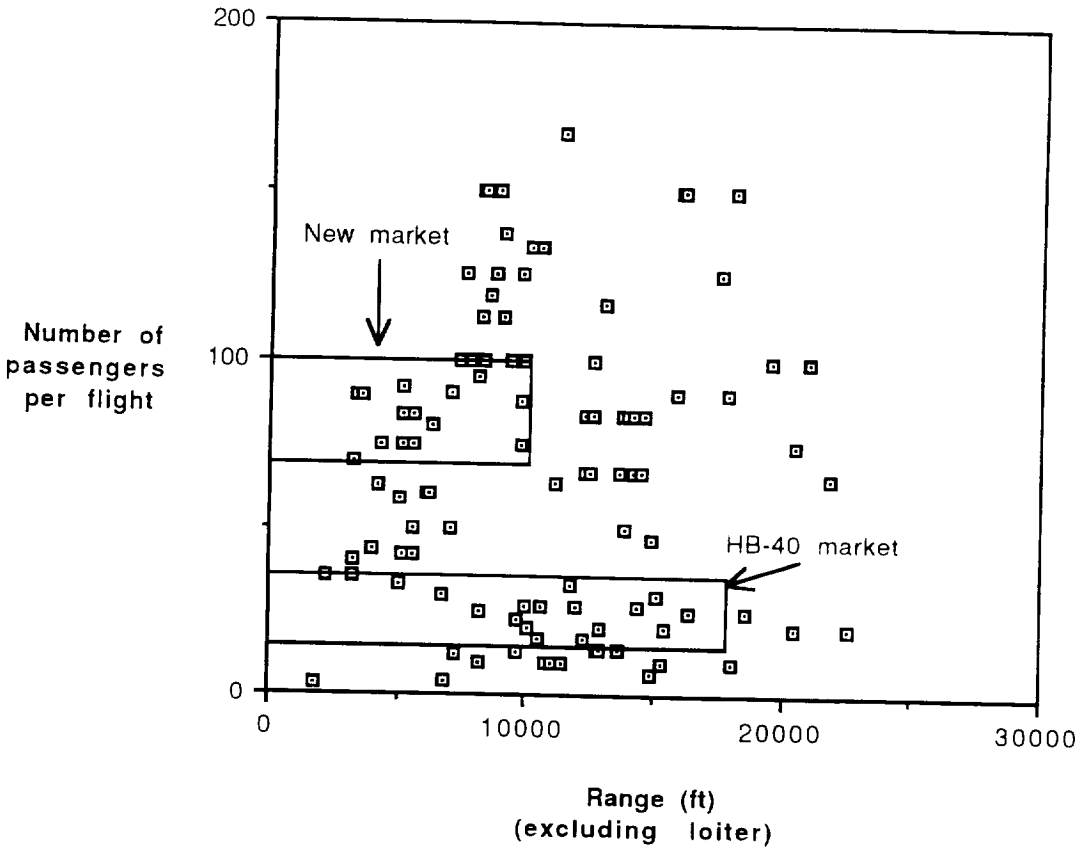

Figure 2.2 Target Markets of the Proposed Aircraft and the HB-40

2.2 Design Requirements and Objectives

2.2.1 Requirements

The design must satisfy the following requirements to successfully operate in the Aeroworld market and meet all of the design constraints. These requirements are firm standards by which the progress of the design can be measured.

Handling and Performance:

- The aircraft must take-off and land in less than 40 ft under its own power to operate in Aeroworld. Thus the design could operate on the longest runway in the market (40 ft).

- A sustained, level, 60 ft radius turn must be executed at 25 ft/s to meet the constraints of the technology demonstrator test area.
- The aircraft must have a static margin greater than 10% c to allow the pilot enough reaction time to successfully fly the transport. This value is half the recommended static margin given as a design objective.

Structures:

- The aircraft must be able to sustain the load factor at its cruise speed and C_{Lmax} to fully utilize its cruise performance capability.
- The complete R/C control system and propulsion system must be easily accessible and be able to be installed in less than 20 minutes as specified in the proposal requirements (Appendix ???).
- The fuselage design must allow for a minimum passenger volume of 8 in^3/passenger for coach and 12 in^3/passenger in first class as specified in the proposal requirements.
- The internal layout must include a two person flight crew and at least one attendant per forty passengers as specified in the proposal requirements.
- The design must have a safe-life greater than 50 hours as specified in the proposal requirements.

2.2.2 Objectives

The following objectives were targeted values to be met by the design. They are intended to guide the design decisions and determine the final prototype configuration. These objectives should be achieved to insure the success of the flight system.

Performance:

- The aircraft should cruise slowly (25 – 30 ft/s) to allow the pilot more time to react to the aircraft's handling qualities. Aircraft which have cruised in this range have successfully operated in Aeroworld.
- The aircraft should have a static margin of 20% c to be easily controllable by the ground-based pilot. This static margin was determined to be adequate from the flight performance of previous Aeroworld RPV designs.
- The range should be at least 10000 ft with a two minute loiter at cruise to service the routes identified in the market analysis.

- The payload capability should be 100 passengers with a 5 person crew to meet the payload goal determined in the market analysis.
- The aircraft should take-off and land in under 32 ft to meet all runway lengths except for cities C and O, as specified in the market analysis.
- The lift-to-drag ratio (L/D) achieved in the cruise configuration should be between 10 and 12 based on performance data from previous Aeroworld aircraft designs.

Structures and Manufacturing:

- The design gross take-off weight should be approximately five pounds based on an analysis of previous designs.
- Construction labor hours are to be minimized by design for manufacturing and are estimated to be 120 hours from the manufacturing data of previous designs.
- The design should be simple when possible to facilitate its manufacture.
- A minimum of wasted construction and hazardous materials should be sought in the design by careful planning of time and resources.
- The design should integrate access to the engine and avionics for maintenance.

Economics:

- The design should have a D.O.C. less than that of the HB-40 (0.9¢ / CPSPK) in the targeted market to be economically competitive.

Design Philosophy:

- The design will be a revolutionary, high risk design to explore the technical and economic feasibility of the joined-wing concept. It will produce data and insight into this configuration and add to the current Aeroworld data base of aircraft.

3. Concept Selection

3.1 Preliminary Concepts

The first step in designing an aircraft is the development of a concept that will allow the design requirements and objectives to be met. With this in mind, the design team generated several configuration which could possibly improve upon designs that had previously been utilized in Aeroworld.

Despite the large number of possible configurations, most of the concepts that were proposed were quite similar. The philosophy behind these proposals was to use a 'safe' design that had already been proven, and make improvements upon them. Along with these more conventional aircraft, a proposal for a joined-wing aircraft was also made which was eventually adopted. Following is a brief description of two conventional proposals along with advantages and disadvantages for each, followed by the a discussion of what influence these concepts had on the final design proposal.

3.1.1 Concept A: Low-Wing, Tail-Dragging Monoplane

The first concept that was proposed, a low-wing aircraft capable of carrying 100 passengers, is illustrated in Figure 3.1. Control for this aircraft was maintained through the use of only two control surfaces, the elevator and rudder, along with the wing dihedral. The horizontal tail was placed at the top of the fuselage and the relative dimensions were similar to most small aviation aircraft. The internal layout consisted of a single level with 25 rows. Each row contained 4 passengers, which resulted in a 'flat', rectangular cross-sectional area that provided little propeller blockage. The total length of this aircraft was six and one-half feet with most of the weight being concentrated near the nose since the engine, servos, and batteries were designed to fit in the forward compartment of the fuselage. Other major strengths for Concept A were the large data base

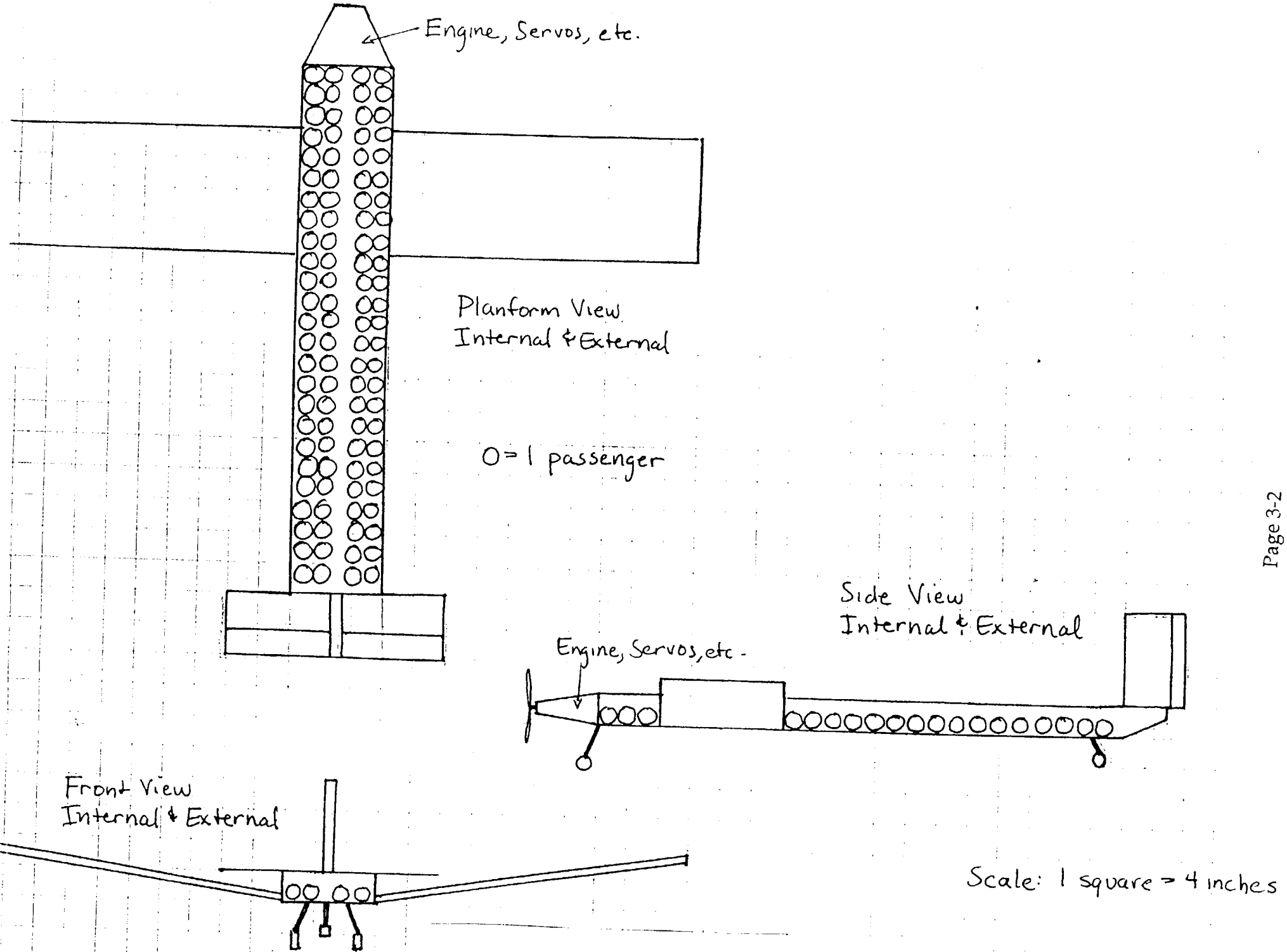

Figure 3.1: Concept A

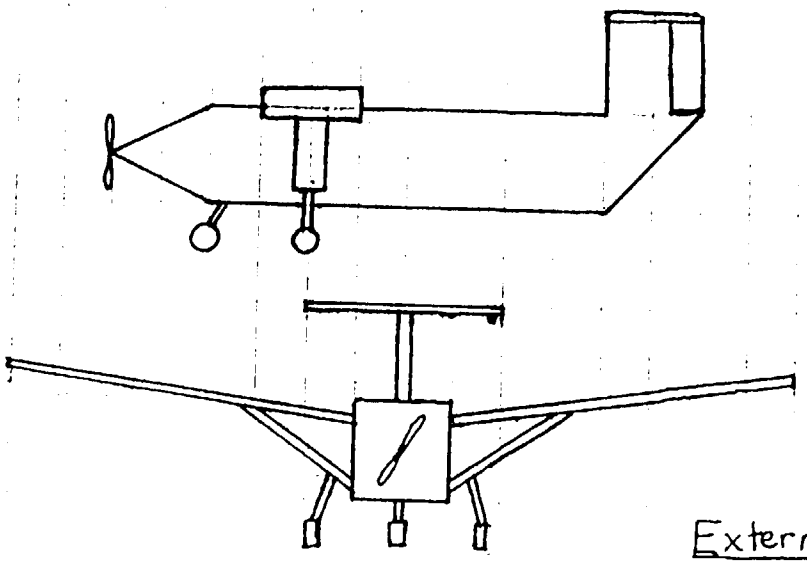

External Views

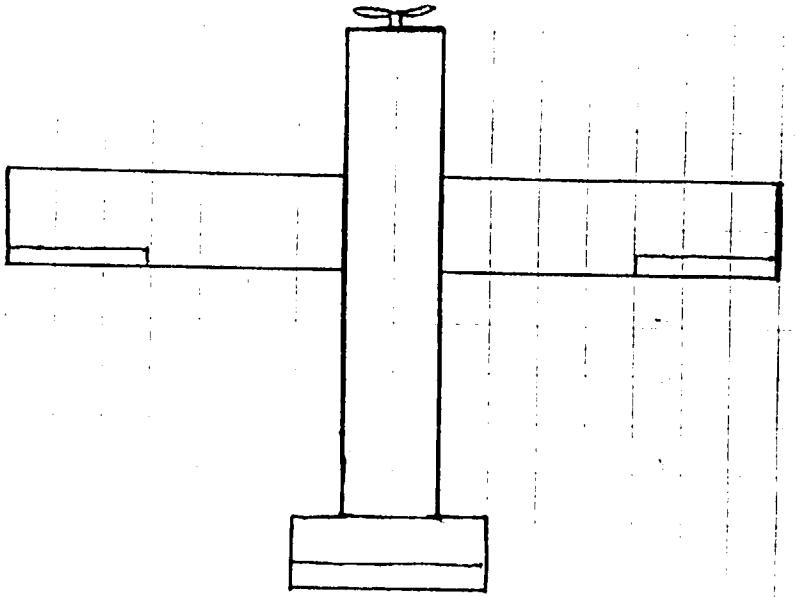

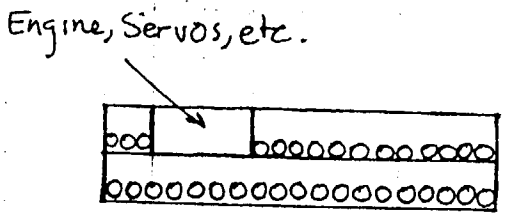

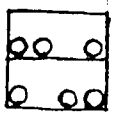

o = 1 passenger

Internal Views

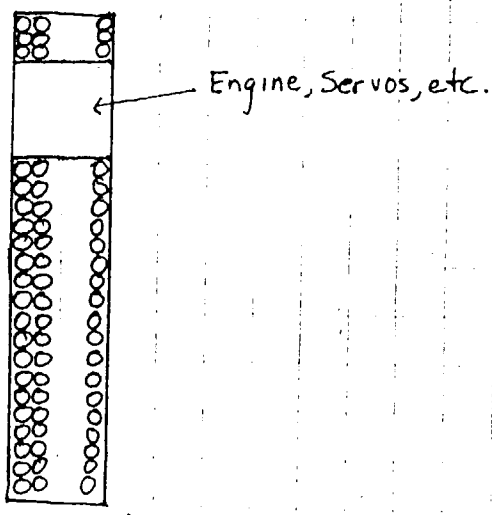

Scale: 1 square = 6 inches

Figure 3.2: Concept B

that was available for reference and the weight savings that can be realized as a result of the minimal structure.

Potential weaknesses include the tail-dragger landing gear, which is not capable of providing as much ground handling ability as a tricycle configuration, and the fact that this design is quite similar to an already proven design. Therefore, Concept A must find some way to improve upon an already successful design in order to succeed in Aeroworld.

3.1.2 Concept B: High-Wing, Tricycle Gear Monoplane

Another proposed concept was the high-wing monoplane that is illustrated in Figure 3.2. This aircraft was controlled through the use of rudder, elevator, and ailerons combined with a dihedral. The battery and servos were located in the middle of the fuselage which caused the cabin to be divided into two compartments. The internal layout consisted of two levels of passengers, each level containing 16 rows of three passengers, resulting in a square cross-sectional area. With this layout, the aircraft would be relatively short (4 feet) considering the fact that it will carry 100+ passengers. Because of the two floors and three servos on Concept B, though, there will be an increase in weight over an aircraft with one floor and two servos.

The empennage was designed as a T-tail configuration, which will minimize the interference effect from the flow that passes over the forward wing. In order to provide extra structural support for the wing, a support strut joined the quarter-span to the fuselage, and connected to the main landing gear. The disadvantage of this strut is that its placement and shape will greatly increase the parasite drag. Lastly, the landing gear consisted of a tricycle configuration in order to provide optimal ground handling capabilities.

	Concept A	Concept B
Major Strengths	. Strength of low-wing carry through . Large existing data base . Minimal structure . Only two control surfaces . Simple fuselage . Little propeller blockage	. High-wing provides additional roll stability . T-tail avoids wing interference . Tricycle gear provides greater ground control . Large existing data base
Major Weaknesses	. Ground handling difficulty due to tail-dragger config. . Need to make substantial improvements on proven design to succeed . C.G. would be near nose	. Drag penalties from wing support struts . Need to make substantial improvements on proven design to succeed . Weight penalties from 3 servos+2 floors

Table 3.1.Strengths and Weaknesses for Concept Proposals

The design that was selected differed greatly from these two concept proposals. However, some of the strengths of both of these designs were eventually incorporated in the design of the *Diamondback*. The design of the fuselage of the *Diamondback* along with its internal layout are almost exactly the same as that of Concept A. The use of only two control surfaces and a low wing design are also characteristics of Concept A.

From Concept B, the Diamondback borrowed the idea of the T-tail concept, which provides the advantage of removing the elevator from the direct wake of the wing. Also, the idea of splitting the cabin into 2 separate compartments was first proposed in Concept B and later adopted by the final proposal.

3.2 Selection of the Joined Wing Concept

After reviewing the conventional designs, our group decided to opt for a more radical concept: the joined wing. Such a design has the potential of both reducing drag and decreasing the structural weight of the wing and tail. By

utilizing the horizontal tail not only as a stability and control device but also as a structural support for the wing, this concept can increase the overall efficiency of the transport. Several difficulties in the design and manufacture of such a concept, however, must be overcome to realize the benefits of the joined wing.

Advantages of the Joined Wing:

1. Drag reduction. In Reference 3.1, the researchers cite an 11% reduction in the cruise drag over a conventional design utilizing the same structural weight and wing area. This savings would allow for a smaller engine, higher cruise speed, a larger fuselage, longer range, and combinations thereof.

2. Weight reduction. The weight of the wing and tail may be reduced by utilizing the tail as a structural support for the wing. Inboard of the wing-tail joint, the bending moments on the wing are reduced by the additional structure of the tail. The weight reduction depends on the span of the tail, with the shorter span weighing less. However, an increase in the tail to wing span ratio brings with it a decrease in total drag. A balance between these two design parameters must be reached in light of the design requirements and objectives.

3. Structural Strength. By connecting the wing and the tail, the joined wing increases the structural stiffness and strength.

4. Sweep. The sweep of the wing provides additional roll control in sideslip and can reduce the need for dihedral.

Disadvantages of the Joined Wing:

1. Stability and Control. With sweep the wing a.c. moves aft and a statically stable aircraft must have the c.g. slightly ahead of the aircraft a.c. Thus the c.g. will move aft with the wing a.c. The pitch authority is proportional to the distance from the c.g. to the tail a.c., with the tail a.c. moving fore with forward

sweep. Thus this distance, l_t, is reduced, requiring a greater tail area or control surface area.

2. Aerodynamic Design. The aerodynamic interference between the wing and tail is significant due to their proximity in this design and will be difficult to model accurately using LinAir, the tool that is available to the design team for aerodynamic modeling.

3. Manufacturing and Structure. The sweep of the wing and tail and the joint may increase the time required to manufacture the aircraft. With manufacturing representing a high proportion of the aircraft total cost such a complication is undesirable. The loads transmuted from the horizontal tail to the vertical tail require additional analysis and will increase the weight of the vertical tail. Such considerations will be addressed with careful planning and structural design.

4. Aerodynamic Design Detail

4.1 Critical Issues of the Aerodynamic Design

The critical design issue of any aircraft is the design of the lifting surfaces. To be effective, the surfaces must be designed to provide enough lift for take-off, have a high L/D at the cruise condition, employ enough control power for maneuverability, and exhibit adequate longitudinal and lateral-directional stability. The aerodynamic design was not an optimal design due to the advanced nature of out proposed joined-wing design. In lieu of this several critical design variables were identified and studied. These studies included the airfoil selection, length of the tail chord, sweep of the wing, and use of winglets.

4.2 Airfoil Selection

A critical step in designing the lifting surfaces of the *Diamondback* is the selection of the airfoil section. Many factors influenced the final decision other than just C_{lmax}. Of primary concern was the performance of the airfoil at low Reynolds Number. After examining the data collected in Reference 4.1 it became apparent that one goal of the design would be to increase the cruise Reynolds Number of the *Diamondback* to a minimum of 150,000. This is due to the fact that the lifting characteristics of airfoils below this Reynolds Number are greatly compromised. This goal was met by selecting an airfoil chord of 12 inches resulting in $Re_{cruise} = 178{,}000$. Unfortunately there were no consistent data at this Reynolds Number, therefore comparisons of different airfoils were made at a $Re \approx 200{,}000$. Consequences of this off-design analysis are: a slightly overestimated stall angle of attack which coincides with an increased C_{lmax}.

In order to arrive at a final selection several measures of merit were identified. The airfoil should:

- have a low C_d at the cruise angle of attack, to reduce the power required.

- demonstrate a gradual stall, to allow the pilot room for error at high angles of attack.
- have a C_{lmax} greater than 1.0.
- have a $C_{mc/4}$ near zero in order to reduce the incidence angle of the tail necessary to trim the aircraft at cruise.
- have a regular cross-section with no regions of high surface contour, (see Appendix ?? for explanation and cross-sections).

Based on these criteria, the Clark-Y airfoil was chosen over the Wortmann FX 63-137, and the SPICA. This decision was primarily based on construction considerations (see Appendix ??), zero lift angle of attack, and its low $C_{mc/4}$. Results of the comparison of these airfoils can be found in Table 4.1. Lift and drag characteristics of the Clark-Y can be found in Figure 4.1.

Airfoil	$C_{d\ cruise}$ *	Stall	C_{lmax}	$C_{mc/4}$	Cross-section	Zero-lift AOA
Clark-Y	0.0105	gradual	1.2	-0.09	good	-3.0 ^{o}
Wortmann	0.0144	gradual	1.6	-0.24	poor	-5.50 ^{o}
SPICA	0.0117	gradual	1.4	-0.11	good	-2.52 ^{o}

Table 4.1 Comparison of Different Airfoils
* This term is rather ambiguous because the drag penalty comes when the tail has to be mounted at increasing (negative) angles of attack in order to trim the aircraft. The increasing angle of attack is caused by the increasing (negative) $C_{mc/4}$.

The aerodynamic modeling program LinAir 1.49 by Desktop Aeronautics was used extensively in the design process. Limitations of this program are discussed in section 4.5. This program was used to compare the contribution of the tail to the total lift, drag, and L/D of the joined wing. These results used the same airfoil section for the wing and the tail, and are represented in Figure 4.2. As evidenced by this figure, the tail lift is only 37% of the wing lift at the cruise condition, at stall this increases to nearly 60%. As a result, the C_{lmax} of the tail section does not need to be as large as that of the

wing. For a wing and tail of equal area, the tail only needs a C_{lmax} which is only 60% of the wing's. Any additional lifting capability would be wasted since the wing would stall be fore this additional lift could be utilized. Accordingly, the NACA 0012 was chosen for the tail section because its Clmax = .82, and has the aditional advantage of $C_{mc/4} = 0.0$. Lift and drag characteristics of the NACA 0012 can be found in Figure 4.3

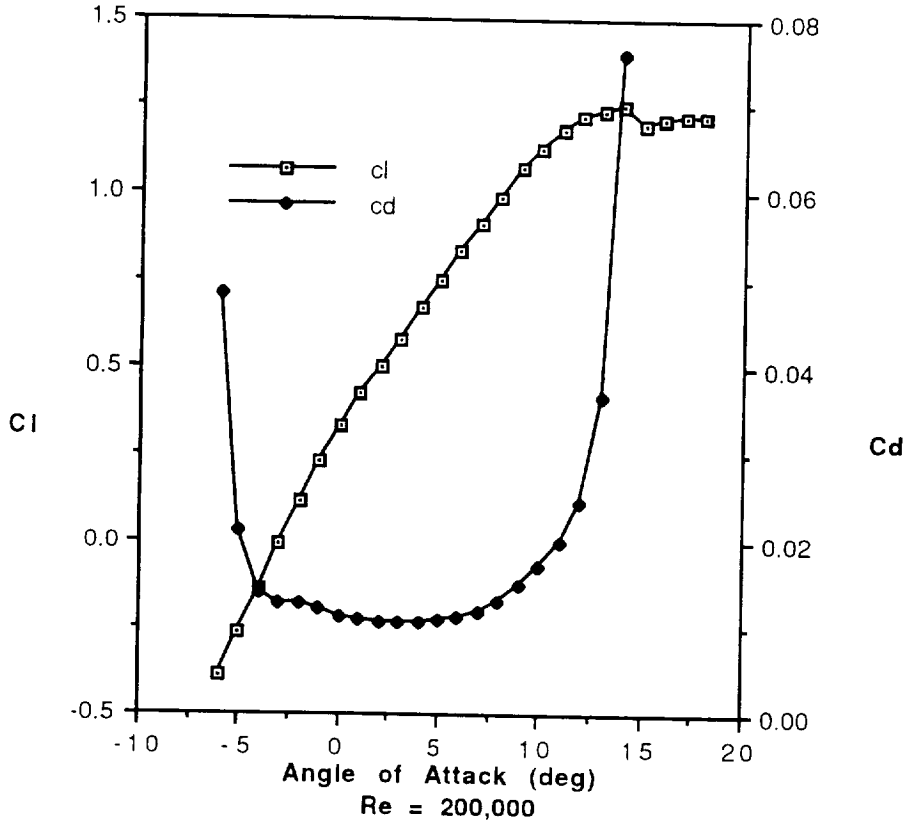

Figure 4.1 Lift and Drag Characteristics of the Clark-Y

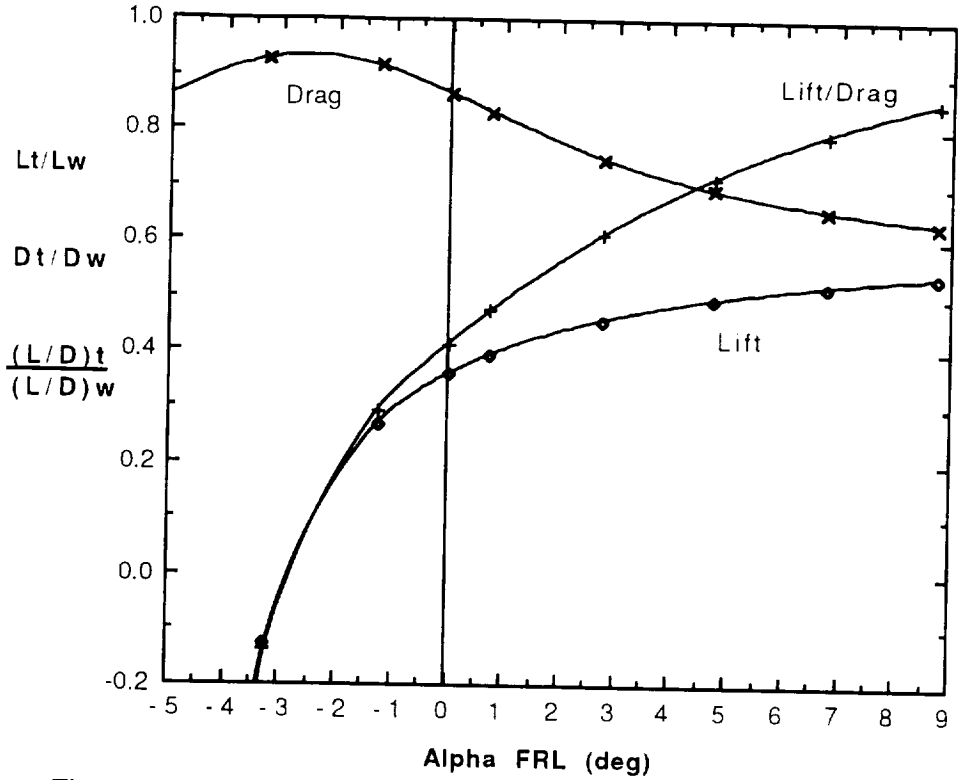

Figure 4.2 Comparison of the Tail Contribution to the Wing Lift, Drag, and L/D of the aircraft

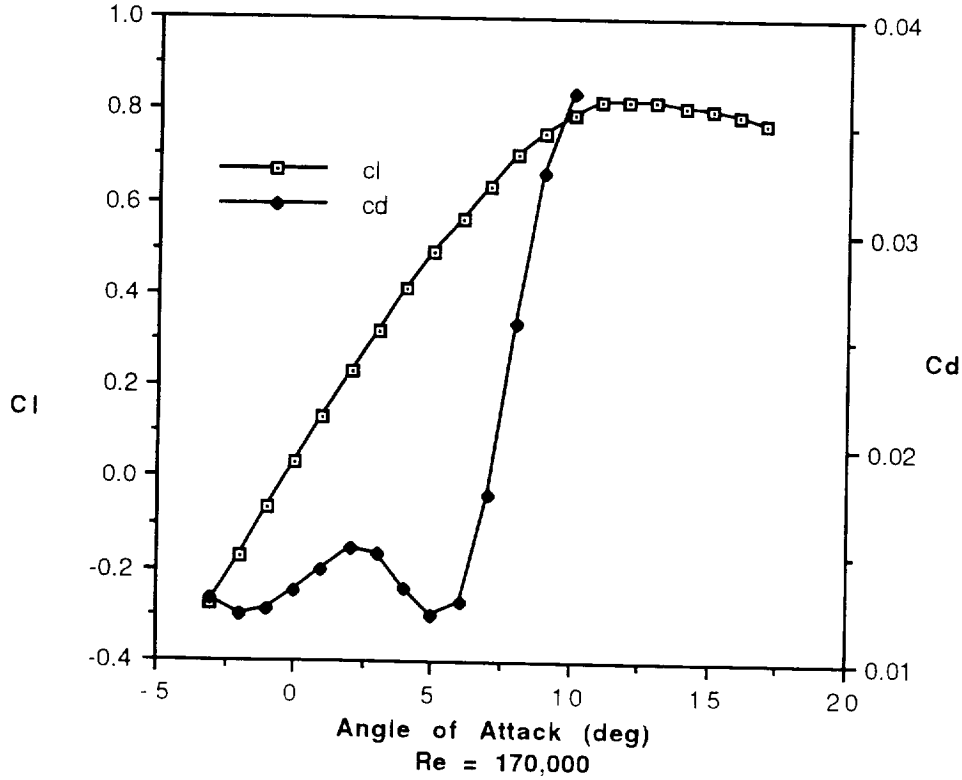

Figure 4.3 Lift and Drag Characteristics of the NACA 0012

4.3 Wing Design

The primary goal of the wing design was to increase $(L/D)_{max}$, and to have $(L/D)_{max}$ occur as close to the cruise angle of attack as possible. By achieving this goal the range of the aircraft will be maximized. Modeling of the wing design for the *Diamondback* was difficult due to the coupling of the wing and tail. For lack of a better modeling technique, LinAir 1.49 was used exclusively to set the final design. In most cases, conventional techniques which were developed for a standard wing and tail combination are not applicable. These conventional techniques account for neither the large aerodynamic interference caused by the joined wing, nor the exceedingly large tail section.

Another difficulty with the design was that several variables were not independent of one another. For example, given that the fuselage length was set by passenger requirements, anytime the sweep of the wing changed, the sweep of the tail also changed. This coupling was also apparent in the dihedral of the wing and tail.

Numerous design variables were identified for the joined-wing concept including: wing and tail areas, chord, span, dihedral, span ratio, wing sweep, and wing tip spacing. A discussion of how each of these parameters were set can be found in Appendix ??. Table 4.2 summarizes the results from this analysis.

	Wing		Tail
Area	9.65 ft^2		9.65 ft^2
Chord	1.0 ft		1.0 ft
Span	9.65 ft		9.65 ft
Dihedral	9.9°		-1.9°
Span ratio *		1.0	
Sweep	18.2°		-18.2°
Wing tip spacing **		0.5 ft	
Effective dihedral ***		8.0 °	

Table 4.2 Summary of Important Wing and Tail Sizing

* ratio of the span of the tail to the span of the wing

** vertical spacing between the quarter chord of the wing and tail tips

*** defined as: $\Gamma_{eff} = \Gamma_{wing} + \Gamma_{tail}(\frac{S_{tail}}{S_{wing}})$

4.4 Drag estimation

Minimizing the drag of the aircraft is the major concern in the design of the lifting surfaces. The consequences of reducing the drag can be seen in several design areas. Reducing the drag of the aircraft reduces the power required to cruise, thereby reducing the size and weight of the engine necessary to propel the aircraft. Reducing the drag of the aircraft also reduces the fuel consumption of the engine, increasing both the range and endurance of the aircraft.

In order to predict the drag of the aircraft, a level 2 component drag breakdown of the aircraft as described in Reference 4.2 was performed to establish C_{D_0}. The parasite drag term, C_{D_0}, was built up by using the equation:

$$C_{D_0} = \frac{\sum C_{D\pi} A_\pi}{S_{wing}}$$

The contributions of the various parts of the aircraft to the total C_{D_0} can be found in Table 4.3. Due to the interference effects associated with the joined-wing design, the contribution of the wing-tail combination was determined using LinAir. For the wing-tail combination, C_D was plotted as a function of C_L^2, and the intercept of the line was assumed to be the wing-tail contribution to the aircraft C_{D_0}. The contributions from the build up method, and the wing-tail combination were then added together and multiplied by a factor of 1.15 to obtain the total C_{D_0}. The 15% multiplication factor is recommended by Reference 4.3, to account for surface roughness, protuberances, and fuselage interference. Values of $C_{D\pi}$ for the fuselage and landing gear were taken from Reference 4.4, Figures 32, 49, and 53, while an estimate for the verftical tail was taken from Reference4.3.

Component	$C_{D\pi}$	A_π	% of C_{D_0} total
Fuselage	0.82	0.148	30
Front Landing Gear	0.59	0.016	8.6
Rear Landing Gear	0.20	0.012	1.0
Vertical Tail	0.008	0.400	7.4
			$C_{D_0} = 0.014$
Wing and Tail		$C_{D_0} = 0.023$	53%

C_{D_0} total = 1.15*(0.014+0.023) = 0.043

Table 4.3 Component Breakdown of Drag

The Oswald span efficiency factor was also determined by a build up method according to the equation:

$$\frac{1}{e} = \frac{1}{e_{wing}} + \frac{1}{e_{fuselage}} + \frac{1}{20}$$

The efficiency factor of the wing-tail combination was taken directly from LinAir. Figure 4.4 illustrates how the span efficiency of the wing increases slightly as the aircraft angle of attack increases. Figure 4.4 was used to determine the span efficiency of the wing-tail combination. At cruise, $e_{wing} = 1.19$. The contribution of the fuselage to the span efficiency of the aircraft was determined from Figure 4.5 as $1/e_{fuselage} = 0.03$. This figure was taken from Reference 4.3, and is based upon empirical data. The final term is conventionally included to account for other influences. This build up results in a cruise span efficiency e = 1.09 for the entire aircraft.

Knowing C_{D_0} and e, the complete drag characteristics of the aircraft can be determined. The drag polars in Figure 4.6 were compiled by adding the C_{D_0} from the component buildup method, to the C_D's predicted by LinAir. The parabolic nature of the drag polar illustrates that at low C_L's the drag term is dominated by the parasitic drag term, while at high C_L's the induced drag term dominates. The consequences of this can be seen in Figure 4.6. At angles of attack less than two degrees the wing and the tail have equivalent C_D's. However as the angle of attack increases, the C_L of the wing and tail, separately, increase. This results in an increase in the C_L^2 term of the

wing which is greater than that of the tail yielding an increase in the induced drag generated by the front wing. One advantage of the joined wing is that it has a higher than normal span efficiency factor. Therefore, at the cruise condition the induced drag comprises a smaller fraction of the total drag. This in turn increases the dependence of the C_D on C_{D_o}. Hence any reduction in C_{D_o} will have an increased effect on reducing the cruise C_D.

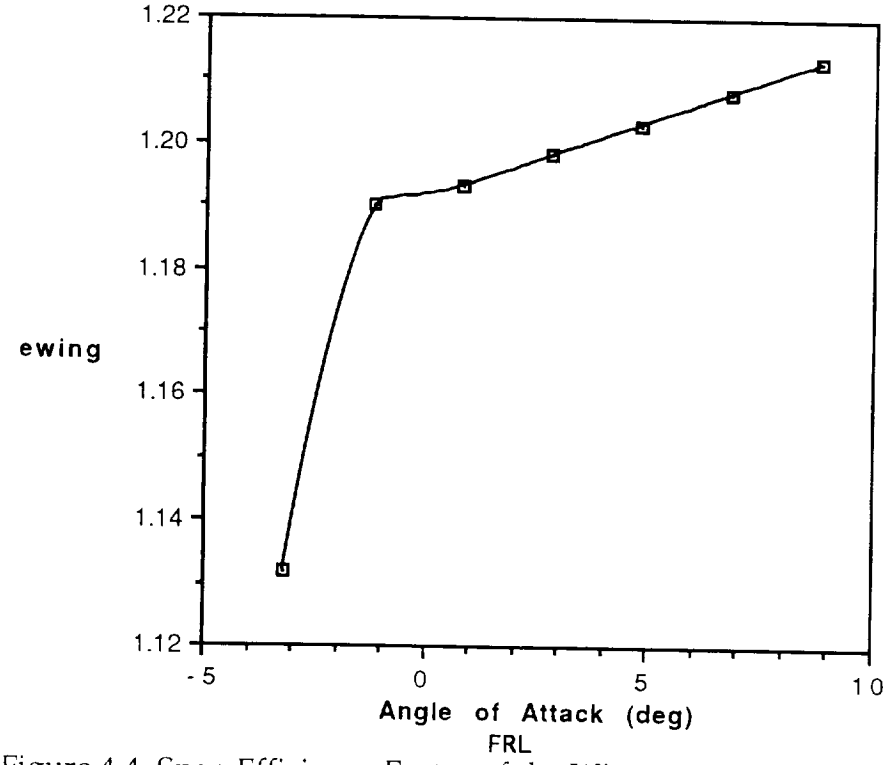

Figure 4.4 Span Efficiency Factor of the Wing-Tail Combination

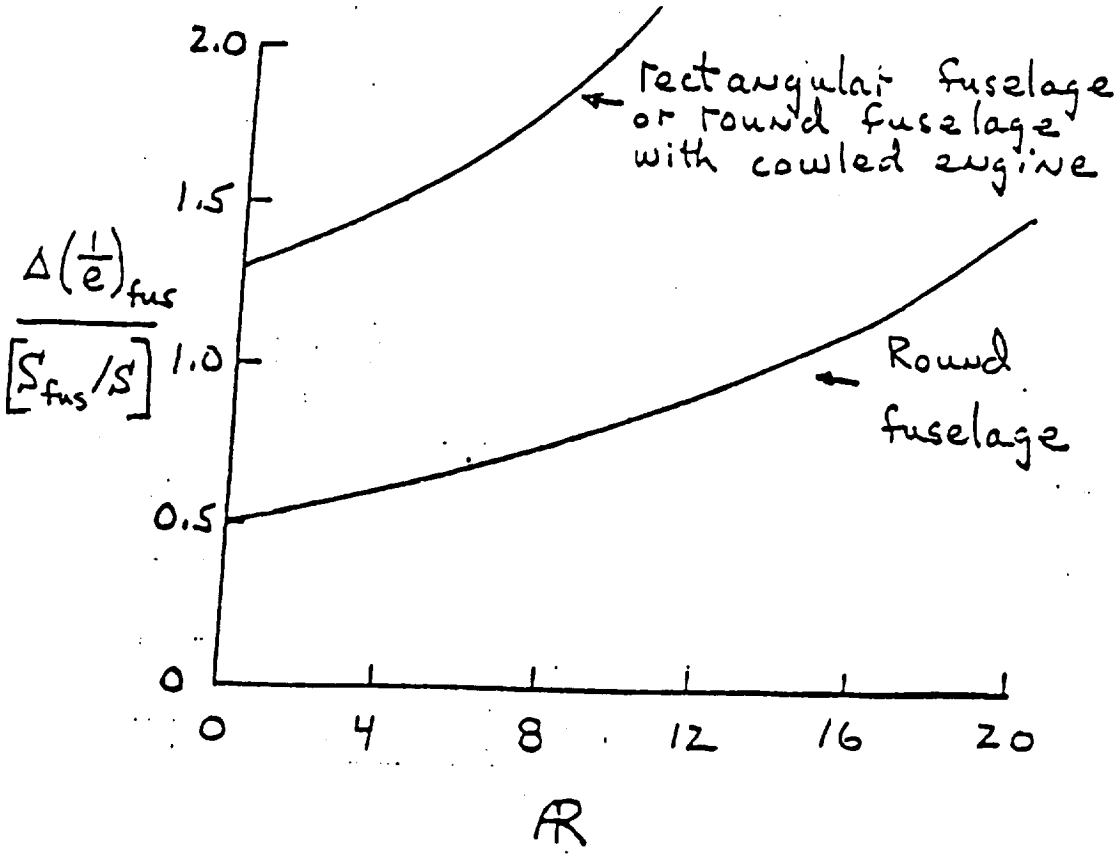

Figure 4.5 Span Efficiency Factor for the Fuselage

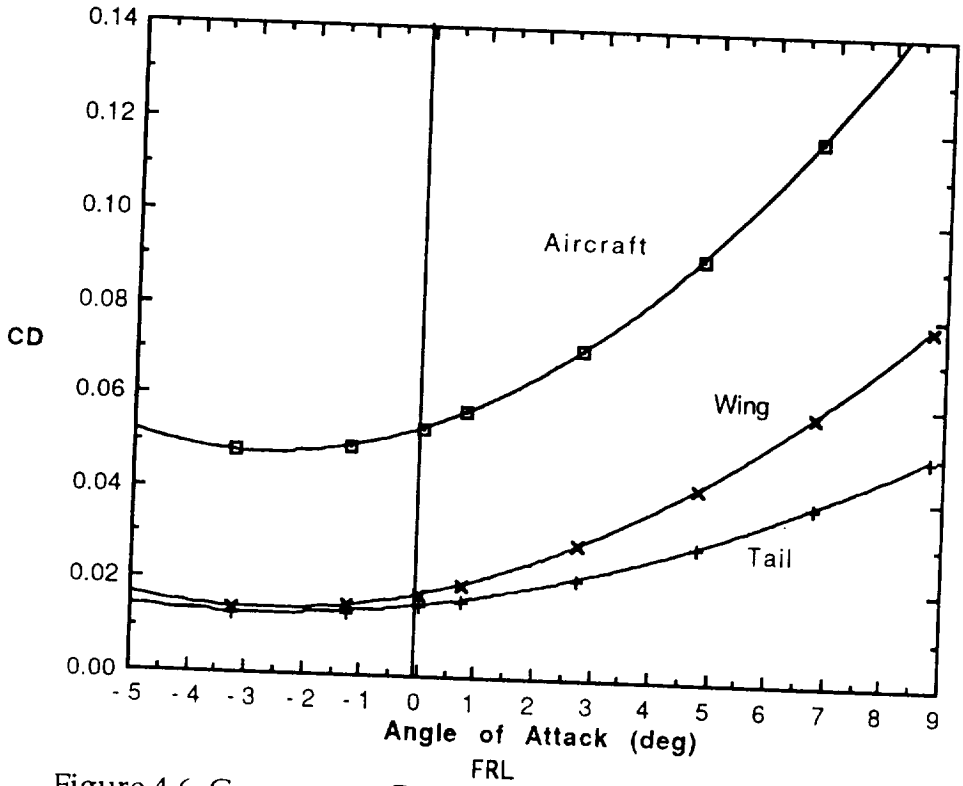

Figure 4.6 Component Contributions to the Drag Polar

Having fixed all of the design variables and determining the drag characteristics of the complete aircraft the lift to drag ratio can computed. The total L/D as well as the wing and tail contributions can be seen in Figure 4.7. As evidenced by this figure the *Diamondback* is not flying at the aircraft $(L/D)_{max}$ at the cruise condition. This results in reduced performance of the aircraft, namely a decrease in the range and endurance. The drag polar and lift curve of the aircraft can be seen in Figures 4.8 and 4.9. For the lift curve, stall was determined by examinining the section C_l distribution on the wing. The wing was estimated to be stalled when the section $C_{l\,max}$ was greater than the $C_{l\,max}$ of the Clark-Y.

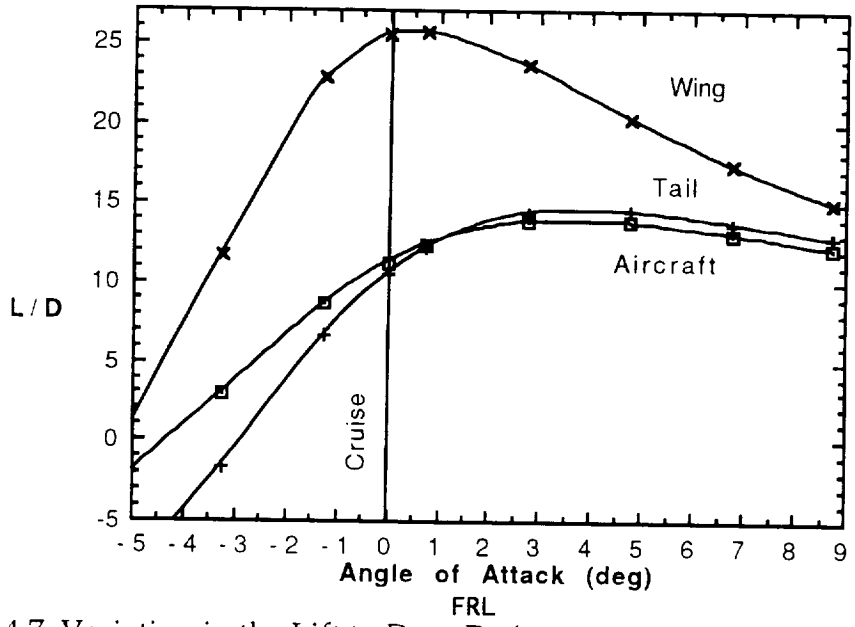

Figure 4.7 Variation in the Lift to Drag Ratio as a Function of Angle of Attack

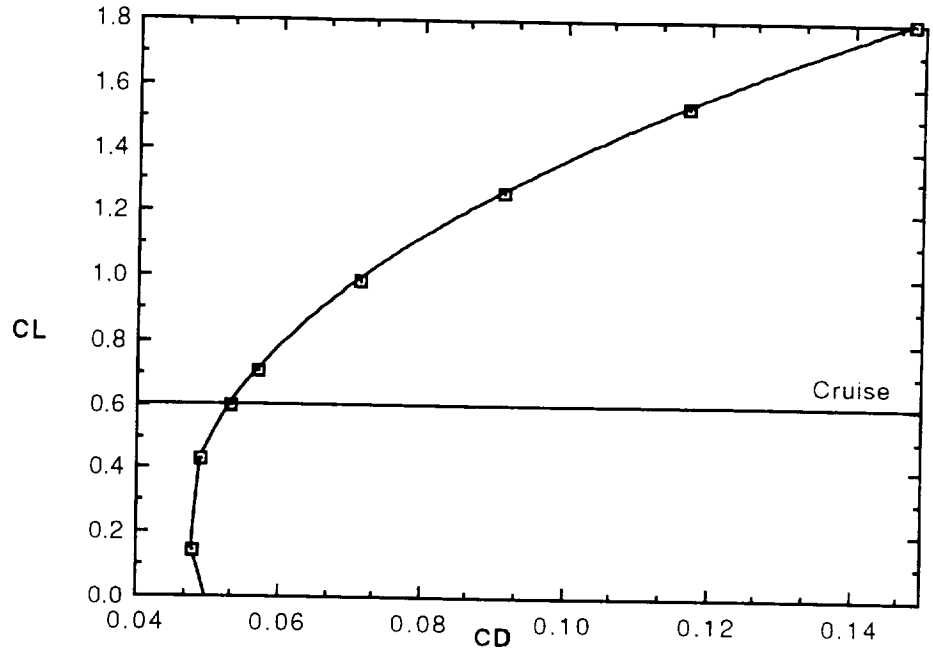

Figure 4.8 Drag Polar of the Diamondback

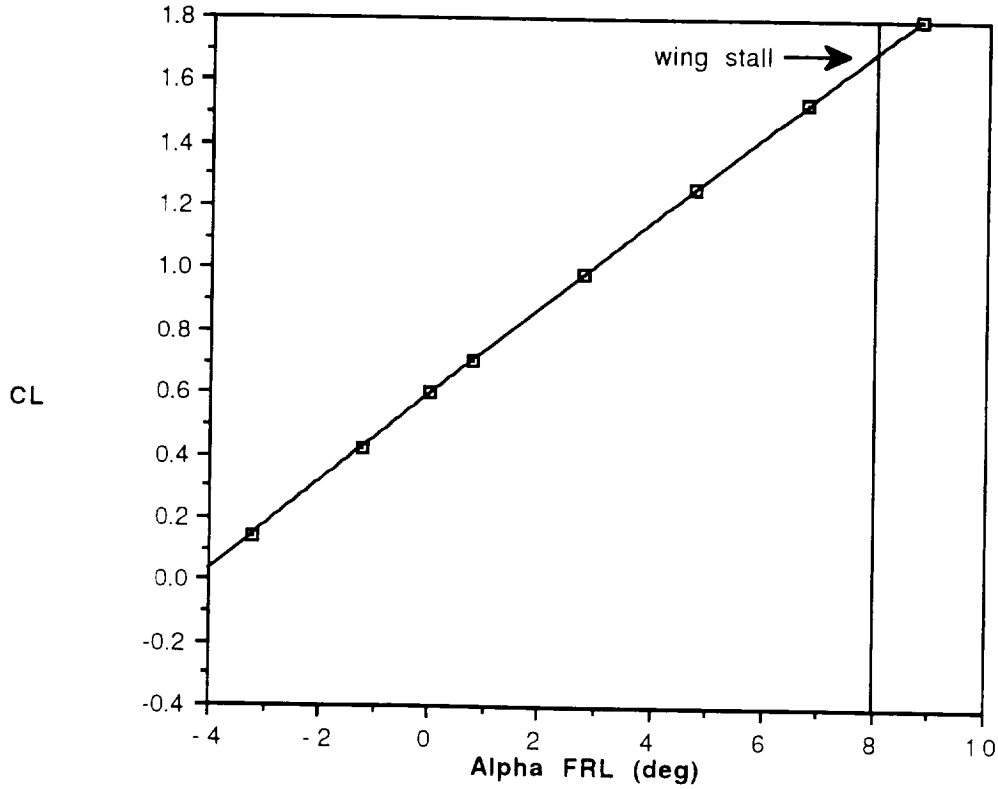

Figure 4.9 Lift Curve of the Diamondback

4.5 Modeling Problems

Due to the complex nature of the flow field around the joined-wing design, it was not possible to use a conventional approach to the design of the aircraft. The software package LinAir 1.49 was used to model the aerodynamic performance of the aircraft. LinAir 1.49 solves the Prandtl-Glauret equations for irrotational, inviscid, linearized flow, Reference 4.5. This program, however, has several shortcomings. First of all, LinAir does not account for viscous effects and therefore can not predict stall. Consequently, the joined wing was considered to be stalled when the local C_l in the spanwise C_l distribution indincluded a C_l higher than the airfoil C_{lmax}. Another inconsistency is that LinAir almost always under predicts the induced drag. The accuracy of the drag prediction increases as the number of panels on the wing are increased. However due to the increased computational time required by increasing the number of panels, studies were conducted with 20 panels on the wing and tail. This typically results in a C_{Di} which is 2% - 3% low, Reference 4.5. In order to simplify the analysis, ground effects were ignored during the take-off and landing phases.

One specific problem in the modeling of the aircraft, was an inability to fit a parabolic curve to the section drag data of the NACA 0012. The curve fit for the tail, used in LinAir, overpredicts the drag at moderate angles of attack 3 - 8 degrees, and underpredicts it at high angles of attack greater than 8 degrees.

In conclusion, the most notable deficiency in the aerodynamic design, is the inability to verify the results given by LinAir. This inability to validate the results is of great concern.

5. PROPULSION SYSTEM DESIGN DETAIL

5.1 Initial Concerns

Takeoff performance was the driving concern in the selection of the components of the propulsion system because one of the primary requirements of the *Diamondback* is that it must takeoff from the ground under its own power. In addition, the propulsion system should be such that the overall weight is minimized while performance specifications are maintained. Initially, the importance of this requirement appeared somewhat trivial, but the additional constraint of a 32 foot maximum takeoff distance played a crucial role in motor, propeller, and battery selection.

5.2 Motor Selection Considerations

The selection of the propulsion system began with an analysis of the data base of past designs and a comparison of the weights of various configurations, their power requirements, the types of motors and propellers employed, and their takeoff distances. This information provided a reasonable range of propulsion system performance parameters for various configurations and a starting point from which a range of motor sizes and propeller characteristics were analyzed. The primary criteria used to rate the motor performance was the power output capability.

Initial motor analysis included the Astro-05, Astro-15, and the Astro-25 motors. The information in the data base demonstrated that the power output of the Astro-05 of about 160 Watts at the fuse current draw of 20 Amps was insufficient to meet our 32 foot takeoff requirement. For this reason, the Astro-05 was dropped from consideration as a candidate motor. However, the data base has shown that both the Astro-15 and the Astro-25 motors have demonstrated their capabilities in powering aircraft of comparable size to the *Diamondback* to successful short takeoffs under 32 feet. Upon further analysis of these two candidates, it was observed that the voltage required by the Astro-25 to achieve a certain motor RPM exceeded that of the Astro-15 by as much

as 2.5 volts. During the critical takeoff run, in which a high propeller RPM is required, the Astro-25 requires two more batteries to achieve the same RPM as the Astro-15 if both motors were turning the same propeller. However, the greater power capability of the Astro-25 would allow it to turn a much larger propeller than the Astro-15 could. It could do this at a lower RPM and achieve comparable thrust and takeoff performance characteristics as the Astro-15 without the weight penalty of two extra batteries. Nevertheless, the Astro-25 motor itself is about 2 ounces heavier than the Astro-15 and thus would be less desirable if comparable takeoff performance estimates were achieved. The lighter Astro-15 coupled with a smaller propeller would be the obvious choice in this case since weight is such a critical issue in RPV design. However, as takeoff performance is the overriding figure of merit, the final engine selection could not be made until the propeller and battery combinations had been considered.

5.3 Propeller Selection Considerations

As with the candidate motors, the data base of past designs was an important tool in taking the first step toward propeller selection. This entailed the consideration of several propellers which had been used on a wide range of past aircraft designs, some aircraft with weights as low as 3.5 pounds and others as heavy as 8.0 pounds.

The actual analysis of propellers began by obtaining the thickness, chord, and angle measurements of several candidate propellers including a Zinger 10-6, a Zinger 11-7, a Topflight 12-4, and a Topflight 12-6. The propeller performance program listed as reference 5.1 was used to analyze the performance characteristics of each. The propellers were modeled with a NACA44XX low Reynold's Number airfoil and the analysis included induced velocity and tip losses and utilized blade element theory as the basis for its calculations. One possible source of error involved with using this program is that the propeller thicknesses could not be properly modelled near the hub with the NACA44XX airfoil series. The maximum thickness available in the series was

.2 inches and the airfoil thickness was modelled as such if it exceeded this value. The program output included the power coefficient, thrust coefficient, and propeller efficiency at various values of the advance ratio. These results illustrated that the Topflight 12-4 propeller demonstrated significantly less efficient performance at low velocities encountered during cruise than any of the remaining candidates. Therefore, this propeller was no longer considered.

Utilizing the manufacturer's motor performance specifications and the propeller performance characteristics, a short spreadsheet program was written which calculated the propeller thrusting capabilities as a function of propeller RPM, the resulting torque loads, and the corresponding voltage and current draw requirements of both candidate motors. Data base estimates of the required static thrust for effective takeoff indicated that a minimum of about 2.5 pounds is desirable. With this in mind, each propeller was analyzed at the necessary RPM such that the static thrust of the propellers met this requirement. The results demonstrated that the torque loads of the Topflight 12-6 associated with the chosen RPM were such that the required current draw exceeded the fuse current level of 20 Amps by almost 50% when it was coupled with the Astro-15, but remained within the limiting current level when coupled with the Astro-25. Meanwhile, both the Zinger 10-6 and the Zinger 11-7 performed such that the maximum current draw was within the 20 Amp limit while utilized with the Astro-15 motor. Analysis of these results showed that sufficient levels of static thrust could be achieved with the Astro-15 motor paired with either the Zinger 10-6 or the Zinger 11-7, and with the Astro-25 motor linked with any one of the remaining three propeller candidates.

Considering the weight penalties associated with each combination, it was observed that the lightest system would utilize the Astro-15 motor and either the 10 inch or 11 inch propeller. Use of the Astro-25 motor would incur a severe weight penalty not only because the motor itself is heavier than the

Astro-15, but also because it would necessitate the use of two more batteries to satisfy its voltage requirement to achieve a satisfactory RPM. For these reasons, the Astro-25 motor was dropped from consideration which left only the Astro-15 motor for consideration and thus, the Astro-15 motor was selected as the motor to be used in the *Diamondback*.. This decision narrowed the field of propeller candidates to the Zinger 10-6 and the Zinger 11-7. A graph of their efficiencies at various values of the advance ratio is shown in Figure 5.1 and graphs of their thrust and power coefficients as functions of the advance ratio are included in Appendix B.1.

In attempting to assess the ground roll performance characteristics of the remaining propulsion system candidate combinations, it became blatantly obvious that the static thrust alone cannot be used as an accurate gauge of takeoff performance. In other words, the entire ground roll phase cannot be judged solely by one static parameter. The thrust and torque levels during a takeoff run are continuously changing as are the lift and drag characteristics. Therefore, the validity and accuracy of the preceding analysis came into serious question. Time constraints involved with the selection of a final propulsion system did not allow the above analysis to be corrected or repeated, so the decision was made to move forward with further analysis of the possible systems at hand.

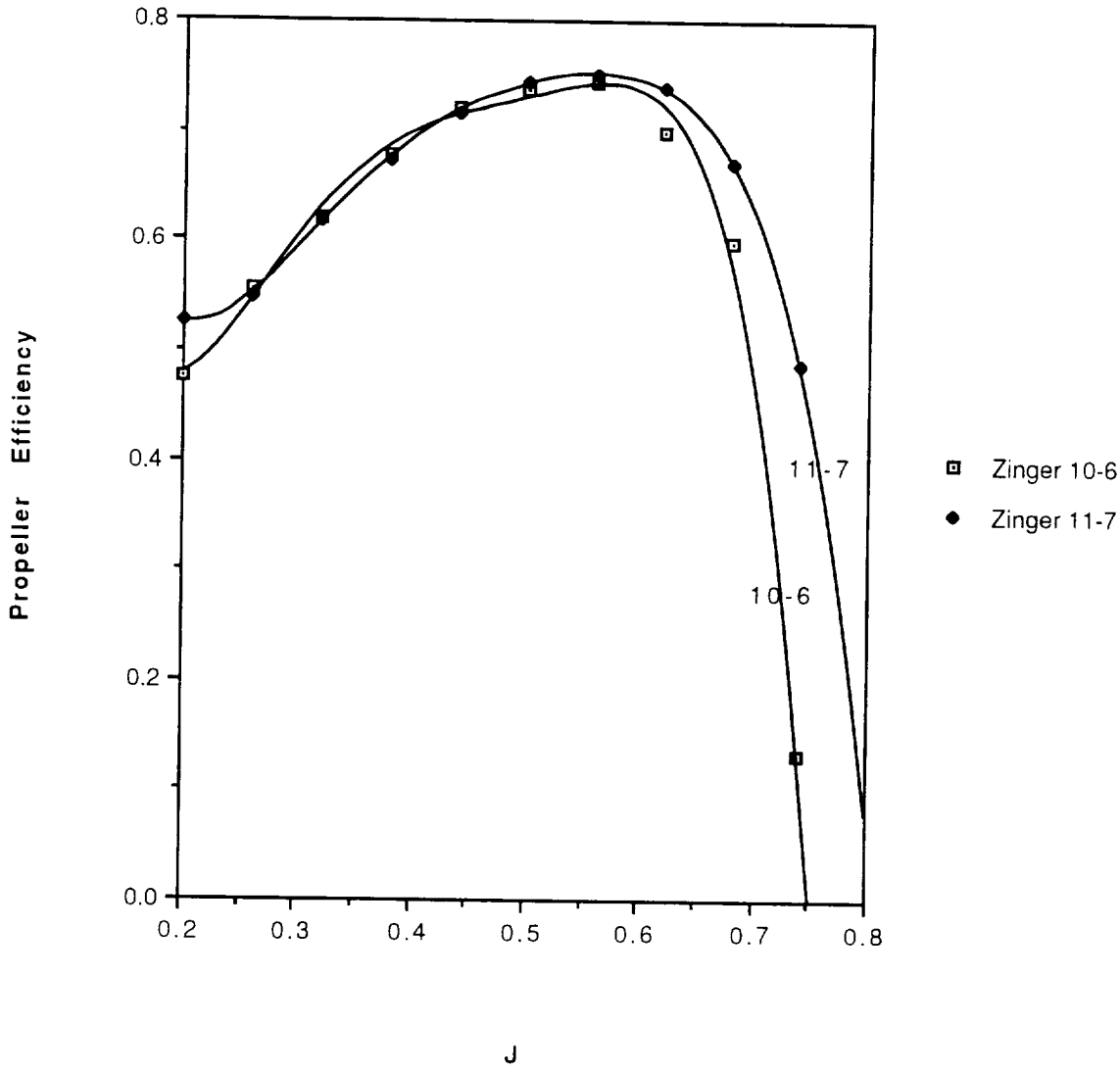

Figure 5.1 Propeller Efficiencies verses Advance Ratio

5.4 System Integration and Battery Selection

The last crucial factor in the selection of the propulsion system was the battery pack. This component typically has the largest weight fraction of any of the individual propulsion system components and therefore, it is critical to minimize. The driving criteria in the selection of the battery pack is the pack voltage because that parameter is what determines the maximum motor RPM which directly effects the takeoff distance. In addition, once the pack voltage has been determined, the capacity of the batteries (measured in Amp-hours) must be chosen such that the range of the technology demonstrator is at least as far as the desired design range including the required loiter capability.

At this point, a takeoff performance program included in Appendix E was utilized to further assess the effectiveness of the motor and propeller candidate combinations. This program utilizes the motor specifications, detailed propeller data, and battery characteristics as well as weight, lift, drag, and friction estimates to analyze a takeoff run and compute the minimum takeoff distance for the given configuration. The ability to takeoff within a field length of 32 feet is one of the objectives of this design. Using the Astro-15 motor specifications, the takeoff distance was analyzed at various voltages corresponding to integer numbers of batteries for both of the remaining candidate propellers. The results are summarized in figure 5.2.

From these results, its is shown that for the Zinger 10-6 to achieve a takeoff distance under 32 feet, the battery pack voltage must be above 15 volts which means that the pack must contain 13 batteries. However, the Zinger 11-7 is able to achieve takeoff at a voltage above 13.5 volts which corresponds to a battery pack containing 12 batteries. It becomes apparent that the lighter overall propulsion system would utilize the 11 inch propeller since it requires the use of one less battery than a system integrating the smaller 10 inch propeller.

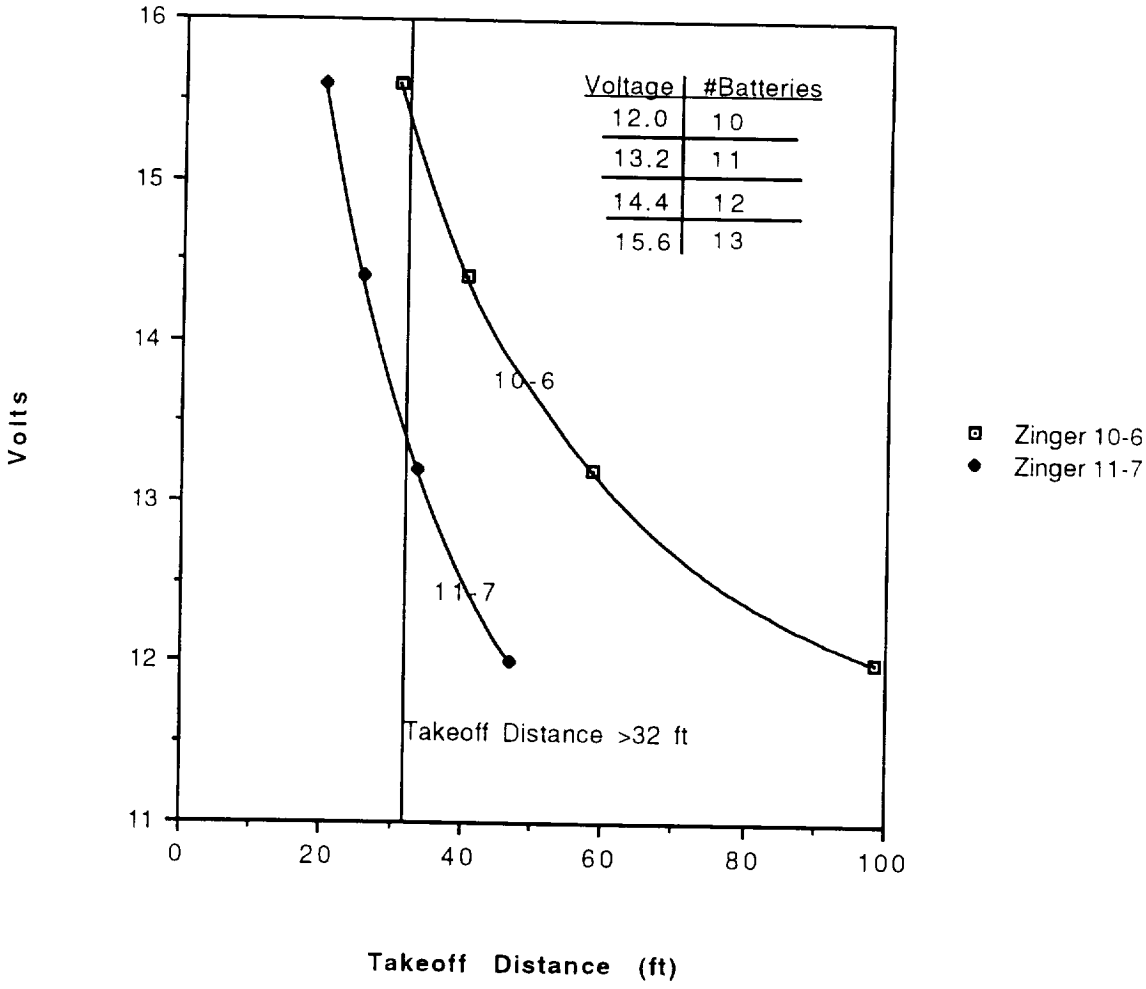

Figure 5.2 Battery Pack Voltage verses Takeoff Distance

At this point in the design phase, the propulsion system had been decided to the point that it was known that the motor would be the Astro-15, the Zinger 11-7 had been chosen as the propeller, and the battery pack would consist of 12 batteries connected in series. However, the exact size of batteries had yet to be determined.

In order to choose the best size of batteries compatible with our design, it was necessary to know the current draw out of the batteries in the cruise condition. A TK

Solver program which is included as Appendix E was written to solve for the armature current and other motor and aircraft performance parameters given the flight conditions, motor specifications, and propeller parameters. It was found that at the cruise condition , the motor draws 4.95 Amps of current at about 8 volts. Using these results, the required battery capacity is calculated to be about .657 Amp-hours. Unfortunately, the available technologies in Aeroworld do not manufacture a battery that exactly matches the capacity that is needed. For the purposes of the prototype, an existing technology must be used due to the high cost and time requirements involved with developing a new technology. The smallest battery in existence that at least satisfies the capacity requirement is the Panasonic P-90SCR900 battery which has a capacity of .90 Amp-hours. The effect of such a high capacity is that the effective range of the technology demonstrator increased by almost 5,000 feet to about 18,300 feet.

5.5 Configuration

In the *Diamondback*, the propulsion system accounts for about 32% of the overall weight of the aircraft. Therefore, the placement of the two heaviest components, the motor and the battery pack, is vitally important not only for structural considerations, but also for maintenance of stability and controllability.

The motor is placed in the nose of the aircraft and is mounted centerline. Its weight of over 11 ounces and its large moment arm causes it to provide a nose-down moment about the center of gravity. The battery pack will be included in what is called the avionics tray which will be placed aft of the center of gravity and will help to balance the nose-down moment created by the motor . It includes components such as the motor speed controller, the servo power supply, the servo motor, and of course the battery pack. The avionics tray has a significant weight fraction of about 23% and will aid significantly in placing the center of gravity at the desired location. In addition, the

main function of the speed controller is to control the voltage across the motor and thus the motor RPM.

		Weight (oz)
Motor Type:	Astro Cobalt 15	11.05
Propeller Type:	Zinger 11-7	.614
Speed Controller:		1.6
Battery Type:	P-90SCR	1.23/battery
Battery Capacity:	.90 Ah	
Number of Batteries:	12	14.76
Battery Pack Voltage:	14.4 volts	

Table 5.1 Summary of Propulsion System Parameters

5.6 Final Considerations

Upon further analysis with the Takeoff Performance program and the realization that the initial method of analysis was not proven and could have yielded unreliable results, it was observed that the overall weight of the propulsion system could have been reduced slightly. First of all, the conclusion reached that the Topflight 12-6 propeller could not be used with the Astro-15 motor was false simply because the static conditions of thrust and torque are only instantaneous because the aircraft begins to move. As the velocity increases from zero, the thrust and the torque values decrease significantly. The Takeoff Performance Program indicated that comparable and satisfactory takeoff distances could be achieved by using either the Zinger 11-7 propeller with a 12 cell battery pack or by using a Topflight 12-6 prop coupled with a 10 cell battery pack. However, changing to the lighter system would alter the weight significantly, thereby forcing another iteration of design calculations for the center of gravity, stability parameters, and control system calculations which is an impossibility given the already compressed time frame allowed for this design. In conclusion, if another design iteration were available in the completion of this project, the use of a Topflight 12-6 propeller and a 10 battery pack would definitely be implemented and have a positive influence on the design evolution.

6. Weight Estimation

The weight of the *Diamondback* was of primary concern throughout the design process. Since this factor drives all aspects of the design, estimates were constantly improved upon in order to arrive at the most accurate predictions. By integrating the novel techniques that were utilized in other designs such as spar placement and drilling holes in unnecessary structure, our design would be able to carry 2.5 times as many passengers as the HB-40 with only a 12% increase in weight.

The values for the preliminary weight estimates of each part of the *Diamondback* were arrived at by different means. For example, accurate estimates of the weight of the propulsion system, avionic control system, and passengers were able to be made based on manufacturing specifications and mission requirements and objectives. The weights of the fuselage, wing, and empennage were estimated from a data base that was compiled from Aeroworld designs of the previous two years . After specifying the wing size of 9.65 ft^2, its weight was determined based on an average of 1.55 oz/ft^2. Similarly, the fuselage weight was based on the desired fuselage volume of 1200 in^3, and a calculated average of 0.0075 oz/in^3 from the data base. One major difficulty that was encountered when weight estimates were made in this manner was the lack of a data base for the weights of joined wing aircraft. Because the preliminary weight estimates were based on planes with conventional configurations, the actual weight of a joined wing model would not necessarily fall within the range of previous designs.

In order to minimize the aircraft weight it was useful to quantify the contribution each component made to the total aircraft weight. Figure 6.1 illustrates the percentage of total weight for each component.

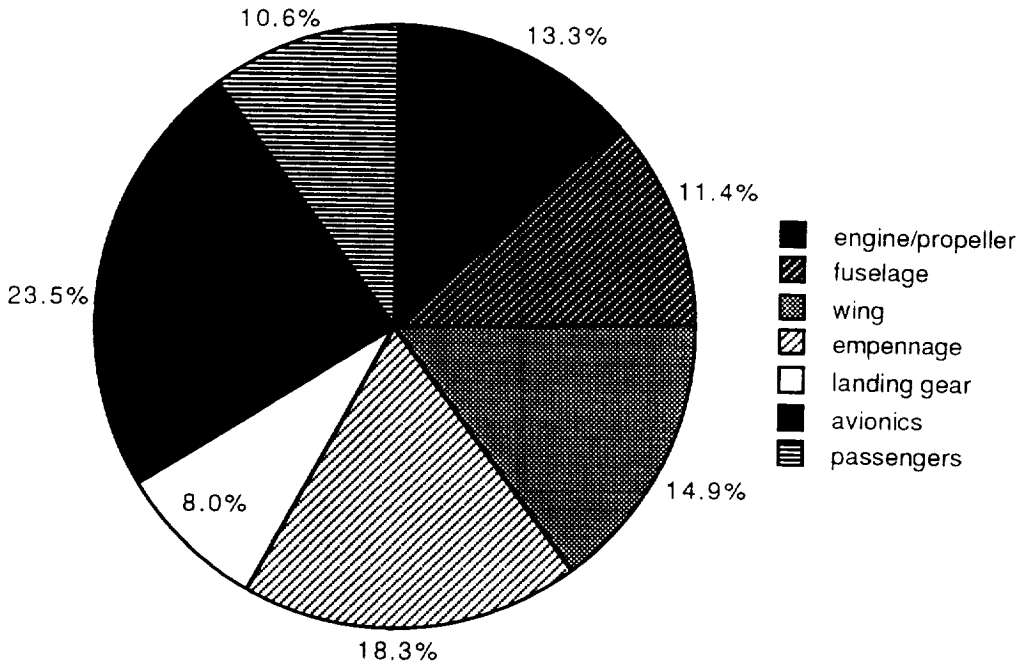

Figure 6.1 Weight Percentages for Each Component

One characteristic of this graph which stands out over a conventional design is the large weight fraction of the horizontal tail. Also, the component which incurs the largest weight percentage is the avionics, which will be a critical factor in determining the center of gravity location.

The specific location of the center of gravity was driven by stability and control design requirements. In order to place the c.g. of the aircraft 27.8 inches behind the nose as stability requirements dictated, the avionics pack containing the servos, speed controller, and batteries was manipulated. Using a Microsoft Excel spreadsheet, the exact location of the avionics pack was determined according to the required location of the c.g.. The location of the avionics pack determined the number of rows of passengers that needed to be placed in the fore and aft comparments. The results of this spreadsheet, including the

locations for each component's c.g., the aircraft c.g., and the movement of the c.g. between full and empty configurations are listed in Table 6.2. For further clarification, Figure 6.2 shows a schematic of the the location and relative magnitude of each weight component.

Along with locating the c.g. at a specific point for stability and control purposes, it was also necessary to minimize the movement of the c.g. which occurs between maximum capacity loading and an empty aircraft. Because the plane must be able to fly empty or fully loaded, it is critical to maintain a relatively stable center of gravity for control purposes. For this reason, the c.g. of the *Diamondback*, only moves forward 0.99 inches when all of the passengers are removed from the aircraft. This allows the plane to maintain stability and control whether it flies full or empty.

Component		c.g. (in		Weight (oz)		
	X-loc	Y-loc	Z-loc			
propeller	0	0	2	0.614		
engine	2	0	1.25	11.05		
fuselage	33.5	2.25	1.25	10		
wings	20.5	33.25	6.3	13		
tail (v)	60	0	10.25	3		
tail (h)	51.5	33.25	17	13		
front gear	25.5	5	-5	4.67		
rear gear	62	0	-2	2.33		
avionics tray	17.5	2.25	1.5	20.56		
front passeng.	11.13	2.25	1.25	1.45	Wfull	W emp
rear passeng.	40.88	2.25	1.25	7.79	5.47 lbs	4.89 lbs
	Fully Loaded				Empty	
Xcg	Ycg		Zcg	Xcg	Ycg	Zcg
27.8 in	0 in		4.3 in	26.8in	0 in	4.7 in
c,g travel=0.99 in						

Table 6.2 Component Weights and C.G., and Travel of Aircraft C.G.

The coordinate system that was utilized for Table 6.2 was:

x = 0 in – nose of fuselage x = 67 in – rear of fuselage

z = 0 in – base of fuselage z = 2 in – top of fuselage

Note: All weights are in ounces.

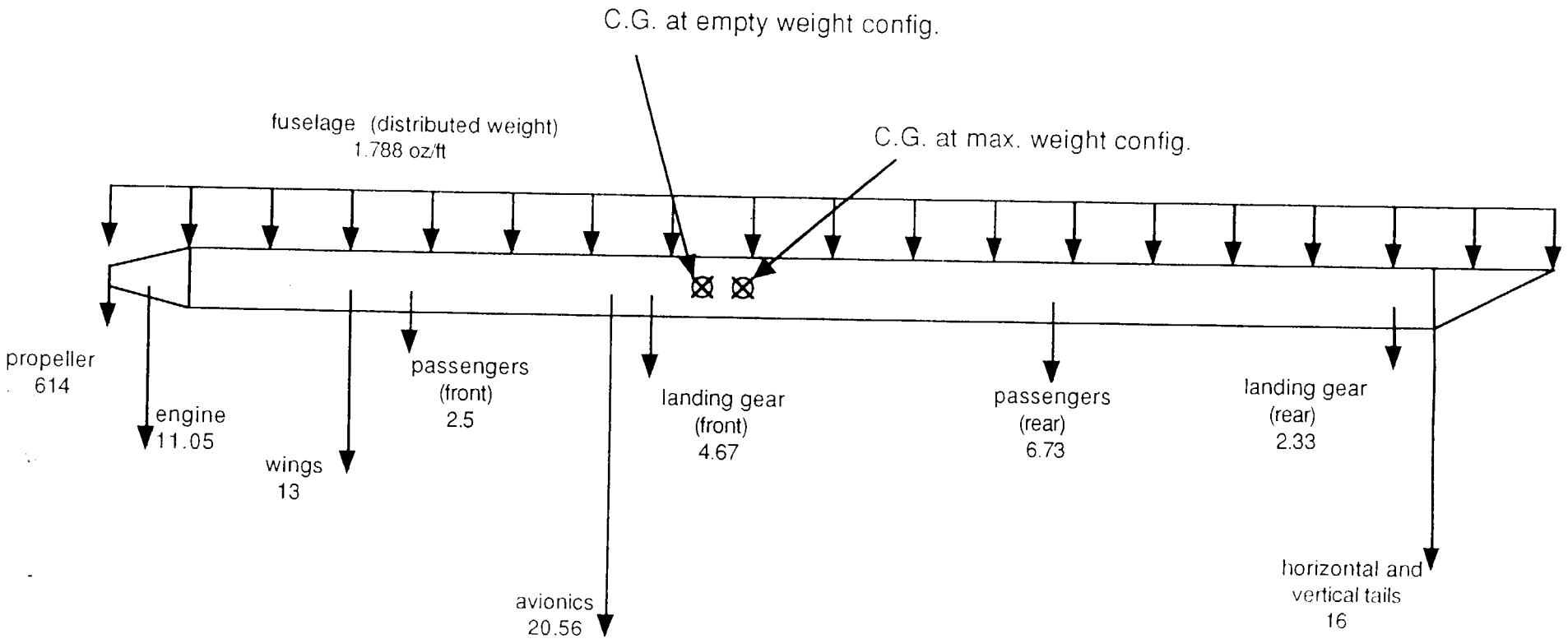

Figure 6.2: Weight Placement Diagram

7. STABILITY AND CONTROL

7.1 System Requirements

Several stability and control requirements must be met to successfully operate an aircraft. For the *Diamondback*, the following requirements were set:

- Maintain steady, level flight with minimal pilot load.
- Longitudinal static stability must be achieved with a static margin > 20% c.
- Lateral stability must be achieved with dihedral.
- Directional stability must be achieved with the vertical tail.
- Pitch control provided with elevator and must be able to trim at C_{Lmax}.
- Must execute a steady, level 60-ft-radius turn at cruise to successfully navigate in Aeroworld.
- Turning achieved with rudder deflection (sideslip) and dihedral.

7.2 Longitudinal Stability

The longitudinal stability of an aircraft is quantified though a parameter termed the static margin. The static margin (S.M.) is a measure of the change in pitching moment due to a change in aircraft total lift and is defined as:

$$\text{S.M.} = -\frac{dC_M}{dC_L} = \frac{X_{np}}{c} - \frac{X_{cg}}{c}$$

For this class of RPV a static margin of 20% c is desirable to provide adequate stability for the pilot. This value is significantly greater than the 5% c – 10% c standard for conventional designs due to the fact that the RC pilot has limited visual cues and a slower response time, thus requiring greater stability.

The static margin reflects that an increase in angle of attack (α) will bring about an increase in lift ($\Delta C_L = dC_L/d\alpha \; \Delta\alpha$) acting at the aircraft's neutral point (X_{np}). To achieve static stability, the change in moment produced must be negative (nose down) to oppose the increase in α and bring the aircraft back to its original α. This is attained if the n.p. is aft of the c.g., and thus the magnitude of the change in moment is equal to the change in lift multiplied by the moment arm ($X_{np} - X_{cg}$). When the position of the

n.p. and c.g. coincide, the aircraft is neutrally stable and this represents the most aft position that the c.g. may have and still satisfy static stability.

For the *Diamondback*, the S.M. at cruise is 24% c. Unlike conventional designs, the S.M. is not constant and increases with α. This aspect will be discussed later. With X_{cg} = 22.8 in behind the wing apex, this reveals the neutral point position is at 25.7 in behind the wing apex.

Several complications arise in the stability and control analysis of the joined-wing configuration. Factors which affect these calculations are:

- Wing-Tail Interference. Unlike conventional designs where the wing and tail are separated by a number of chord lengths, the joined wing brings the wing and tail in close proximity, thus significantly increasing the aerodynamic interference between the surfaces.
- Sweep. The sweep of the wing and tail complicate the calculation of the positions of their respective aerodynamic centers. These locations are needed to calculate their moment arms from the c.g..
- T-Tail. Because the joined wing projects a diamond shape in both the front and plan views and because of the dihedral needed in the wing, the tail must be mounted atop the vertical tail. Thus, the drag from the tail becomes significant in the moment calculations due to its vertical moment arm to the c.g.. The Diamondback is even more sensitive to this since the tail area is as large as the wing area and thus produces a significant drag.
- C.G. location. The centers of gravity of the wing and the horizontal tail both lie above the fuselage, bringing the aircraft c.g. above the fuselage centerline. As a result, the propulsion and both the tail and wing drag provide a nose-up moment, while the fuselage drag provides a nose-down moment.

These complications required that new tools be developed to determine the stability and control characteristics of the *Diamondback* and define its final configuration. The method and computer codes used to define the configuration are provided in Appendix C.1 and Appendix E.

For this design, the wing and tail spans were set equal as were the wing and tail sweeps to ease the analysis. With a fixed fuselage length, these parameters constrained the design. In fact, the neutral point was nearly set by this configuration, and in order to achieve the correct static margin, the c.g. had to be placed correctly. A weight analysis concluded that it should not be difficult to locate the c.g. roughly 24 in. from the wing apex, the distance needed to achieve the desired static margin of approximately 20% c. Thus, the c.g. location became a dependent variable as long as it did not deviate more than a few inches from this location.

To assist in the design of the tail, the following plot was made with LinAir data to assess the effect of the tail incidence angle on C_L, C_D, C_M, L/D, and S.M.. Appendix C.1 outlines the role that this plot played in the design and illuminates critical sensitivities of the configuration. Figure 7.1 graphically demonstrates that as the tail incidence increases the nose-up moment increases, the lift decreases, and the lift-drag ratio decreases.

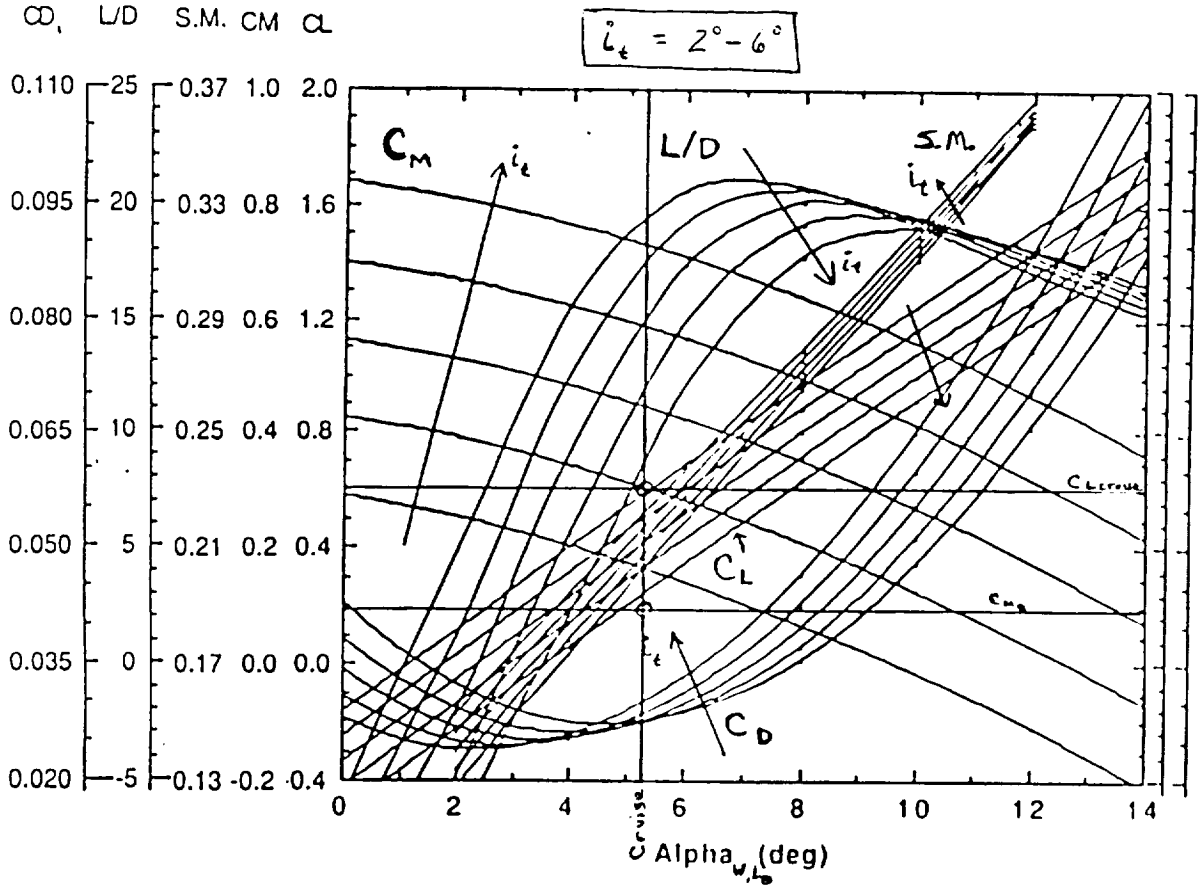

Figure 7.1 Effect of Incidence Angle

The final design was fixed with $i_t = 1.6°$ and $\alpha_{W,L_0} = 5.2°$ ($\alpha_{FRL} = 0$) giving the *Diamondback* a $C_L = 0.6$, C_M (including C_{M_0}) = 0, and S.M. = 0.24% c.

Horizontal Tail Area:	S_h	=	9.65 ft^2
Horizontal Tail Aspect Ratio:	AR_t	=	9.65
Length to Horizontal Tail:	l_t	≈	24 in
Tail incidence to Wing Zero-Lift Line (+ nose down):	i_t	=	1.6°
Incidence to Fuselage Ref. Line (+ nose up):	$i_{t,FRL}$	=	3.6°
Static Margin (cruise):	S.M.	=	24% c
Design C.G. (behind wing apex)	X_{cg}	=	22.8 in
C.G. Travel			21.6 - 23.0 in

Table 7.1 Horizontal Tail Design

This analysis neglected the contribution of the fuselage and the propulsion system to the static margin. Reference 7.1 provides a method of estimating the fuselage contribution to C_M (pp. 49-51), but due to the unique nature of the configuration, this method was not utilized since it assumes a standard configuration. These omissions from the analysis are unknowns and will probably decrease the static margin due primarily to the fact that the fuselage is usually destabilizing. The projected moment coefficient curves are provided in Figures 7.2 and 7.3.

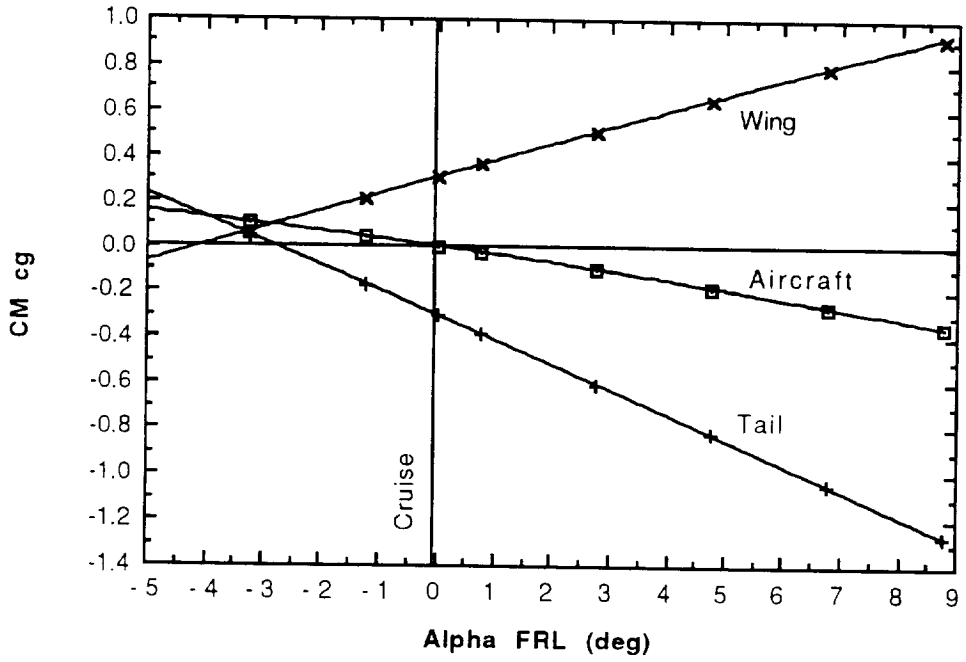

Figure 7.2 Coefficient of Moment vs Alpha

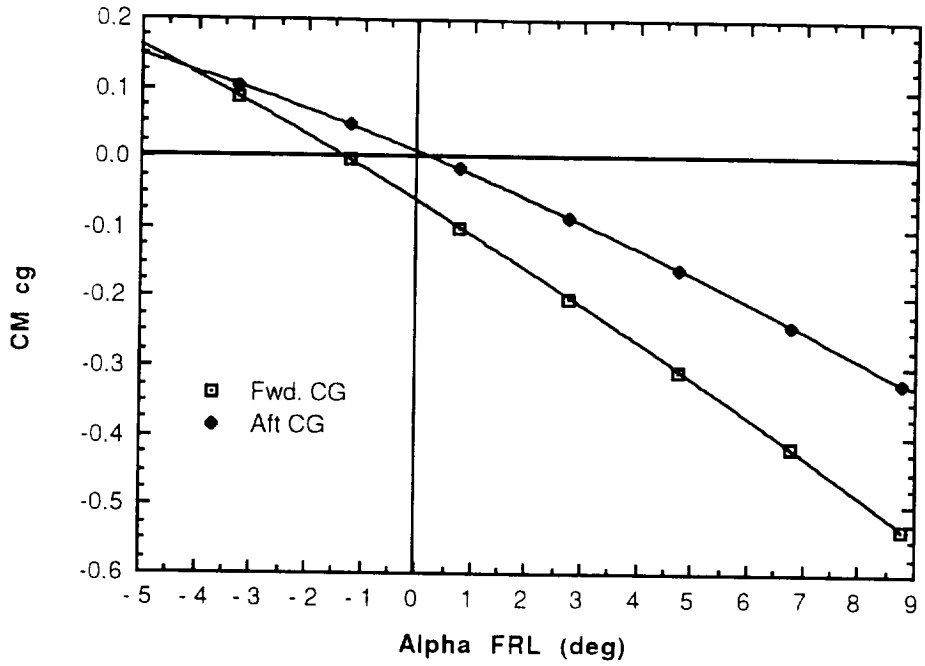

Figure 7.3 Coefficient of Moment vs Alpha for Most Forward and Aft C.G.

7.2.1 Change in Static Margin

As noted in Section 7.2, the static margin (S.M. = $-dC_M/dC_L$) changes as a function of angle of attack. This result, though unexpected, is evidenced in the data from LinAir. The data clearly show an increase in S.M. as the angle of attack increases. Thus the aircraft is more stable at higher angles of attack. Figure 7.4 documents this phenomena.

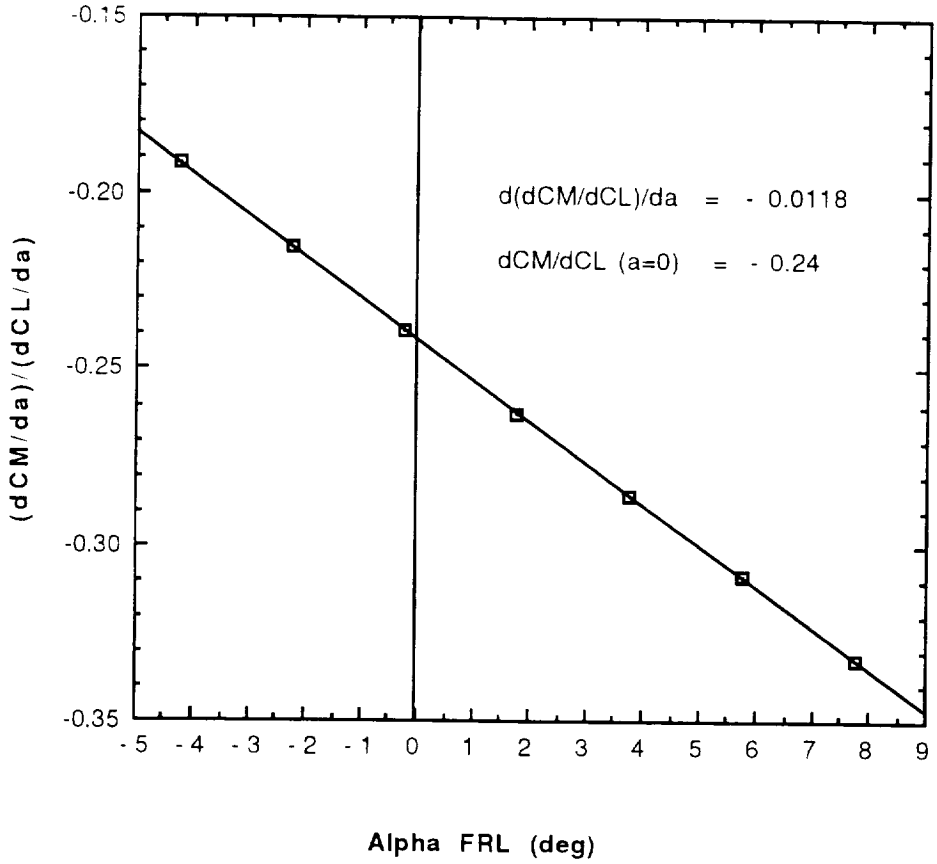

Figure 7.4 Static Margin Movement

It was initially believed that the span loading was changing with the angle of attack, and Figure 7.5 shows the span loading at cruise and near stall for the configuration. The lift distribution has been normalized such that the average C_l is unity.

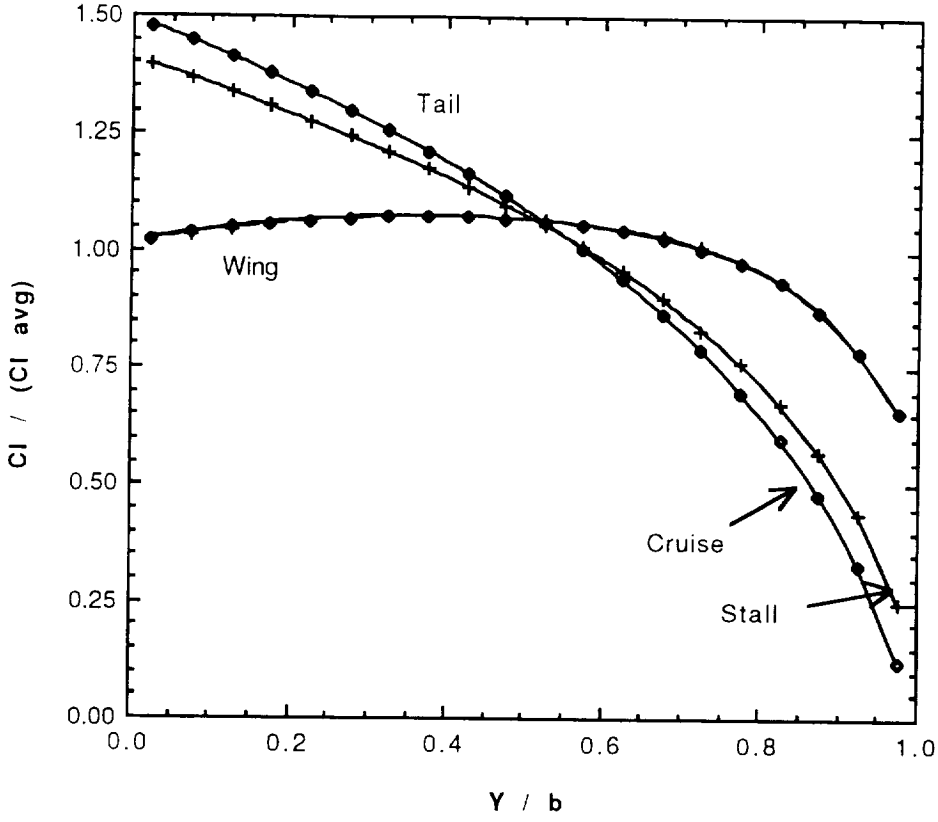

Figure 7.5 Wing and Tail Span Loading

As can be seen from the plot, the wing lift distribution changes negligibly, though the tail center of pressure moves slightly outboard as the angle of attack increases to the stall angle. This, however, should decrease the tail moment arm since the tail is swept forward and produce a less negative moment contribution from the tail. Thus this plot suggests the static margin should decrease with an increase in alpha.

No acceptable explanation of the increase in S.M. with alpha has been determined. Both the wing and the tail contribution to the moment have $dC_M^2/d\alpha^2 < 0$ so that the curves are slightly concave down. Thus both contribute to this increase in static margin with angle of attack (or, alternately, both move the aircraft neutral point aft).

A significant risk in this design is that it has had to greatly rely on data obtained from LinAir to establish the configuration. The non-linearity in $C_{M\alpha}$ is not surprising in light of the aerodynamic coupling of the wing and tail, but it is unclear whether or not it is an accurate depiction of the real aircraft response.

7.3 Longitudinal Control

The longitudinal control for the *Diamondback* is obtained using an elevator located on the inboard portion of the tail. This control device will allow for the pitch control needed to fly at all desired angles of attack, to rotate for take-off, to climb and descend, and to flair at landing. The elevator was designed to allow the *Diamondback* to trim at stall at the design c.g. (i.e. the fully loaded c.g.) with an elevator deflection of -15°. The maximum elevator deflection, however, is ± 20°, allowing the aircraft to trim at stall when the c.g. moves forward of the design point by 1.2 inches ($X_{cg,forw}$ = 26.6 in. behind the nose = 21.6 in behind the wing apex). Without payload, the c.g. moves only 1.0 inches forward of the fully loaded c.g. position, thus the aircraft can trim at stall at its empty weight. However, Figure 7.6 demonstrates that if the *Diamondback* is loaded from the front, the c.g. will move ahead of the forward limit and the aircraft will not be able to trim at its stall angle. It is recommended, therefore, that the aircraft be loaded from the rear.

Appendix C.2 outlines the method used to obtain the elevator design and the final design variables are outlined below. Figure 7.7 presents the moment data for several elevator deflections for the design c.g.

S_e/S_t	=	0.042
c_e/c_t	=	0.012
$C_{M\,\delta e}$	=	0.021 deg^{-1}
$\delta_{e\,max}$	=	± 20°

Table 7.2 Elevator Design

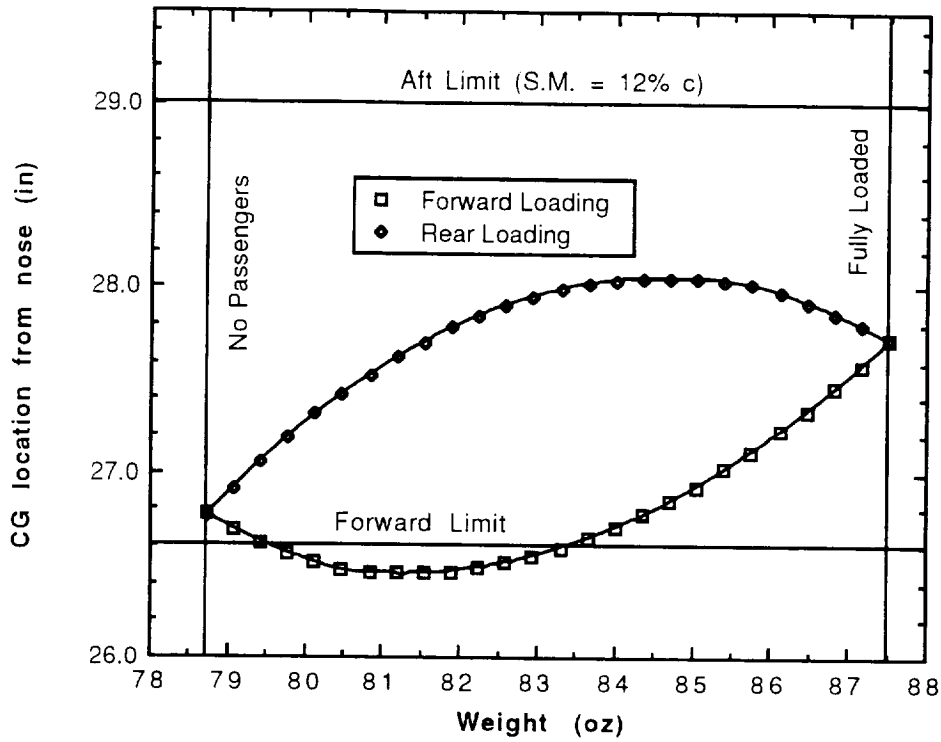

Figure 7.6 Weight Balance Diagram

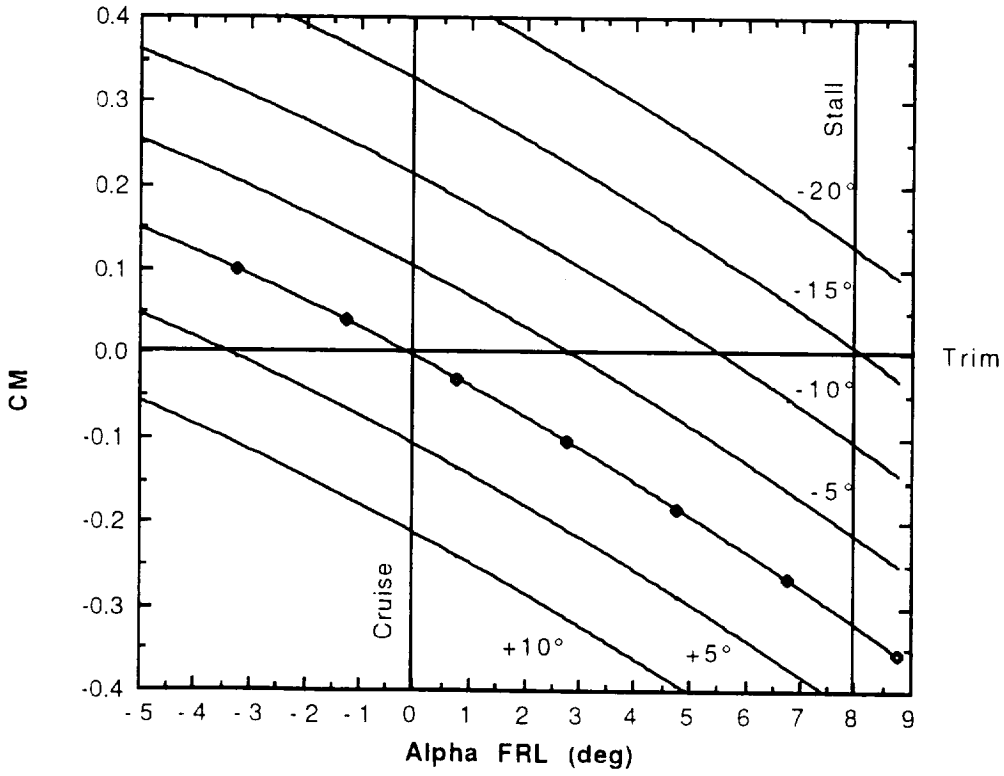

Figure 7.7 Moment Curve with Elevator Deflection

7.4 Lateral Stability

The airplane's lateral stability is provided by the wing dihedral. Reference 7.2 states that for a R/C, mid-wing aircraft utilizing rudder and dihedral for roll control, a $7° - 8°$ dihedral is recommended. Since the *Diamondback* has both wing dihedral (Γ_w) and tail anhedral ($\Gamma_t < 0$), an equivalent dihedral was defined as

$$\Gamma_{eff} = \Gamma_w + \Gamma_t \frac{S_t}{S_w}$$

such that the aircraft would act as one with a wing of area S_w and a dihedral of Γ_{eff}. This approximation should be a conservative estimate since the wing carries a majority of the lift and the roll moment should actually exceed that predicted by the effective dihedral. The effective dihedral was set at 8° early in the design in order to calculate the aircraft geometry for LinAir, and the following analysis determines the effectiveness of this value.

The roll stability coefficient ($C_{l\beta}$) due to the dihedral was approximated with the following relation,

$$C_{l\beta} = -\frac{y_{cp}}{b} C_{L\alpha} \Gamma_{eff}$$

Again Γ_{eff} is a conservative approximation because the location of the wing c.p. is more outboard of the tail c.p. thus having a longer moment arm, y_{cp} (see Figure 7.5). $C_{L\alpha}$ is the lift curve slope of the wing and tail and utilizing an approximation for the c.p. of the wing, $C_{l\beta} = -0.0087\ deg^{-1}$.

In addition to the wing and tail contribution, the position of the wing on the fuselage affects the roll stability. However, since the fuselage is only 2.5 in. high while the wing thickness is 1.4 in, this is assumed to be negligible. Nevertheless, the wing will be a low wing to capitalize on any additional roll stability provided by this configuration. The horizontal tail is a high tail and it is expected that it placement will contribute to an undetermined amount of roll instability. The influence should be small and it has been neglected.

In sideslip, both the wing and tail will experience a change in angle of attack due to the dihedral ($\Delta\alpha = \tan^{-1}(\tan \Gamma \sin \beta) \approx \Gamma \beta$). The wing, however, will experience a much larger $\Delta\alpha$ because the magnitude of its dihedral is greater than that of the tail. Care must be exercised not to stall the wing in a turn by over sideslipping the aircraft and increasing the wing α above stall. At $\beta = 22°$, $\Delta\alpha_w = 3.7°$. The wing stalls at $\alpha_{FRL} = 8°$, so that in cruise ($\alpha_{FRL} = 0$) the wing is far from its stall angle even with a 22° sideslip during a turn. As will be shown in Section 7.6, this value for the sideslip is the maximum attainable by the *Diamondback*.

Γ_w	=	9.9°
Γ_t	=	-1.9°
Γ_{eff}	=	8.0°
$C_{l\beta}$	=	-8.7×10^{-3} deg^{-1}

Table 7.3 Lateral Stability

7.5 Directional Stability

The directional stability for the joined wing is difficult to estimate with conventional methods. Examining the side view of the aircraft, it is evident that the wing projects a large area into the x-z plane. Because the wing is ahead of the c.g. this will yield a destabilizing influence in yaw. The tail should be a stabilizing influence in yaw, though Reference 7.3 states it only is 50% effective due to the "vane" effect of the vertical tail (p. 172). With the tools available in this design, the side-force on the wing and horizontal tail due to yaw was not quantified. Appendix C.3 provides the methods used to obtain the breakdown of the directional stability coefficient in Table 7.4 below.

	$C_{n\beta}$ (deg $^{-1}$)
Vertical Tail	0.0015
Winglets	0.0003
Wing & Fuselage	-0.0007
Aircraft	0.0011

Table 7.4 Directional Stability Component Breakdown

In determining $C_{n\beta}$, conservative estimates of $C_{L\alpha}$ for the fin and winglets were utilized and it is probable that these surfaces will contribute more directional stability than predicted. However, the effect of the wing and fuselage on $C_{n\beta}$ has a great degree of uncertainty associated with it and it may be more destabilizing than predicted. To effectively analyze this configuration with its unique characteristics, some aerodynamic modeling tool is needed to analyze asymmetric flow conditions or a flight test must be performed.

Vertical Tail Area:	S_V	=	1.08 ft^2
Vertical Tail Aspect Ratio:	AR_V	=	3.1
Vertical Tail height		=	15.5 in
Vertical Tail chord	c_V	=	10.0 in
Length to Horizontal Tail:	l_V	=	27.9 in
Vertical Tail Volume:	V_V	=	0.026

Table 7.5 Vertical Tail Design

7.6 Lateral and Directional Control

Both lateral and directional control are provided by the rudder. The rudder directly controls the yaw angle of the *Diamondback*, and indirectly controls the roll angle through lateral-directional coupling and dihedral. This control is essential for the successful operation of the aircraft in Aeroworld.

Maximum rudder deflections ($\delta_{r\,max}$) of ±20° are common for this class of vehicle and this deflection was taken to be the maximum deflection for the *Diamondback*. The yaw coefficient was determined by

$$C_n = C_{n\beta}\,\beta + C_{n\,\delta r}\,\delta r$$

and at steady state where $C_n = 0$, the sideslip caused by the rudder was approximated as $\beta \approx C_{n\,\delta r}/C_{n\beta}\ \delta r$. Knowing $C_{n\beta}$ from Section 7.5, the sideslip was found as a function of the rudder control effectiveness ($C_{n\,\delta r}$) and the rudder deflection. Additionally,

$$C_{n\,\delta r} = -\eta\ V_v\ C_{L\alpha v}\ \tau$$

and assuming $\eta \approx 1$, $C_{n\,\delta r}$ is a function of the rudder effectiveness factor (τ). The rudder effectiveness can be found as a function of the ratio of rudder area to the fin area (S_r/S_v) in Reference 7.1, p. 60. Thus the sideslip was found as a function of $\delta_{r\,max}$ and the rudder area.

Knowing the sideslip, the roll moment may be calculated

$$C_l = C_{l\beta}\,\beta + C_{l\,\delta r}\,\delta r = C_{l\beta}\,\beta + \frac{z_v\ S_v}{b\ S}\,\tau\ C_{L\alpha v}\ \delta r$$

For the design, $S_r/S_v = 0.63$ ($\tau = 0.70$) yielding

S_r/S_v	=	0.63
c_r	=	7 in
$C_{n\,\delta r}$	=	$-0.0012\ deg^{-1}$
$C_{l\,\delta r}$	=	$0.0029\ deg^{-1}$

Table 7.6 Rudder Design

8. PERFORMANCE ESTIMATION

8.1 Initial Considerations

The initial performance requirements were defined by the need to fulfill the target market demand and to be compatable with the existing airspace and airports in Aeroworld. The only performance requirements set forth by the management of AE441, Inc. in compliance with the geographical restrictions inherent in Aeroworld include that the technology demonstrator must be able to takeoff from the ground under its own power, land effectively, and perform a sustained level turn with a maximum radius of 60 feet at a speed of 25 ft/s. The most pressing requirement was imposed by the size of the airports in Aeroworld. The standard airport runway length in Aeroworld is 40 feet. However, three of the airports have significantly shorter runways than this. The short runways at airports O and C, of 20 and 24 feet respectively, are purposely excluded from consideration since they place considerable demands on the aircraft servicing them and the passenger loads to and from these locations are not very significant. By process of elimination, the next shortest runway is at airport B and is 32 feet long. Naturally, the takeoff distance objective of our aircraft became 32 feet and is a reasonable and feasible design goal.

8.2 Takeoff and Landing Estimates

The Takeoff Performance program included in Appendix E was used exclusively to analyze the takeoff performance of the *Diamondback*.. The input values of this program included the aircraft weight, reference area, lift and drag characteristics, battery and motor data, as well as propeller characteristics. The important results of the program calculations include the take-off velocity, take-off distance, static thrust, static current draw, and the thrust at takeoff. A copy of the input and output files of this program for the *Diamondback* are included in Appendix E.

The selection of the propulsion system was based on its ability to achieve the takeoff distance objective of 32 feet. Recall figure 5.2 which demonstrates that an 11 cell battery pack providing 13.2 volts is not sufficient as it drives the system to a takeoff distance of about 33 feet. Therefore, a 12 cell battery pack was chosen. Using the selected propulsion system including the Astro-15 motor, the Zinger 11-7 propeller, and a 14.4 volt battery pack, the takeoff distance is computed to be 25.4 feet which is well below the objective of 32 feet. This system is thus capable of operating at airport B and the other unrestricted cities in Aeroworld.

The estimate of the landing distance was obtained using an equation found in Reference 8.1 and is shown below.

$$Xland = \frac{1.69\ W^2}{g\ \rho S\ Clmax\ [D+\mu(W-L)]}$$

Using this equation, the landing distance was found to be about 53.5 feet by estimating the coefficient of rolling friction to be .2 and Clmax to be 1.5.

8.3 Range and Endurance Estimates

The range and endurance calculations were done using an electric motor performance iteration scheme adapted to a TKSolver program and is included in Appendix E. This program calculates parameters such as the power required, power available, range, endurance, RPM, current, and the voltage when given input values of the velocity, weight, motor constants, resistances, efficiencies, and the battery capacity. It was found that at the cruise condition where the velocity is equal to 28 ft/s and at the maximum payload capacity of 100 passengers which corresponds to WMTO=5.47 lbs, the range obtained was about 18,300 feet and

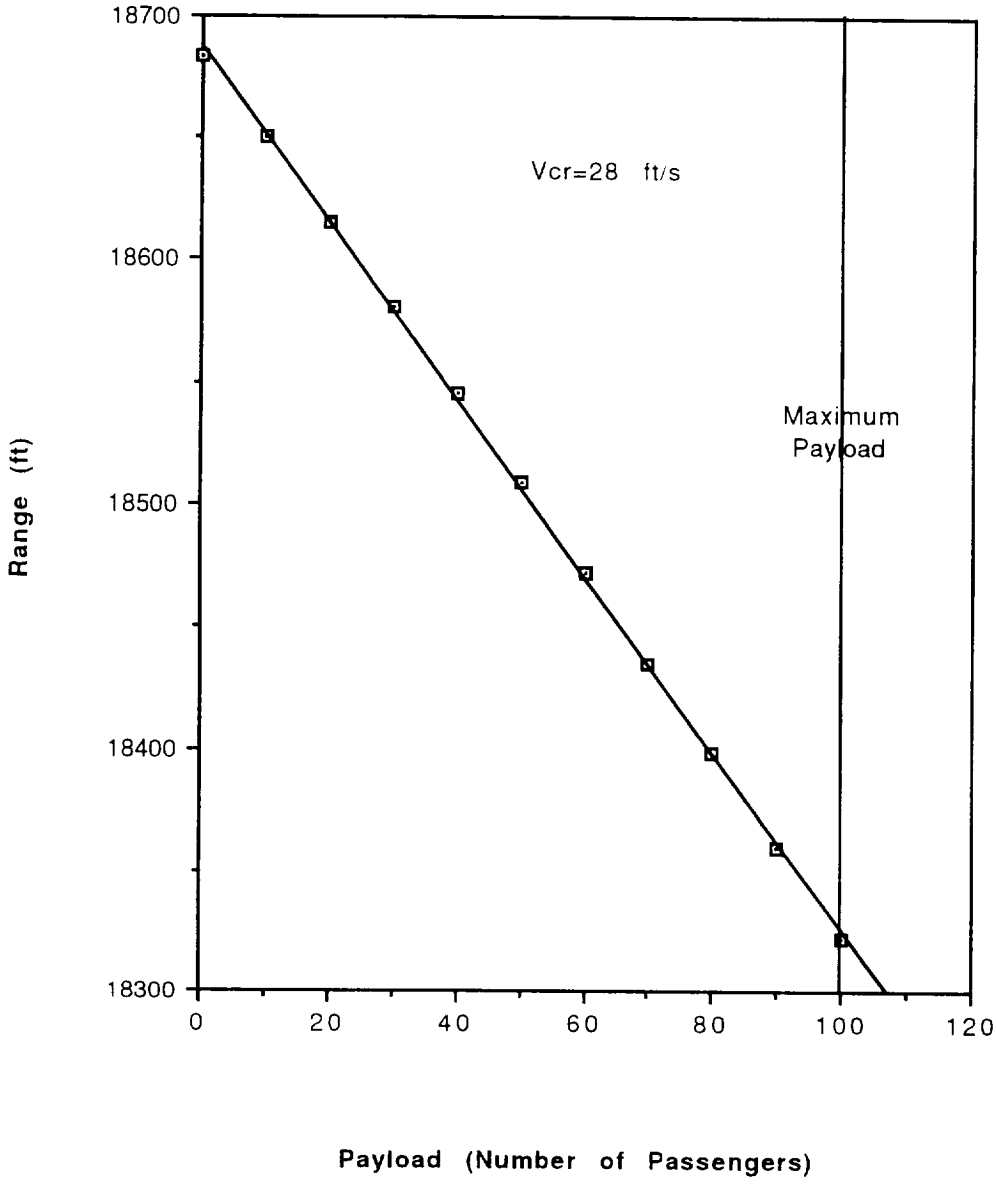

Figure 8.1 Range-Payload Diagram for a Cruise Velocity of 28 ft/s

the endurance was found to be about 10.9 minutes. However, at the minimum payload capacity of WMTO=4.92 lbs and at the cruise velocity, the range increases to about 18,700 feet and the endurance increases to about 11.1 minutes. The reasons why the effective range is about 5000 feet greater than the design range was discussed previously in section 5.4. A graph of the range verses the number of passengers is shown in figure 8.1. It shows a linear relationship and that the range increases as the number of passengers and thus the weight decreases.

Other important performance parameters are the maximum ranges at maximum and minimum takeoff weights and the maximum endurance. The TK Solver program found in Appendix E was used to find them. It calculated each of these parameters through a series of velocities extending from the stall velocity of about 18 ft/s through the maximum velocity of about 50 ft/s which is calculated in the next section. The maximum range at the maximum takeoff weight was calculated to be about 18,330 feet and occurs at a velocity of 26 ft/s. At the minimum takeoff weight the maximum range was found to be about 18,820 feet and also occurs at 26 ft/s. Likewise, the maximum endurance was found to be about 13.2 minutes and occurs at a flight speed of about 22 ft/s. It was observed that the endurance would increase at lower velocities, but to fly any slower than 22 ft/s is too close to stall and thus it would be unreasonable to expect the aircraft to fly in this regime. Therefore, the maximum endurance was calculated such that the velocity was no lower than about 1.2 times the stall velocity.

8.4 Power Estimates and Maximum Rate of Climb

The estimates of the power available and the power required at various values of the velocity were also calculated using the TKSolver program of Appendix E. The program calculated these power quantities through a range of

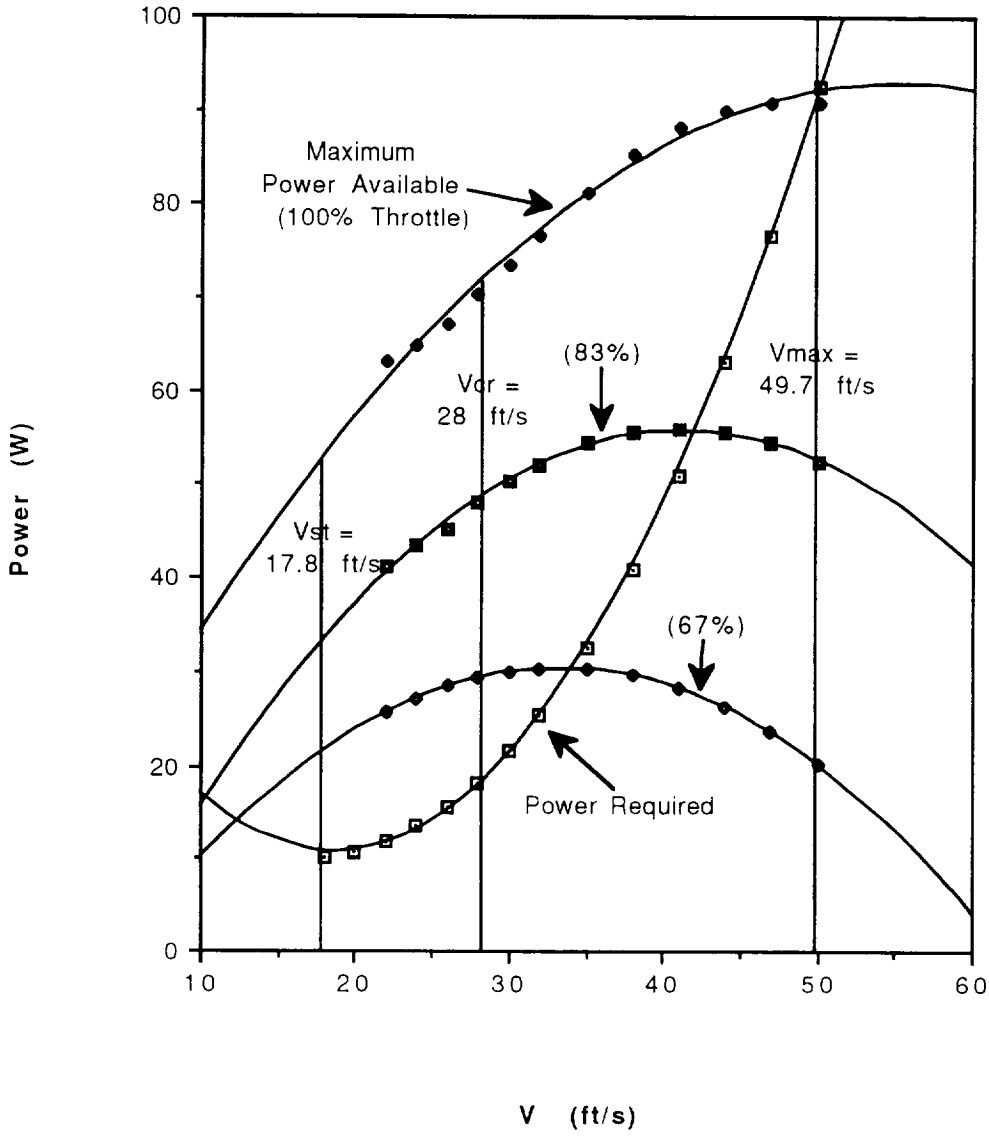

Figure 8.2 Power Available and Power Required versus Velocity

velocities extending from the stall velocity up until the power required exceeded the power available. A plot of the results is shown in figure 8.2.

From this graph it is seen that within the flight regime of our aircraft, the selected propulsion system has about 50 Watts of excess power for climbing or accelerating. More specifically, the rate of climb can be calculated from this data by the following equation and the results are shown below in figure 8.3.

ROC = (Power Available - Power Required)/Weight

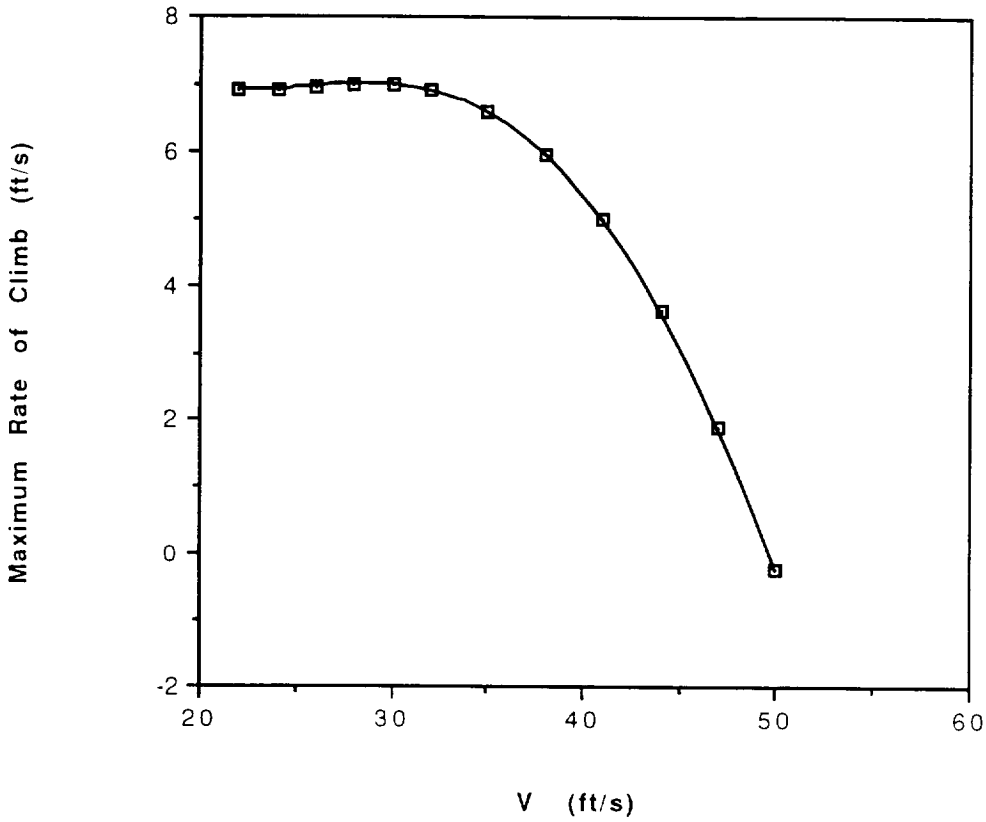

Figure 8.3 Maximum Rate of Climb verses Velocity

This graph demonstrates that the rate of climb is near the maximum throughout the proposed flight regime of this aircraft. The exact interpretation of this data is that the maximum rate of climb is the maximum vertical velocity that can be achieved at a

specified forward velocity. Another important aspect of this graph is that the point at which the rate of climb becomes zero dictates the maximum velocity at which the aircraft can fly. In our case, the *Diamondback* has a maximum velocity of 49.7 ft/s.

8.5 Turning and Gliding Performance

One of the primary performance requirements specified by the management of AE441, Inc. is that the technology demonstrator must be able to perform a steady level turn with a maximum radius of 60 feet. By analyzing simple force vectors in a turn, the turn radius was determined as a function of the velocity, bank angle, and the gravitational constant.

$$R = \frac{V^2}{g \tan \phi}$$

The bank angle, however, is a function of the load factor as shown.

$$\cos \phi = \frac{1}{n}$$

The maximum load factor allowed in a maneuver for the *Diamondback* has been set at about 1.35 by the structures expert. A graph of the turning radius as a function of the bank angle is shown in figure 8.4. This graph shows that to achieved a turn radius less than 60 feet while flying at 25 ft/s, the aircraft must bank at least 18 degrees. At the cruise velocity of 28 ft/s, the aircraft must bank at least 23 degrees. These turns occur at load factors of only 1.05 and 1.08, respectively. Therefore, the *Diamondback* is able to satisfy and far exceed the turn radius requirement of 60 feet because it can withstand a much greater load factor than is necessary as demonstrated by the results in figure 8.4.

In addition the gliding performance is an important parameter, especially on the landing approach. If the minimum glide angle is too large, then the aircraft is going to land hard and possibly sustain damage or injure passengers. A small minimum glide angle is obviously desired. The equation which yields the minimum glide angle is shown below.

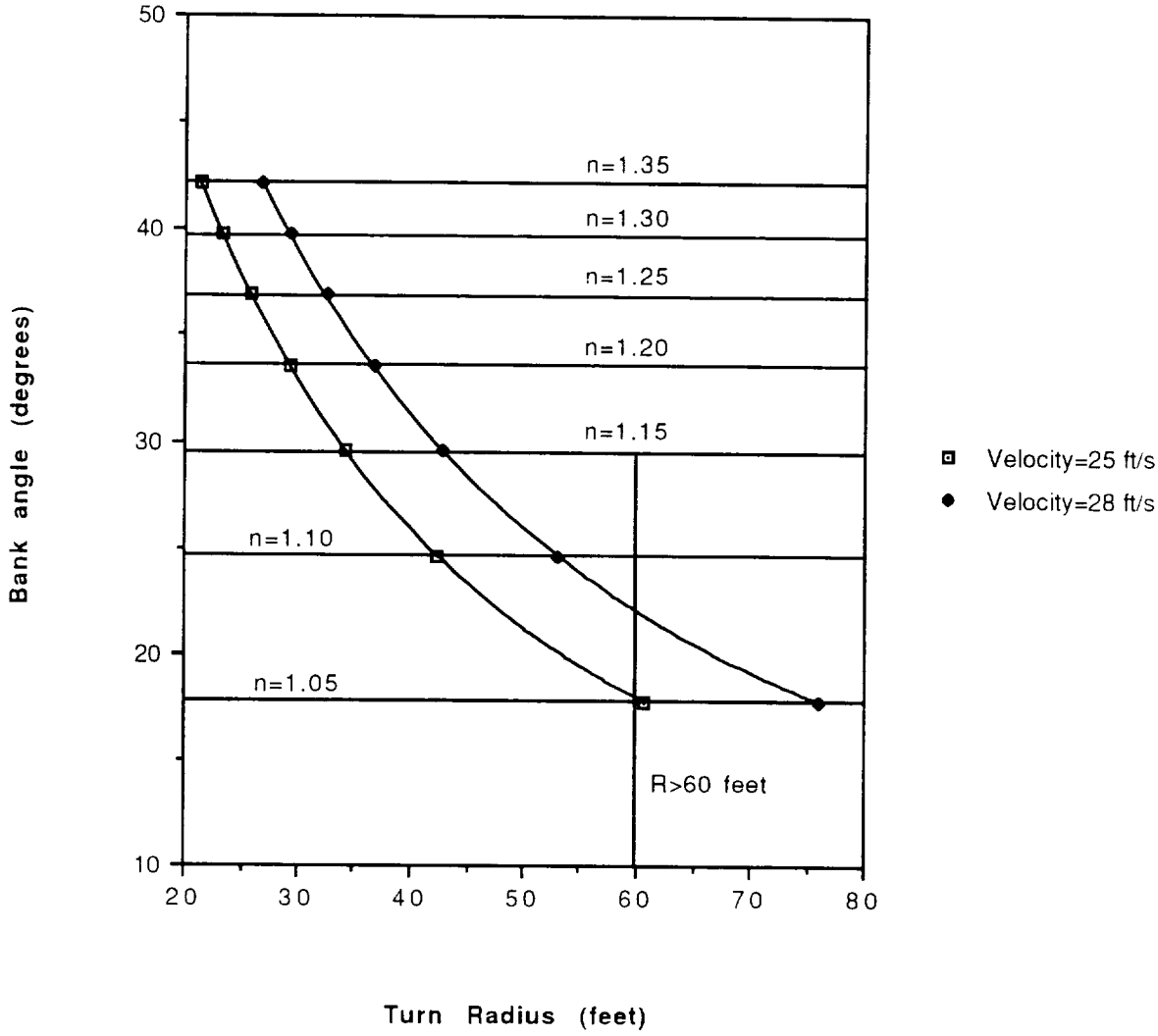

Figure 8.4 Turning Performance of the *Diamondback*

$$\gamma\text{min} = \arctan\left(\frac{1}{(L/D)\text{max}}\right)$$

For the Diamondback, the (L/D)max is about 14 which corresponds to a minimum glide angle of about 4.1 degrees.

9. Structural Design Detail

9.1 V-n Diagram

In order to examine the extremes that the aircraft structure could encounter while in flight, a velocity versus load diagram was constructed. The V-n diagram for maximum and minimum capacities shown in Figure 9.1 was constructed using the relationship:

$$n = 0.5*\rho*V^2*C_L*S/W$$

with $C_{Lmax} = 1.54$ and $C_{Lmin} = -0.25$.

The value for the positive yield load (n yield) was based upon the maximum load factor that would be generated during a turning maneuver. This is equivalent to the maximum load that could occur during the flight of the *Diamondback*, since there will be no gusts or wind shear in the testing facility, and the loads at take-off will be small because there will no rotation, only a slow ascent. Assuming that dihedral and rudder control can maintain a 60 foot radius turn at $V_{max} = 49.5$ ft/s, the load factor experienced would be equal to:

$$n = \sqrt{(V_{max}^2/gR)^2+1} = 1.65$$

In keeping with Aeroworld conventions, a factor of safety (F.S.) equal to 1.4 was utilized for the entire structure based on Aeroworld conventions and a high regard for passenger safety. Based on a F.S. = 1.4, the maximum load that can be sustained during flight without violating the facotor of safety is n = 1.35. When the required 60 foot turn is executed at $V_{cruise} = 28$ ft/s, the load factor of the plane is n = 1.08, which means that a load limit of n = 1.35 does not present any foreseeable restrictions.

A majority of the envelope that is shown in Figure 9.1 will not be utilized since it is predicted that the *Diamondback* will not exceed speeds of 35 ft/s while in operation. However, this diagram does provide a useful visual representation of the range of loadings that could be endured at various velocities.

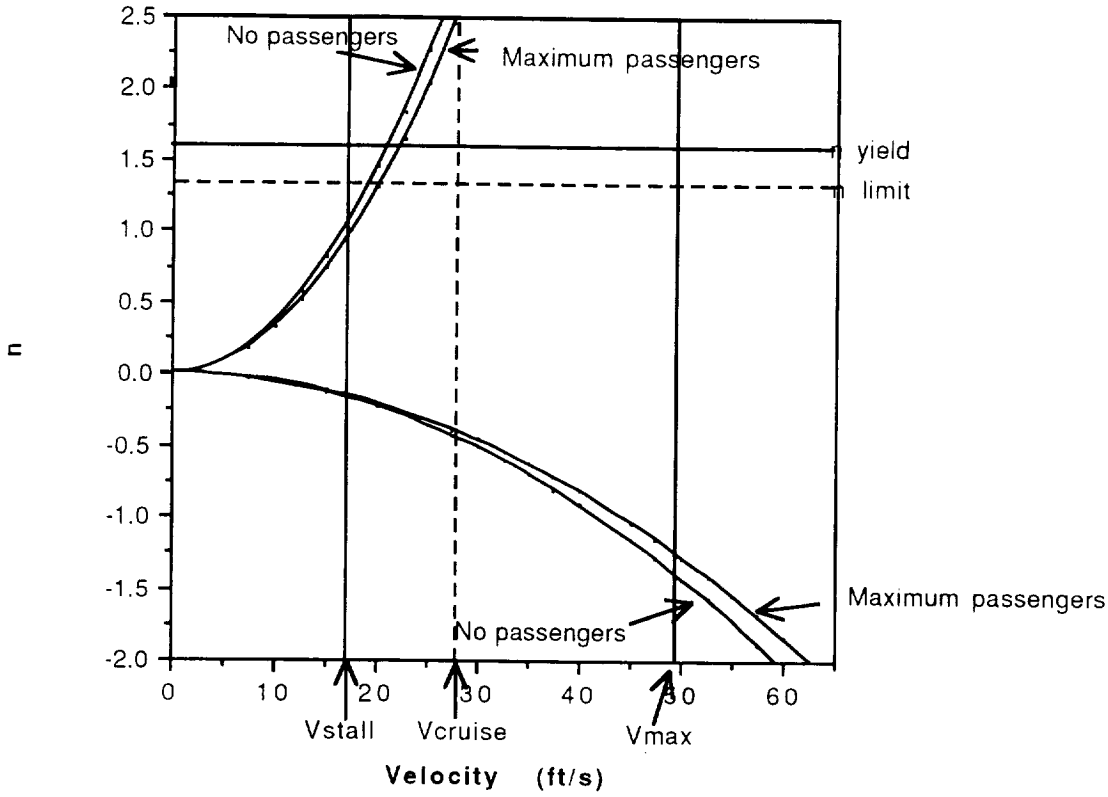

Figure 9.1: Velocity vs. Load Factor for Minimum and Maximum Capacities

9.1.2 Flight and Ground Loading

The loads encountered by the aircraft both while on the ground and while in flight were analyzed by modeling the fuselage of the aircraft as a beam which undergoes transverse loading. To analyze the in-flight loads encountered by the aircraft, it was assumed that the aircraft was at cruise. The cruise velocity of the *Diamondback* is 28 ft/s. At cruise, the lift is equal to the weight of the aircraft. From Figure 9.2, it can be seen that at cruise (C_L ~ .58) the wing is responsible for approximately 73% of the aircraft's total lift.

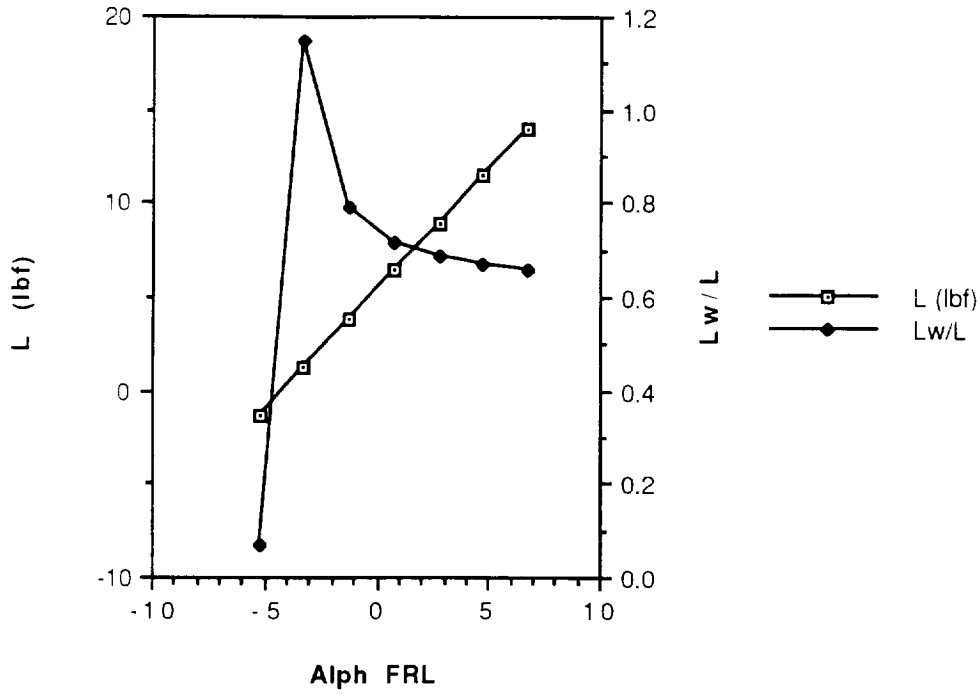

Figure 9.2 Wing / Tail Lift Distribution

Therefore, the wing is producing approximately 4 lbs of lift while the tail produces 1.47 lbs. From this information, it is possible to construct the shear and bending moment diagrams for the fuselage (Figures 9.3 and 9.4).

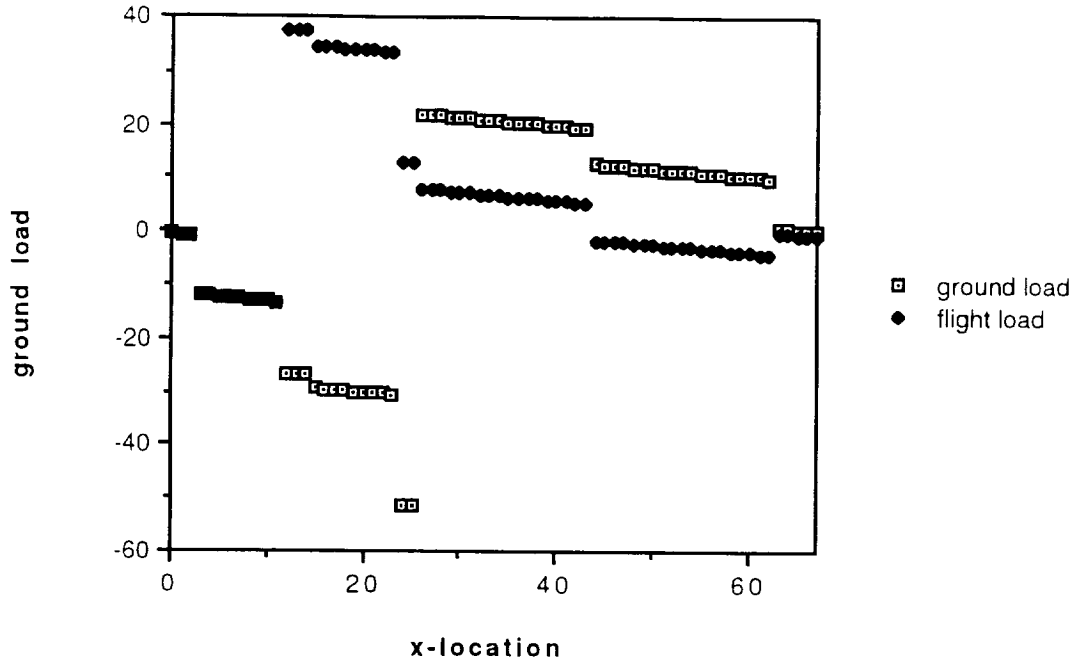

Figure 9.3 Fuselage Shear Diagram

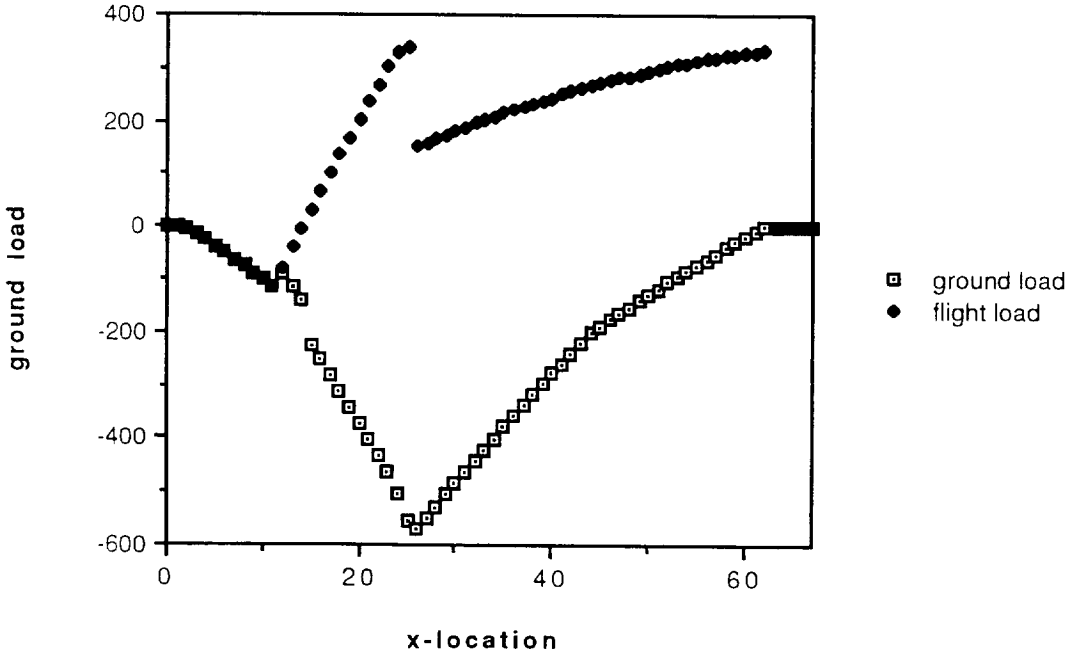

Figure 9.4 Fuselage Bending Moment Diagram

9.2 Structural Components

9.2.1 Fuselage Structure

The main fuselage of the aircraft is important to the design in that the fuselage serves many purposes. The most obvious purpose which the fuselage serves is to hold the equipment used in the aircraft as well as the passengers, or cargo. However, the fuselage also transmits loads from one part of the aircraft to another. The fuselage for this particular aircraft was designed keeping several key factors in mind. First, the fuselage had to be big enough to carry 100 passengers, 5 crew members and the electronic and propulsion systems required to fly the aircraft. Second, the fuselage had to be designed to withstand the loads which are encountered during take-off, flight and landing. A third driving factor in the design of the fuselage was drag minimization. Because the fuselage does not contribute much lift, its drag must be reduced as much as possible. With these three factors in mind, the fuselage dimensions were determined. The height, width and length of the fuselage were set at 2.5, 8.5 and 67 inches, respectively. These dimensions were influenced by the passenger volume requirements. A fourth factor which influenced our choice of fuselage shape was its ease of manufacturing. A rectangular configuration was chosen over a cylindrical one because the rectangular fuselage is much easier to build.

For the major load-carrying members of the fuselage, spruce will be used. Balsa will be used for the non-critical members of the fuselage. Balsa is extremely light, yet strong, and has adequate allowable stresses. The fuselage will then be entirely covered with monokote. In addition to covering the fuselage, this material will contribute stiffness and will lend to the overall strength of the fuselage. The fuselage will consist of four main spars positioned longitudinally. These spars will be supported and strengthened by smaller spars transversely positioned in a truss-like fashion. Since it appears that the side forces which the aircraft will encounter will not be as severe as the longitudinal forces, the top and bottom of the fuselage will not need as much support as

the sides. In addition to the smaller spars, other supports will be used internally to help maintain the integrity and shape of the fuselage. The firewall, in addition to serving as a place to mount the motor, will lend support to the fuselage. The wing carry-through structure will also indirectly serve to strengthen the fuselage. The firewall and the carry-through structure will help prevent folding in the y-z plane. An access hatch will be placed in the top of the fuselage which will enable easy installation and adjustment of the aircraft's avionics system. The fuselage will be tapered at the nose and at the rear of the aircraft to reduce drag. The same type of balsa spars will be used at these locations.

9.2.2 Wing Structure

The wing design for this particular concept presents some challenging problems and yet also results in structural benefits. Aside from its aerodynamic aspects, the joined wing concept results in increased wing strength and stability with a reduced wing weight, which helps to minimize the total weight of the aircraft. The wing and tail are joined at the tip, providing increased stiffness for both the wing and the tail. In this configuration, the wing tip and tail tip are both additionally constrained due to the wing/tail joint. This joint minimizes tip deflection and therefore reduces the stresses in the members. The joint also helps withstand any torsion incurred by the wing or tail. Any torsion incurred on the wing is counteracted by the tail, and vice versa.

The wing and tail "box" structures will consist of two spruce wing spars and balsa shear webs. The spars will be placed at .25c to reduce the torsion which would be caused if the spars were placed elsewhere. Spruce spars will run the span of thw ing connecting the upper and lower surfaces of the ribs. The shear webs will be used to connect the top and bottom spars. Full ribs will be used intermittently with partial ribs (approximately .4c). The partial ribs, or riblets, will be used to minimize the overall weight of the wing and to maintain the aerodynamic integrity of the leading edge. The

riblets will provide shape for the monokote skin covering and will extend back to the thickest part of the airfoil section where the airflow is most critical. The ribs and riblets will be placed approximately 3 inches apart to prevent sagging of the monokote and to increase the wing's effectiveness. The ribs will also be cored out where ever possible to reduce their weight.

9.3 Material Selection

The selection of the materials used for the construction of the *Diamondback* was again based on several important factors. The most important of these factors is that the materials must be able to withstand the loads encountered during normal and critical conditions. The weight is also an important factor to consider when selecting materials. The material used should be the lightest possible which will still withstand the maximum loads encountered during operation. Finally, economic considerations must also be taken into account. The selected material should be inexpensive in order to keep manufacturing costs down.

Although wood would seem to be the obvious choice of material, several other types of materials were considered. Metals are extremely strong but they they are usually heavy and expensive. The adverse effects of the weight and cost of metals outweigh the benefits obtained from their strength. A second type of material considered were composites. Composites are extremely lightweight and relatively strong, but tend to be extremely expensive. A third type of material considered was plastics. Plastics have relatively low weight and cost, but they are not very strong.

Material	Strength	Weight	Cost	Availability
Wood	good	excellent	good	good
Metal	excellent	poor	good	good
Composites	excellent	excellent	poor	poor
Plastics	poor	good	good	good
Ceramics	poor	poor	poor	poor

Table 9.1 Material Characteristics

In light of these facts, we determined that wood was the best material to use in the manufacturing of the *Diamondback*. Wood is relatively inexpensive, easily acquired and easy to manipulate with simple tools. Therefore, wood was chosen as the principle material for construction of the *Diamondback*.

Several different types of wood were considered. Balsa and spruce are the two types of wood most commonly used for these types of applications because of their high strength to weight ratio. Although balsa is not as strong as spruce, the greater amount of balsa necessary to compensate for this lack of strength is usually less than the spruce required for the same application. It is important, however, when using balsa, to make sure that no excessively large deflections occur that would cause instabilities for the plane while it was in flight. Below is an abbreviated listing of some of the materials considered and their properties (Table 9.2). Spruce was chosen for the main spar caps on both wings, and for the main load-bearing elements of the fuselage because of high values of allowable normal stress, in both tension and compression. Balsa was used for the noncritical parts of the fuselage and empenage structures, and the leading and trailing edge spars of the wings because of its low weight. For areas of high loads, such as the engine mount, landing gear mount, and the webbing near the root chord of the wing and tail, birch plywood was selected because of its high value of allowable shear stress. This plywood has a much higher modulus of elasticity and isotropic in-plane characteristics which are desirable for these areas.

The grain orientation of the material used must be taken into account. When an element is axially loaded, the shear force on a plane which is 45 degrees from the loaded axis will typically exceed the material shear stress before the compressive or tensile stresses are exceeded. While an isotropic material such as plywood will have a σ_{xx}, σ_{yy} and σ_{xy} which are related to the various surfaces of an element rotated in the x-y plane, the values of compression or tension for spruce are relative only to the grain orientation. Allowable stress values due to forces applied perpendicularly to the grain boundaries

are smaller than the allowable stress levels due to forces applied along grain boundaries. The maximum values of the tensile stresses of the materials were used in the analysis of the structures. This was done because the allowable tensile stresses are smaller than the allowable compressive stresses. In the event that the RPV were loaded in a negative sense, it would be as strong as it would be under normal flight loadings.

The final material selection was the skin covering. Monokote was the only material considered. This material not only covers the frame of the aircraft, but contributes to the strength of the frame and helps reduce skin friction drag.

Material	$\rho(lb/in^3)$	σ_{com}(psi)	σ_{ten}(psi)	σ_{xy}(psi)	E(psi)
Balsa	0.0058	600	400	200	65000
Spruce	0.016	9000	6200	750	1.3e6
Plywood	0.0231	2500	2500	2500	2.01e6
Monokote	0.125e-6	N.A.	25	25	

Table 9.2 Material Properties

9.4 Landing Gear

The geometry of the landing gear is illustrated in Figure 9.5. The *Diamondback* employs a tail-dragger configuration which will weigh less than a tricycle configuration, while providing an adequate amount of ground stability and control. Aluminum was chosen as the strut material because it is lightweight and its flexibility will help to absorb the impact of landing. Foam tires were chosen over air filled ones because they deformed more easily, which will also allow more of the impact to be absorbed.

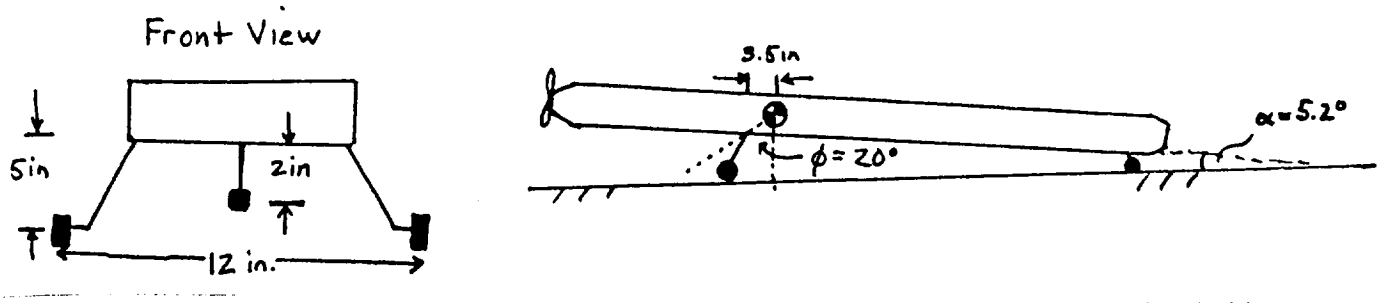

Figure 9.5 Configuration of the Landing Gear

The design of the landing gear for the *Diamondback* was based on the following considerations:

(1) Propeller clearance.

The propeller must provide propeller clearance during take-off and worst-case landing scenarios, and absorb landing impact. The Zinger 11-7 has an 11 inch diameter, so the landing gear must be able to provide 5.5 inches from the propeller nose to the ground. Furthermore, when calculating propeller clearance, the fact that the landing gear will deflect during landing must be taken into account. While at rest the configuration of the landing gear provides 8.38 inches of clearance. Therefore, during landing the gear must not deflect more than 2.88 inches or the propeller will hit the ground.

The amount of deflection for the landing gear was based on a worst case scenario in which all the load is concentrated on one wheel. In order to estimate the amount of vertical deflection (y) that will occur during impact, it was assumed that the strut could be modeled as a cantilever beam with a concentrated load applied at one end. Based on this assumption, the equation $y=PL^3/3EI$ was utilized, with P=applied load, L=vertical length of landing gear strut, E=modulus of elasticity, and I=moment of inertia ($I=\pi r_{strut}^4/4$). The maximum applied load was estimated as 16 lbs using the equation F t = m v, with t~0.1s, and v=rate of descent~10 ft/s (worst case scenario). Using these

constraints, the maximum deflection for the struts was calculated as y_{max}=1.4 inches, which is below the allowable 2.38 inches.

(2) Drag.

In order to minimize drag, the length of the struts and the diameter of the wheels were minimized while maintaining the necessary amount of support. With this criteria in mind, the size of the wheel and struts were determined as:

D_{front}=1.5 inches D_{rear}=0.75 inches L_{strut}=5.7 inches

Since most of the impact of landing will be concentrated on the forward wheels, the diameter of the rear struts could be decreased and the drag therefore reduced. Furthermore, the wheel diameters are equivalent to the smallest diameters that have been placed on any previous Aeroworld design.

(3) Take off angle of attack.

In order to minimize take-off distance, it was desired that the wing be as close to C_{Lmax} during the take-off as safely possible. According to Reference 9.1, α_{to}~$0.8\alpha_{stall}$ accounts for ground effects and safety factors. Based on this, the fact that α_{Wstall} occurs at 10° for our design, and the wing being mounted at an incidence of 2.24°, the fuselage reference line should be set near 5.7°. When the tail wheel is placed 33 inches behind the center of gravity and the vertical length is 2 inches, the fuselage reference line is set at an angle of 5.2° to the ground.

(4) Configuration guidelines.

The first convention requirement was that the turnover angle be less than 60°. The turnover angle requirement, found and explained in Reference 9.1, is necessary in order to provide a wide enough wheel base to prevent the plane from tipping over sideways while on the ground. A wheel base of 12 inches results in a turnover angle of 60.1°, which is near enough specified limits.

The other guideline consists of a standard military specification which requires an angle between 15°-20° from the center of gravity to the point on the ground directly

below the point of attachment of the front landing gear. This forced the front landing gear to be located near the x-distance of the center of gravity. With the front landing gear height of 5 inches, the front spars needed to be attached 3.5 inches in front of the c.g..

10. Economic Analysis

10.1 Initial Considerations

When designing an aircraft, the economic consequences of the design must always be included in the analysis of the concept. In Aeroworld, the HB-40 has proved to be successful at controlling a portion of the market by keeping its costs low with a CPSPK of 0.9 cents per passenger seat per 1000 ft. Thus, in order for the *Diamondback* to be able to gain a portion of the Aeroworld market, the CPSPK would have to be lower than that of the HB-40. Therefore, it was necessary to design the *Diamondback* for optimum performance, as well as economic feasibility.

10.2 CPSPK Determination

In determining the CPSPK of the *Diamondback*, the first parameters calculated were the total cost of the aircraft and the flight crew costs. The flight crew cost was governed by the number of servos in the aircraft. The *Diamondback* will require the use of two servos, which will yield a flight crew cost of $ 0.2/flight. In order to calculate the cost of the aircraft it was necessary to know the current market prices for various aircraft systems. Table 10.1 is a component cost breakdown of the *Diamondback*.

Component	Price ($)
Radio Trans.	75
Radio Rec.	35
Avionics Bat.	10
Switch Harness	5
2 Servos	70
Speed Control	50
Astro Motor	107
Wiring	6
Batteries	36
Total Cost	394

Table 10.1 Component Cost Breakdown

Thus, the total fixed subsystem costs were $394. The next area to be examined was the materials cost. Knowing the sizing of our aircraft, we were able to determine a good estimate of the materials cost by inspecting the database and finding the materials costs of airplanes of similar sizing. Thus, the raw materials were expected to cost $140.

In order to determine the manufacturing costs, it was necessary to make estimates for the labor hours and tooling costs. It was estimated that the aircraft would be more difficult to manufacture because of the complexity of the joined-wing design. In the manufacturing of most aircraft, there is no joint between the wing and the horizontal tail. For the *Diamondback*, this joint is the fundamental principle of the design and will require additional labor and tooling. Furthermore, because the aircraft is essentially a T-tail design it will be necessary to have a more complicated structure at the joining of the horizontal tail and the vertical tail. Finally, most of the past RPVs have used flat plates for their horizontal tail. In the *Diamondback*, the horizontal tail will be an airfoil section, which will further increase the manufacturing time. Thus, estimates for the labor hours and tooling costs were made larger to account for these considerations. In order to determine the number of labor hours required to construct the aircraft, data from past designs was examined. Believing our aircraft would require additional labor hours because of the complexity of the design, a conservative estimate of 120 labor hours was made. For the present labor rate of $10 / hr in Aeroworld, the labor costs were found to be $1200.

For the tooling costs, it was found that exact estimates for the number of turn-ons and operating times would be very difficult to estimate within a reasonable certainty. Therefore, the tooling costs were found using the data provided from past designs. Including the increased tooling brought on by our design, the tooling costs were estimated to be $260.

Knowing the tooling, raw material, personnel, and fixed subsystem costs it was

possible to determine the total cost of one aircraft. The total cost of the *Diamondback* was found to be $1994.

In determining the CPSPK, it was noted that many of the cost algorithms given by AE441, Inc. were dependent on the performance characteristics of the aircraft. In determining the depreciation costs of the aircraft, the number of flights in the lifetime of the airplane was dependent on the range of the airplane and its cruise velocity. Furthermore, the depreciation costs were dependent on the lifetime of the aircraft which presently stands at 50 hrs in Aeroworld. In the operating costs, the maintenance cost was a function of the range and cruise velocity of the aircraft as well as the number of passengers in the aircraft. The maintenance cost was also a function of the passenger classes. The *Diamondback* was designed to accommodate only coach passengers. AE441, Inc. has set the cost per passenger per hour for coach passengers at $.005. Finally, the fuel costs were heavily dependent on the performance characteristics of the airplane, specifically, the propulsion characteristics. The fuel costs were dependent on the range and cruise velocity, the cost per amp-hour of battery usage and the current draw of the propulsion system.

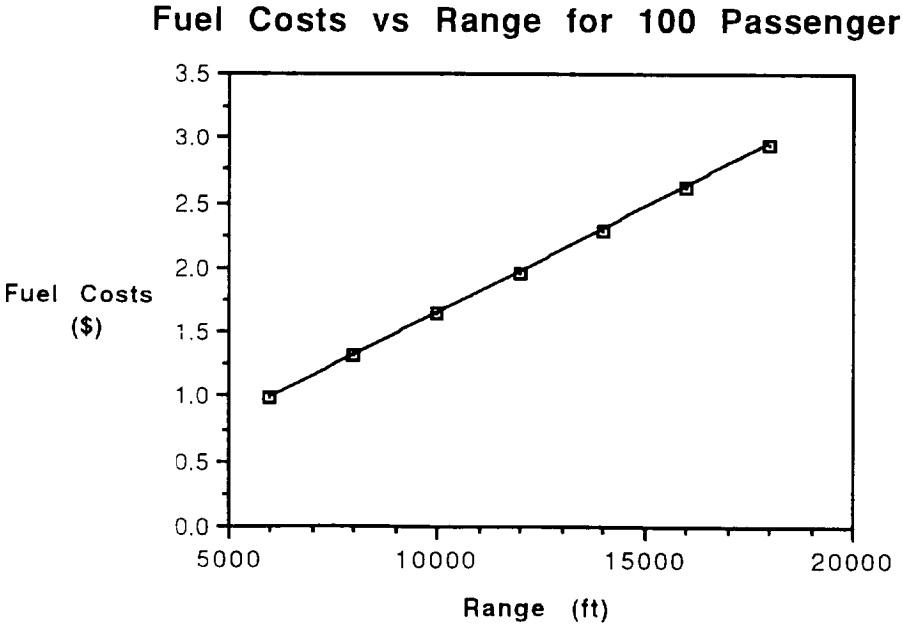

Figure 10.1 Fuel Costs vs Range for 100 Passengers

The effect of the performance characteristics of the aircraft on the fuel costs can easily be seen in Figure 10.1. In this Figure, the effects of increasing the performance characteristic of range on the fuel costs can be seen. As expected, when the range of the aircraft was increased, the fuel costs rose. In Aeroworld, the cost per amp-hour of battery usage was $3.33/amp-hour. It was known that the current draw was a function of the payload of the aircraft. As the payload increased, the current draw would have to rise to accommodate the additional weight. Finally, the CPSPK was a function of the range of the aircraft.

Thus, it would be necessary to develop a model to determine the costs for various range and payload configurations. In order to perform this analysis a spreadsheet was used that would calculate the costs for changing performance characteristics. Using our design range of 10000 ft and our design payload of 100 passengers, it was now possible to determine the various costs of our aircraft.

Cost Breakdown	($/flight)
Depreciation Costs	3.956
Operating Costs:	
Flight Crew	0.2
Maintenance	0.0496
Fuel Costs	1.635
DOC	5.841

Total Aircraft Cost	$1994
Design CPSPK	$.006

Table 10.2 Cost Breakdown

Knowing the CPSPK for our design requirements was very helpful, however, it was known that the aircraft would not always be operating with a full payload, and a range of 10000 ft. Thus, it was necessary to examine the effects of range and payload on the CPSPK of the aircraft. In order to examine these effects, the range was varied from 6000 to 18000 ft for payloads of 50, 75, and 100 passengers. It was then possible to analyze the effects of changing range and payload configurations on the CPSPK.

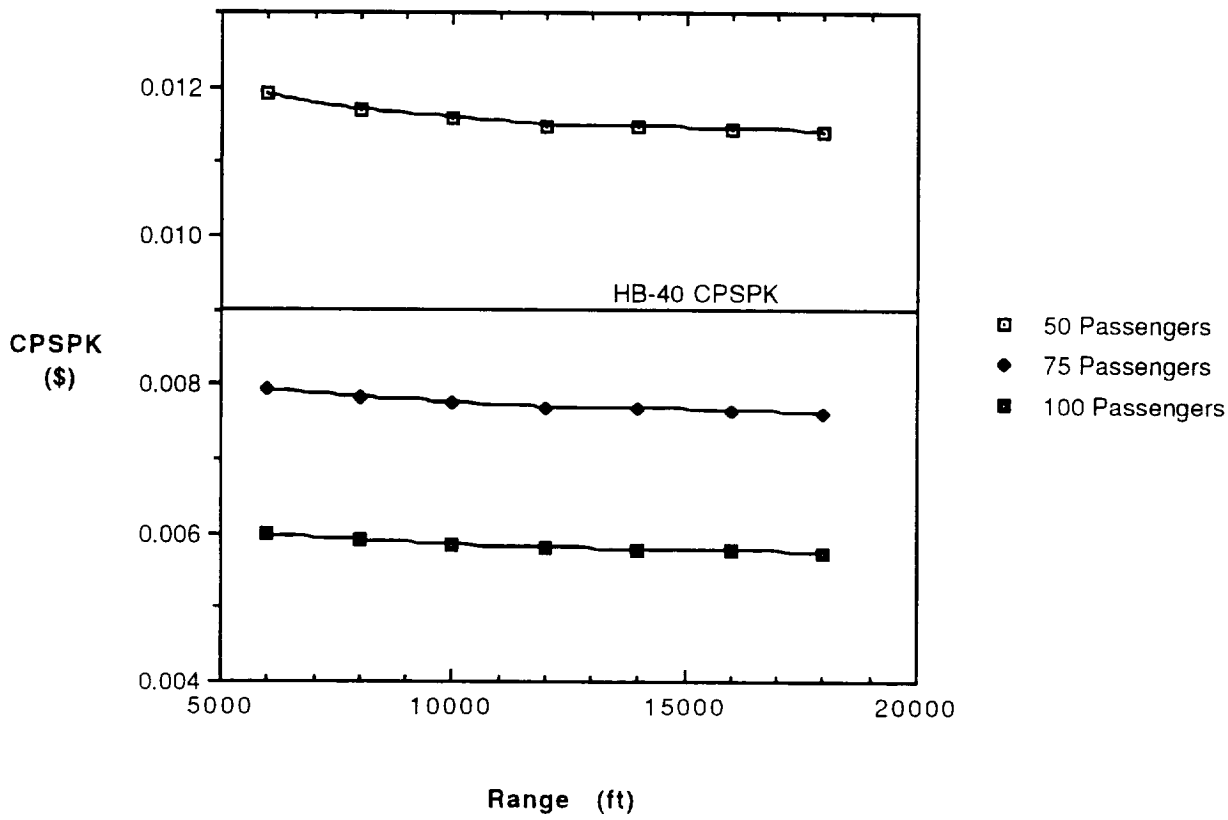

Figure 10.2 CPSPK vs Range for Various Payloads

In Figure 10.2, it can be seen that as the payload decreases the CPSPK of the *Diamondback* will rise dramatically. This trend would be expected because when you operate at less than maximum capacity you are not receiving as much revenue from the consumer. However, when the aircraft was flying at its design payload of 100

passengers, the CPSPK for the aircraft was always near .006. The *Diamondback* offers a CPSPK 35% lower than that of the HB-40.

10.3 Final Considerations

In looking at the economic aspect of the aircraft it was found that it would be best for the aircraft to operate close to the design specifications. Thus, the aircraft was designed to the original requirements. When judging the *Diamondback* against the competition of the HB-40, it was seen that the *Diamondback* was able to operate at a significantly lower CPSPK than the HB-40. The *Diamondback* would therefore be able to operate in a more economically efficient manner than the HB-40. The *Diamondback* should be able to compete in its target market and possibly steal a significant portion of the Aeroworld market from the HB-40.

Appendix A: Aerodynamics Design

A.1 Cross Section and Construction Analysis

Due to the proposed fabrication process of the Diamondback, the cross sectional profile of the airfoil becomes extremely important. The wings of the Diamondback are to be covered with monokote, a shrink-to-fit material. In the region between the ribs of the wing, the monokote is unable to maintain the exact profile of the airfoil section in the longitudinal and latteral directions. Rather in these areas the monokote assumes a nonlinear profile (Figures A.1). Therefore, any airfoil which depends upon areas of detailed contour will not perform as well as expected. A good example of a detailed contour is the lower surface of the Wortmann FX-137 airfoil (Figure A.2). The lifting characteristics of this airfoil are highly dependent upon the large cusp at the trailing edge. However, in the regions between the ribs, the monokote will not retain this profile, resulting in an undetermined decrease in performance. Therefore, the Wortmann FX-137 was not considered as a possibility.

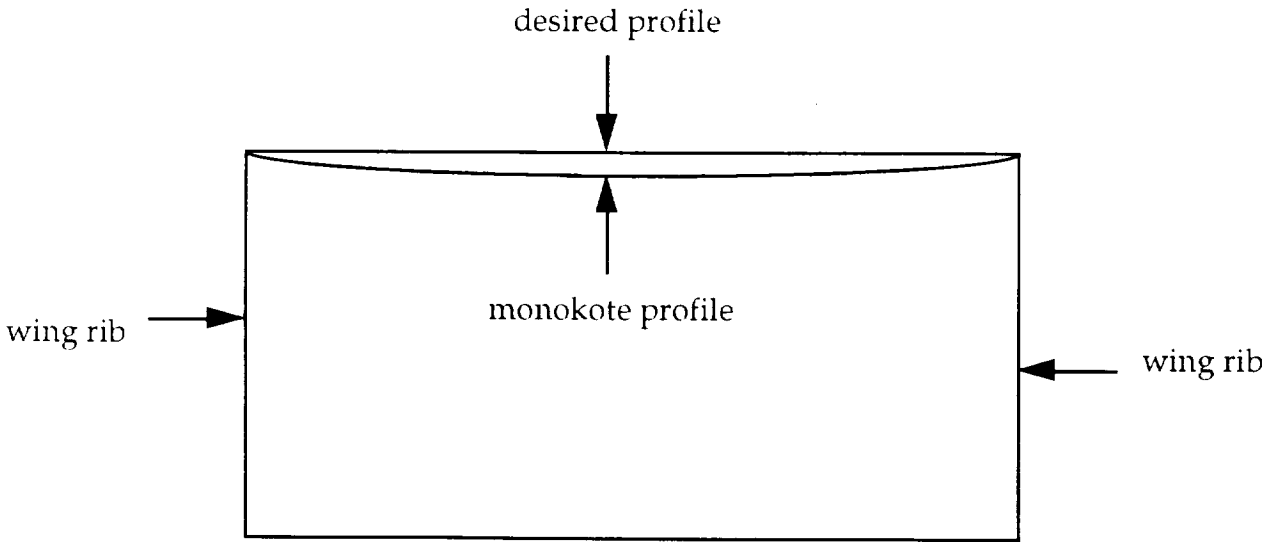

Figure A.1 Profile of Monokote Between Ribs

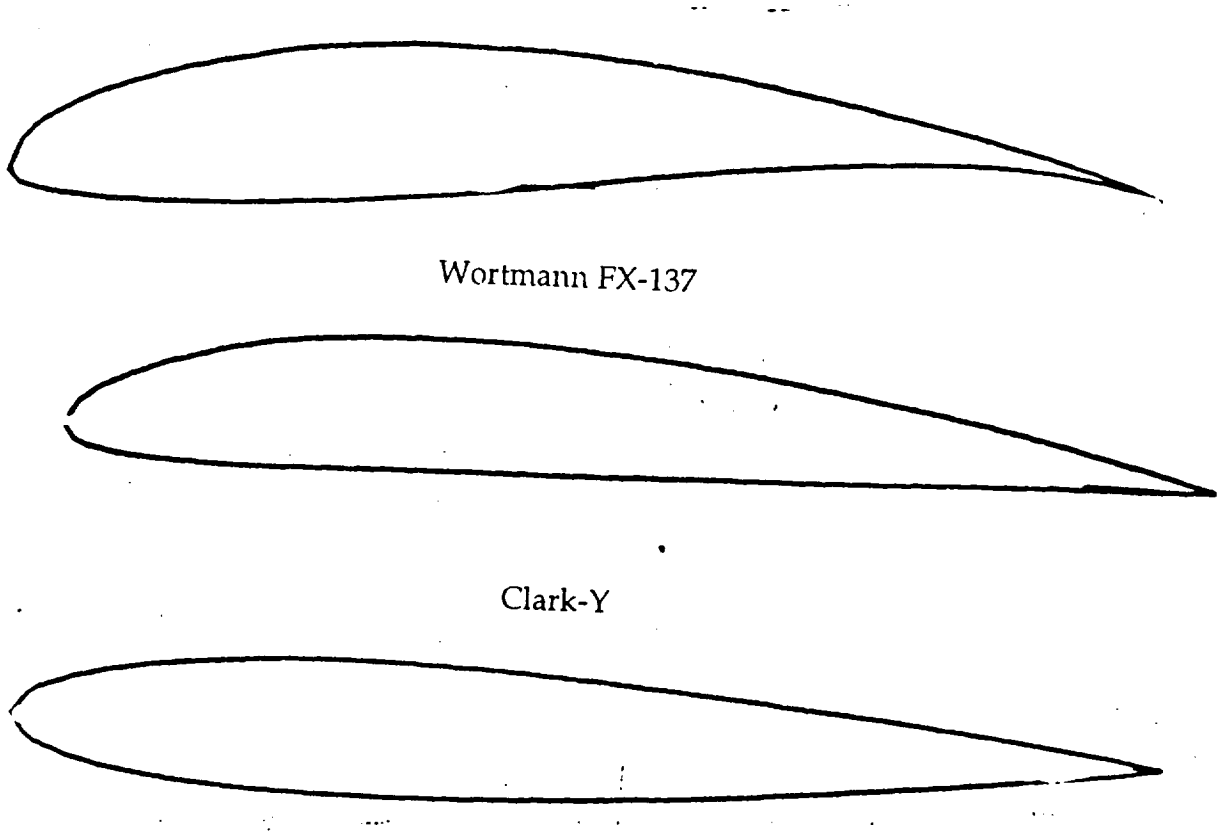

Figure A.2 Comparison of the Wortmann FX-137 the Clark-Y and the NACA 0012

A.2 Method of Aerodynamic Sizing

Many factors were considered in sizing the wing and tail sections. Listed below is the methodology used to establish the basic geometry of the configuration. It is important to remember that this design is by no means an optimal one. Rather, several key areas were determined, and their influence on the lift and drag characteristics were studied.

Initially the areas, chords, spans, and dihedrals of the wing and tail were set using various considerations. The area of the wing was fixed by selecting a moderate $C_{L\ cruise} = 0.6$, based from previous designs, and a relatively slow cruise velocity of 28 ft/s. This low cruise velocity was desired to allow the pilot to fly safely within the

constraints of Aeroworld. The chord of the wing was then selected in order to meet the Reynolds number requirement of $Re_{cruise} > 150{,}000$. This goal was exceeded by setting the wing chord = 1.0 ft, which results in a Re cruise = 178,000. Once the chord of the wing and the area were set, the span was also fixed at $b_{wing} = 9.65$ ft. It was found in Reference A.1 that for this class of aircraft, it is desirable to have a wing dihedral of 8°. Due to the large tail and its destabilizing anhedral effect, it was necessary for us to define an effective dihedral angle as the sum of the dihedral of the wing and the product of the anhedral of the tail and the tail to wing area ratio.

$$\Gamma_{eff} = \Gamma_{wing} + \Gamma_{tail}\left(\frac{S_{tail}}{S_{wing}}\right)$$

Once these basic design variables were set, studies were then to performed to fix the remaining variables. These studies included varying the span of the tail, chord of the tail, sweep of the wing, and use of winglets. The first variable studied was the span of the tail. It was found in Reference A.2 that there was no one optimal span of the tail. From a purely structural stand point the ratio of the span of the tail to span of the wing would be minimized to increase the amount of the load being carried along the spar, i.e., in compression, thereby decreasing the shear and bending moment on the tail root. Conversely, the aerodynamic performance of the joined-wing aircraft is maximized when the wings are joined at the tips. And finally, from a weight and structures standpoint, the optimal design would occur when the span ratio was near 70%. It was decided that the aerodynamic performance was more important than the structural considerations, and the span ratio was set equal to 1. Another advantage to this design is that it allows for the use of a winglet to join the two wings, simplifying the construction.

The next study involved varying the chord of the tail, in order to see what effect it had on the lift and drag characteristics of wing-tail combination. Results of this study can be seen in Figure A.3. Figure A.3 illustrates that as the chord of the tail decreases, (L/D)max increases and the angle at which it occurs decreases. Both of these trends

enhance the performance of the *Diamondback* . However, LinAir does not account for the effects of the decreasing Reynolds Number of the tail which coincides with the decreasing chord. In order to avoid problems associated with premature stall at low Reynolds Numbers, the chord of the tail was set equal to that of the wing. This analysis assumed the use of similar airfoils for the wing and the tail.

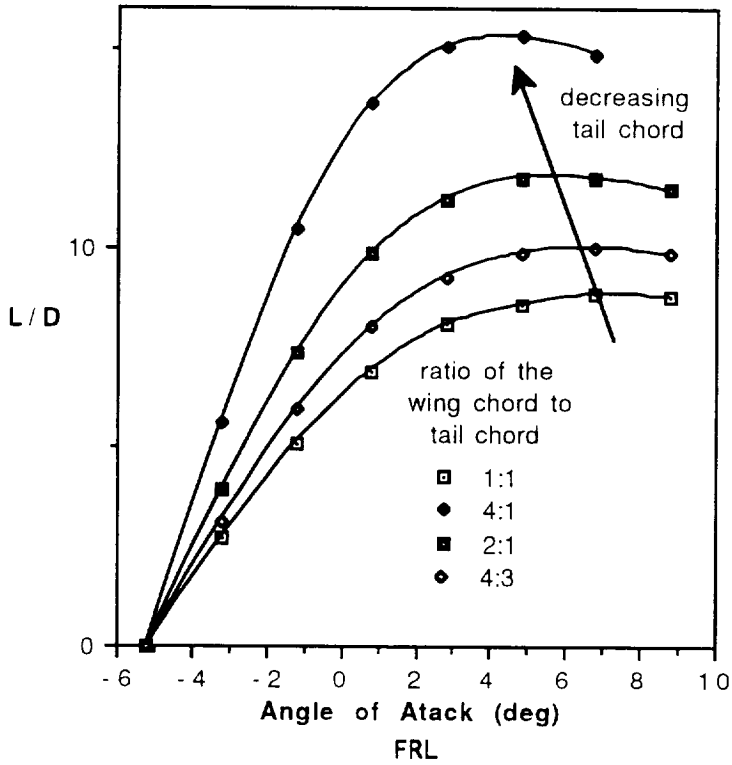

Figure A.3 Comparison of the L/D Curves for Variations in the Chord of the Tail

The next study was performed using LinAir 1.49 to see what effects the variation in the sweep of the wing had on the C_L and C_D of the wing-tail configuration. It was determined using LinAir that the variation in the wing sweep had a negligible effect on the total lift and drag of the wing-tail combination, Figures A.4 and A.5. This is believed to be caused by the coupling inherent in the wing and tail, since a change in the sweep of the wing is countered by an equal but opposite change in the sweep of the tail. This countering effect cancels the effect of changing the wing sweep. This analysis also assumed the use of similar airfoils for the wing and the tail.

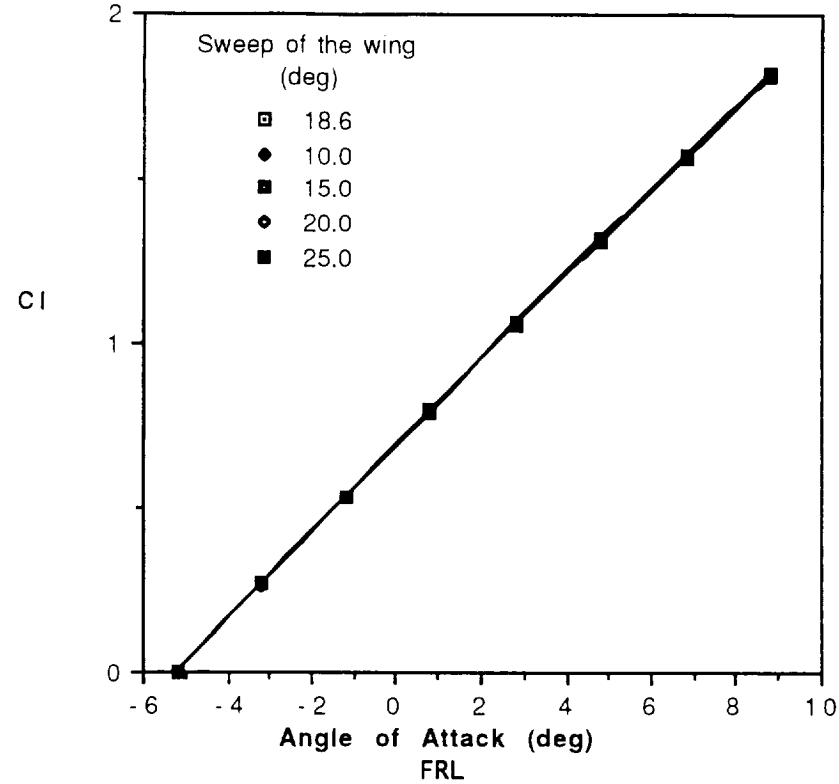

Figure A.4 Variation in the C_L Curve as a Function of the Wing Sweep

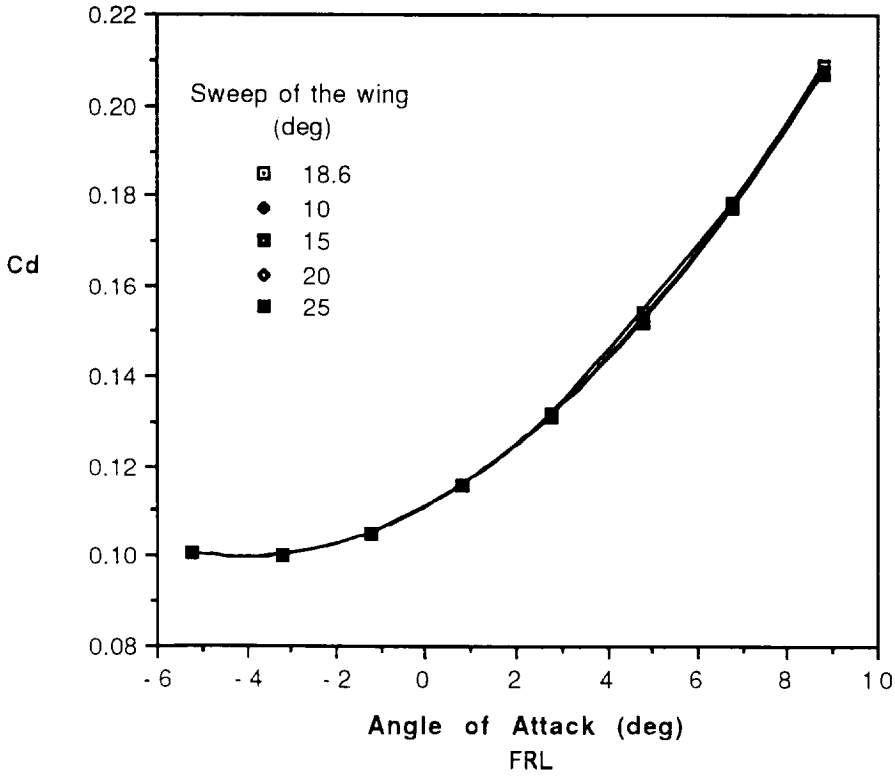

Figure A.5 Variation of the C_D Curve as a Function of the Wing Sweep

One final issue that was raised in locating critical aerodynamic design areas was the wing to tail joint. Several joints were considered, however it was decided that the use of winglets would be the best compromise between structural and aerodynamic considerations. The use of a winglet avoids the problems of flow constrictions (and associated drag penalty) around the wing-tail joint by vertically separating the wing and the tail tips. Another advantage of the winglet is that it also serves to stop the spanwise flow and divert it over the wing surface. A tip separation of 6 inches was decided upon from the analysis above. Addition of the winglet increased the CL of the wing-tail combination approximately 8% at equivalent angles of attack while providing an increase in CD of less than 1%. Unfortunately, by increasing the tip separation the structural advantages of the joined wing are decreased by decreasing the tail anhedral. As mentioned before, decreasing the anhedral of the tail increases the shear and bending moment at the tail root.

Appendix B: Propulsion

B.1 Propeller Performance Characteristics

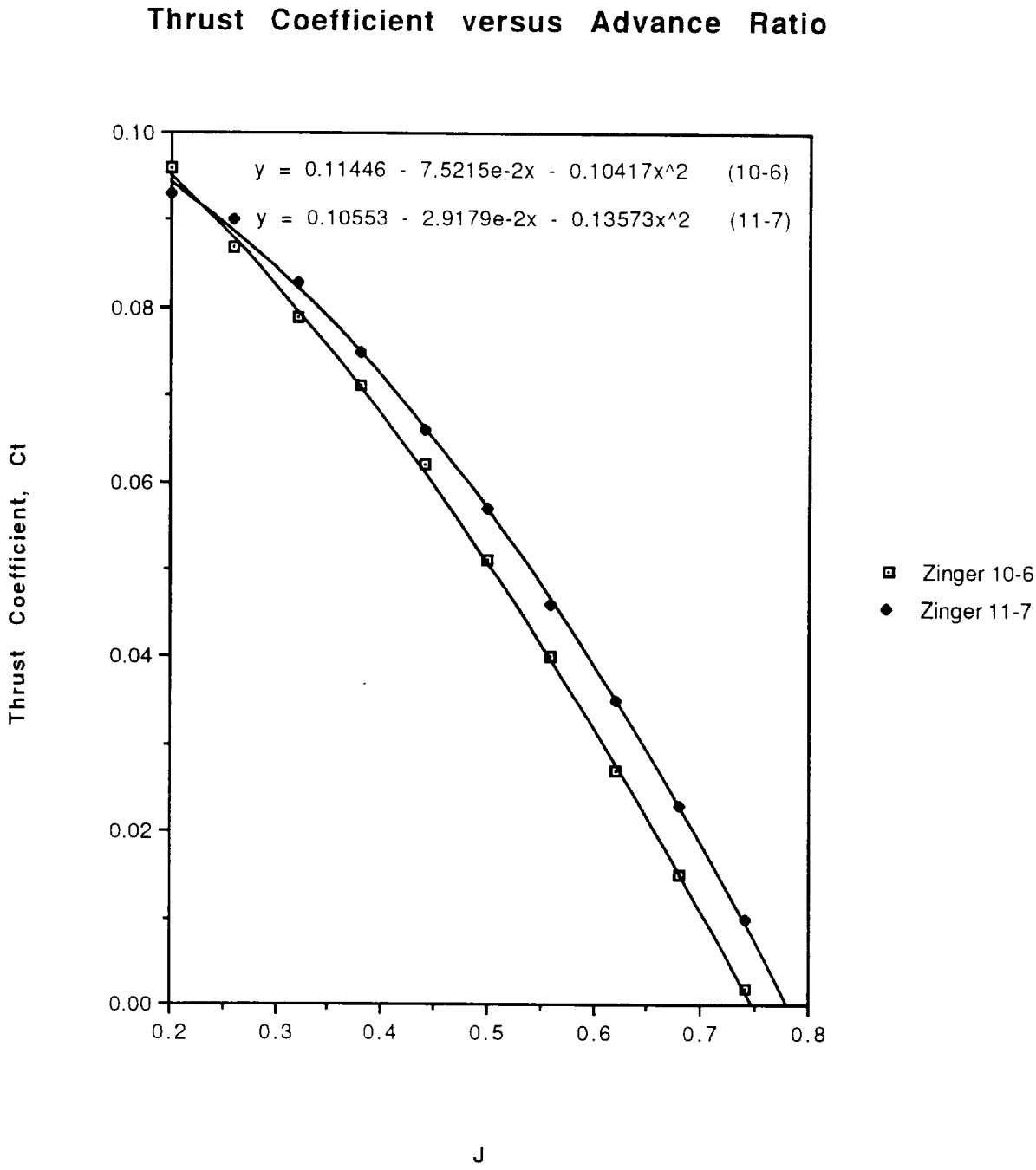

Power Coefficient verses Advance Ratio

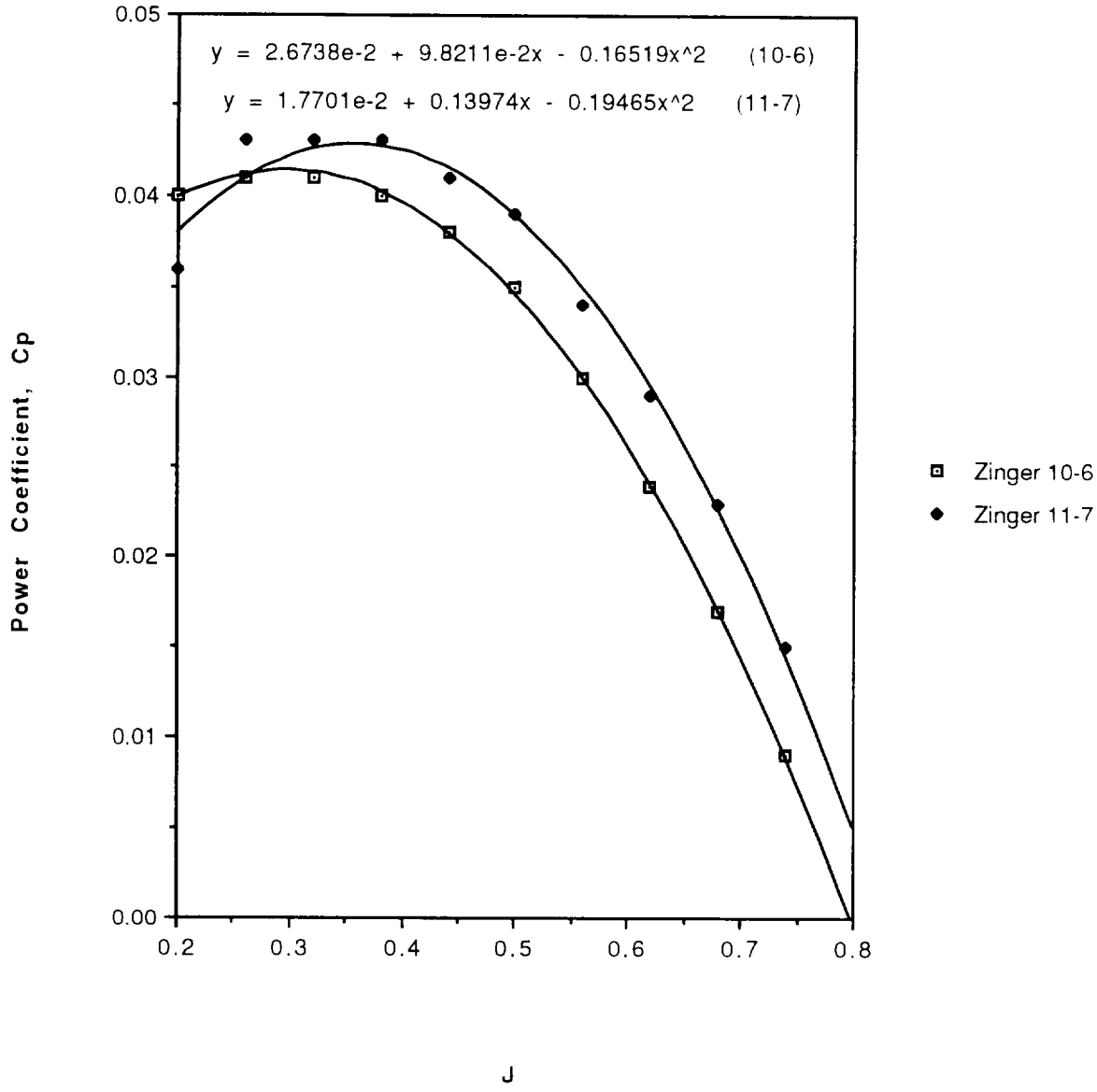

Appendix C: Stability and Control Methodology

C.1 Longitudinal Stability Methodology

As a first step in the analysis, equations modeling the aerodynamic coupling of the wing and the tail had to be developed. Not only will the wing induce a downwash on the tail, the tail will induce a measurable upwash on the wing due to their close proximity. Even when the wing's zero-lift line is parallel to the freestream ($\alpha_{w,L0} = 0$) it will experience a negative upwash due to the tail's negative lift due to the tail incidence (i_t). Thus the wing will experience a negative $\alpha_{w,L0}$ yielding a negative lift, thus inducing a negative downwash on the tail and reducing the tail's negative lift. This relation is circular and will iteratively reach an equilibrium point. Appendix C.4 includes the derivation of the wing and tail angles of attack (from their zero-lift lines) as a function of the upwash on the wing (γ) and the downwash on the tail (ε).

The longitudinal static stability equations were then rederived with these relations. Paralleling the derivation in Reference C.1, pp. 481-2, the equations in Appendix C.5 were developed to include the upwash and downwash due to the aerodynamic interference. The drag component was still assumed to be small and would be dealt with later when the configuration was validated on LinAir.

Armed with these new tools, a TKSolver routine was written to determine the LinAir geometry input parameters as a function of effective dihedral (Γ_{eff}), span, tail to wing span and chord ratios, fuselage length, rudder height, elevator chord, tail incidence, and elevator angle. The routine integrated numerous complicated geometrical relations and greatly increased the turn-around time of calculating configuration geometries.

With the input, the basic configuration was analyzed using LinAir with no tail incidence angle. The wing alone and tail alone configurations were also

analyzed and were then compared to the data for the wing and tail with interference (i.e. the basic configuration). Equation 4 of Appendix C.5 was then utilized to determine the upwash and downwash.

$$C_{L\alpha} = C_{L\alpha,w} + C_{L\alpha,t}$$

$$C_{L\alpha} = C_{L\alpha,w\ alone}\left(1 + \frac{d\gamma}{d\alpha}\right) + \eta_t \frac{St}{Sw} C_{L\alpha,t\ alone}\left(1 - \frac{d\varepsilon}{d\alpha}\right)$$

From the basic configuration, $C_{L\alpha}$ was be determined for the wing and the tail, and with the wing and tail alone $C_{L\alpha}$'s, the $\gamma_\alpha = \frac{d\gamma}{d\alpha}$ and $\varepsilon_\alpha = \frac{d\varepsilon}{d\alpha}$ were determined. Additionally, by comparing the lift, drag, and moment due to the wing and tail separately at several angles of attack, the position of their aerodynamic centers were approximated.

The interference parameters and aerodynamic centers were then input into another TKSolver routine which utilized the relations of Appendix C.5 to calculate i_t, α_{cr}, and x_{cg} for a desired S.M., C_{Lcr} such that $\delta e = 0$ and $C_{Mcr} = 0$.

Returning to LinAir, the tail incidence and angle of attack were input and an analysis was performed at this condition. The variables obtained with Appendix C.5 were found to closely model C_L but the C_M and S.M. were slightly off and the configuration was modified slightly to obtain the desired values.

To assist in the selection of a design point the following plot was made with LinAir data to assess the effect on tail incidence angle on C_L, C_D, C_M, L/D, and S.M..

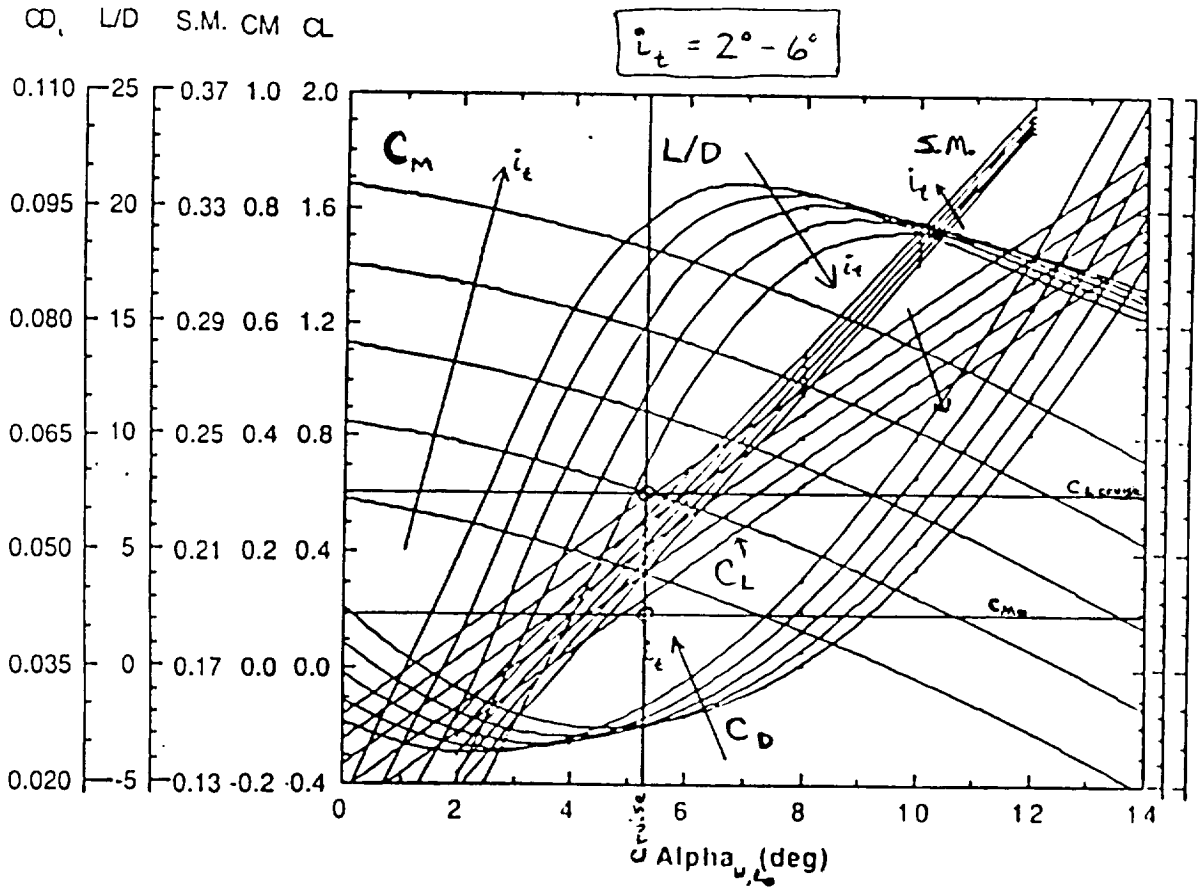

Figure C.1 Effect of Incidence Angle

Because the tail airfoil was changed from the Clark–Y to the NACA 0012 (C_{M_0} = 0) during the design and with a more accurate estimation of C_{M_0} for the Clark–Y (C_{M_0} = –0.09, but the initial estimation was –0.24), the aircraft C_{M_0} which had to be balanced by the LinAir C_M to trim changed from -0.48 to -0.09. Thus on the plot the trim condition moved from C_M = 0.48 to 0.09. By drawing a line at C_L = 0.6 (i.e. cruise) and intersecting the C_L lines for various incidence angles (i_t = 2° to 6°) the angle of attack (from the wing zero-lift line) can be determined for cruise for each i_t. At these angles, the C_M for each i_t can also be determined. Thus each i_t uniquely defines a C_M and an alpha for C_L = 0.6 with the locus of these points forming a line of C_M for C_L = 0.6. At C_M = 0.09 this yields an i_t

1.5° at $\alpha \approx 5°$. The design was finally set at $i_t = 1.6°$ and $\alpha_{w,L0} = 5.2°$ ($\alpha_{FRL} = 0$) giving the *Diamondback* a $C_L = 0.6$, C_M (including C_{M0}) = 0, and S.M. = 0.24 c.

C.2 Elevator Sizing Methodology

The initial elevator sizing was obtained from the $\Delta C_M = +0.31$ required at stall ($\alpha_{FRL} = 8°$) to trim the aircraft with an elevator deflection of – 15°. The elevator contribution to the moment was approximated as

$$\Delta C_M = C_{M\delta e}\ \delta_e = -\eta_h\, V_h\, \frac{dC_{Lt}}{d\delta_e}\ \delta_e = -\eta_h\, V_h\, C_{L\alpha t}\ \tau\ \delta_e$$

For the configuration, the elevator effectiveness factor (τ) was calculated from the other known parameters. In Reference C.2, p. 60, a plot is provided to obtain the elevator area to tail area ratio. This method produced $A_e/A_t = 0.06$. While this ratio may appear somewhat small, when one considers the large horizontal tail ($S_H = 9.65\ ft^2$), it is acceptable.

LinAir was then utilized to verify this calculation using an elevator extending 50% of the span with a chord of 12% c_t. It was determined that this elevator was larger than that needed to trim at this condition, and the elevator was reduced to 35% span. This configuration trimmed the aircraft at stall with a -15° deflection.

C.3 Directional Stability Methodology

The method in Reference C.2 (p. 68-9) was used to estimate the yaw instability due to the wing and fuselage ($C_{n\beta\ wf}$).

$$C_{n\beta\ wf} = -K_n\, K_{R\,l}\, \frac{S_{fs}\, l_f}{S_w\, b}\ \ (deg^{-1})$$

where K_n and $K_{R\,l}$ are empirical constants determined from the aircraft geometry, S_{fs} is the projected side area of the fuselage, and l_f is the length of the fuselage. Unfortunately, the K_n obtained is zero using the configuration

geometry and a value of 0.001 was selected as an "estimate." This method yields a $C_{n\beta\ wf}$ of – 0.0007 deg^{-1}. The uncertainty of the value is large and it may significantly underestimate the instability caused by the wing.

The winglets act much like a vertical tail and were analyzed similarly.

$$C_{n\beta\ wl} = 2\ \eta\ \frac{l_{wl}\ S_{wl}}{b\ S_w}\ C_{L\alpha\ wl}$$

To calculate the lift curve slope of the winglets, the following approximation was utilized.

$$C_{L\alpha} \approx \frac{2\pi}{1 + \frac{2\pi}{\pi\ AR}}$$

This approximation may overestimate the actual slope of standard wings, but bounded by the wing and the tail on both the top and the bottom the winglet appears to the flow to have an artificially large aspect ratio. Thus this approximation is conservative. With the winglet geometry set by aerodynamic and geometry considerations, $C_{n\beta\ wl} = 0.0003\ deg^{-1}$.

The vertical tail was analyzed using conventional methods. The effect of the vertical stabilizer on the yaw stability was approximated as (Reference C.2, p. 70-1),

$$C_{n\beta\ v} = \eta\ V_v\ C_{L\alpha\ v}\ (1 + \frac{d\sigma}{d\beta}) = (0.836 + 1.56\ \frac{S_v}{S_w})\ V_v\ C_{L\alpha\ v}$$

The lift curve slope was approximated like that of the winglets, and like the winglets the fin is bounded on both sides by the fuselage and the horizontal tail. Thus the stabilizing effect of the fin is probably underestimated.

The height (span) of the fin was set in the aerodynamic design at 15.5 inches to provide the vertical spacing between the wing and the tail necessary for the joined-wing configuration. This value was an initial guess based on a consideration of previous designs, but as the design progressed it became fixed since to change its height would be to change the wing and tail dihedral, the gap

between the wing and tail, and the aerodynamic characteristics of the design. (Much of the design was set in such a manner since not only are the aerodynamics of the joined wing coupled, but the geometries of the individual components of the configuration are dependent on those of the other components). Thus the chord became the design variable in the vertical tail.

In light of the uncertainty in the wing and fuselage contribution to $C_{n\beta}$, a large vertical tail was required to ensure directional stability. For a chord of 10 inches, the fin's directional stability coefficient, $C_{n\beta\ v}$, was estimated to be 0.0015.

Interference of Wing & Tail (ignoring blockage)

- Wing induces a downwash angle (ϵ) on tail
- Tail induces an upwash angle (γ) on wing

- Since these induced velocities are due to the circulation (Γ) of the surface causing them, and since the circulation is proportional to the Lift, when the lift on the surface is zero, the circulation is zero, and the induced velocity on the other surface is zero.

Let α be the wing angle of attack from the relative wind (V_∞) as measured from the wing zero-lift line.
Let i_t be the incidence of the tail relative to the wing as measured from the wing zero-lift line to the tail zero-lift line. ($i_t > 0 \Rightarrow$ negative incidence)

Lift on wing: $C_{L_w} = \frac{dC_L}{d\alpha}(\alpha + \gamma) = \frac{dC_L}{d\alpha}\alpha_w$

Lift on tail: $C_{L_t} = \frac{dC_{L_t}}{d\alpha}(\alpha - i_t - \epsilon) = \frac{dC_{L_t}}{d\alpha}\alpha_t$

so $\alpha_w = \alpha + \gamma$
$\alpha_t = \alpha - i_t - \epsilon$

Now, at $\alpha = 0$ the tail will experience an angle of attack (α_t) and thus will induce an angle of attack on the wing (γ_0) which will in turn induce a downwash angle on the tail (ϵ_0).

So, $\alpha_w = \alpha(1 + \gamma_\alpha) + \gamma_0$ where $\gamma_0 \neq 0$, $\gamma_\alpha = \frac{d\gamma}{d\alpha}$
$\alpha_t = \alpha(1 - \epsilon_\alpha) - i_t - \epsilon_0$ where $\epsilon_0 \neq 0$, $\epsilon_\alpha = \frac{d\epsilon}{d\alpha}$

At $\alpha = 0$, $\alpha_{w_{\alpha=0}} = \gamma_0$
$\alpha_{t_{\alpha=0}} = -i_t - \epsilon_0$

but $\gamma_0 = \gamma_\alpha \alpha_{t_{\alpha=0}} = \gamma_\alpha(-i_t - \epsilon_0)$
$\epsilon_0 = \epsilon_\alpha \alpha_{w_{\alpha=0}} = \epsilon_\alpha \gamma_0$

Thus, $\epsilon_0 = -\frac{\epsilon_\alpha \gamma_\alpha}{1 + \epsilon_\alpha \gamma_\alpha} i_t \Rightarrow \boxed{\alpha_t = \alpha(1 - \epsilon_\alpha) - i_t\left(\frac{1}{1 + \epsilon_\alpha \gamma_\alpha}\right)}$

$\gamma_0 = -\frac{\gamma_\alpha}{1 + \epsilon_\alpha \gamma_\alpha} i_t \Rightarrow \boxed{\alpha_w = \alpha(1 + \gamma_\alpha) - i_t\left(\frac{\gamma_\alpha}{1 + \epsilon_\alpha \gamma_\alpha}\right)}$

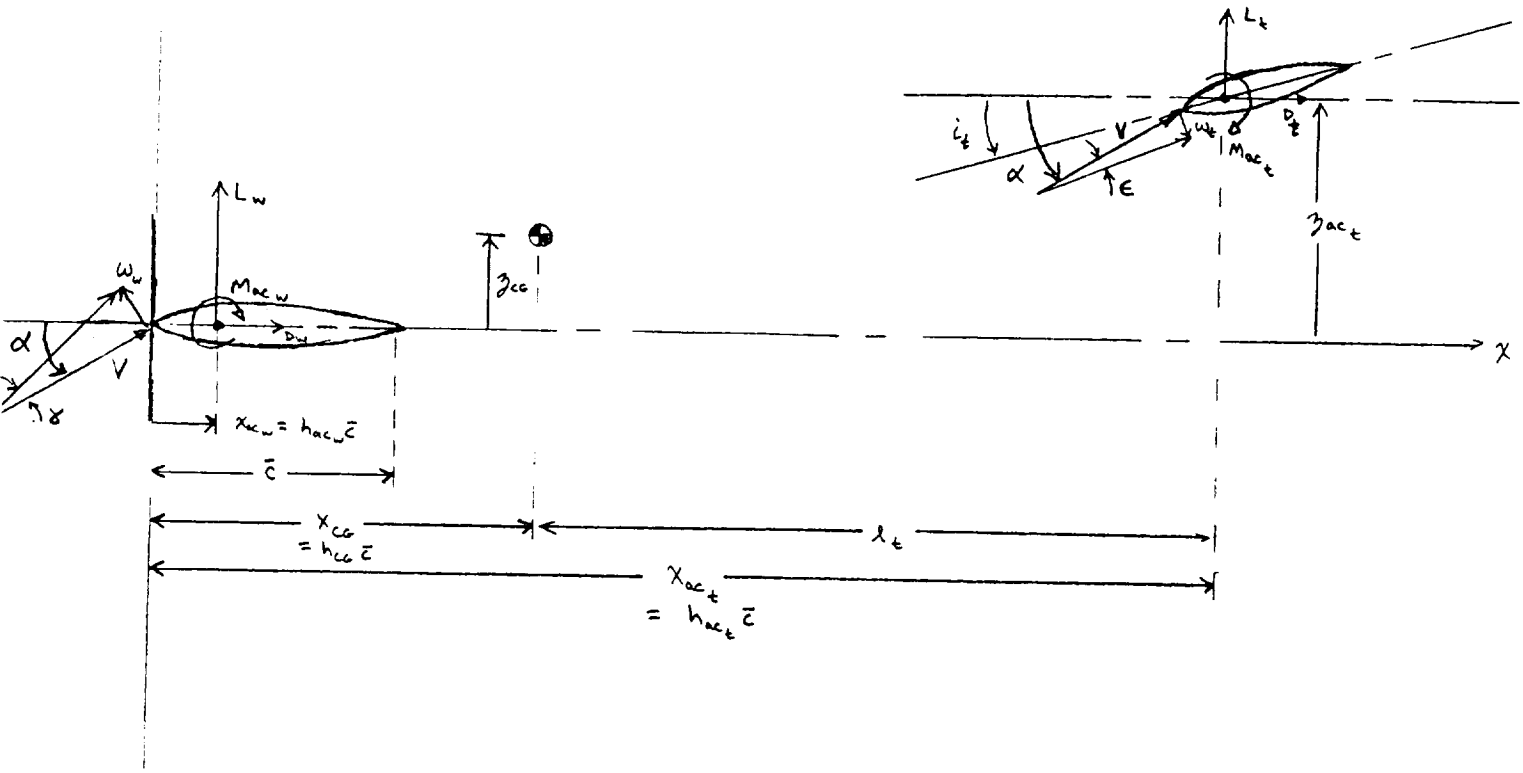
z
L_t
i_t
V
w_t
D_t
M_{ac_t}
α
ϵ
z_{ac_t}
L_w
w_w
M_{ac_w}
z_{cg}
D_w
α
V
γ
x
$x_{ac_w} = h_{ac_w}\bar{c}$
$\bar{c}$
x_{cg}
$= h_{cg}\bar{c}$
l_t
x_{ac_t}
$= h_{ac_t}\bar{c}$

Static Stability (ignoring Fuselage, drag)

$$L_w = q S a \alpha_w = q S a \left[\alpha (1+\gamma_\alpha) - i_t \left(\frac{\gamma_\alpha}{1+\epsilon_\alpha \gamma_\alpha} \right) \right] \qquad \text{where } a = \frac{dC_L}{d\alpha}$$

$$L_t = \eta_t q S_t a_t \alpha_t = \eta_t q S_t a_t \left[\alpha (1-\epsilon_\alpha) - i_t \left(\frac{1}{1+\epsilon_\alpha \gamma_\alpha} \right) \right]$$

$$M_{ac_w} = q S \bar{c} C_{M_{ac_w}}$$
$$M_{ac_t} = \eta_t q S_t c_t C_{M_{ac_t}}$$

- $$C_M = \frac{M_{cg}}{q S \bar{c}} = (h_{cg} - h_{ac_w}) a \left[\alpha (1+\gamma_\alpha) - i_t \left(\frac{\gamma_\alpha}{1+\epsilon_\alpha \gamma_\alpha} \right) \right] + C_{M_{ac_w}} - \eta_t \underbrace{\frac{S_t}{S} \frac{l_t}{\bar{c}}}_{V_H} a_t \left[\alpha (1-\epsilon_\alpha) - i_t \left(\frac{1}{1+\epsilon_\alpha \gamma_\alpha} \right) \right] + C_{M_{ac_t}} \eta_t \frac{S_t}{S} \frac{c_t}{\bar{c}}$$

$$C_M = \alpha \left[(h_{cg} - h_{ac_w})(1+\gamma_\alpha) a - \eta_t V_H (1-\epsilon_\alpha) a_t \right] + C_{M_{ac_w}} + C_{M_{ac_t}} \eta_t \frac{S_t}{S} \frac{c_t}{\bar{c}} + i_t \left[\eta_t V_H a_t - (h_{cg} - h_{ac_w}) \gamma_\alpha a \right] \left(\frac{1}{1+\epsilon_\alpha \gamma_\alpha} \right)$$

$$C_M = C_{M_0} + C_{M_\alpha} \alpha$$

$\Rightarrow$

① $$C_{M_0} = C_{M_{ac_w}} + C_{M_{ac_t}} \eta_t \frac{S_t}{S} \frac{c_t}{\bar{c}} + i_t \left[\eta_t V_H a_t - (h_{cg} - h_{ac_w}) \gamma_\alpha a \right] \left(\frac{1}{1+\epsilon_\alpha \gamma_\alpha} \right)$$

② $$C_{M_\alpha} = (h_{cg} - h_{ac_w})(1+\gamma_\alpha) a - \eta_t V_H (1-\epsilon_\alpha) a_t$$

$\bar{c}$ – t must [illegible] that good stability is obtained

[illegible]

Note: $V_H = \frac{S_t}{S} (h_{ac_t} - h_{cg})$

- $$C_L = C_{L_w} + \eta_t \frac{S_t}{S_w} C_{L_t} = a \alpha_w + \eta_t \frac{S_t}{S} a_t \alpha_t = a \left[\alpha (1+\gamma_\alpha) - i_t \left(\frac{\gamma_\alpha}{1+\epsilon_\alpha \gamma_\alpha} \right) \right] + \eta_t \frac{S_t}{S} a_t \left[\alpha (1-\epsilon_\alpha) - i_t \left(\frac{1}{1+\epsilon_\alpha \gamma_\alpha} \right) \right]$$

$$C_L = C_{L_{\alpha=0}} + C_{L_\alpha} \alpha$$

$\Rightarrow$

③ $$C_{L_{\alpha=0}} = -i_t \left(a \gamma_\alpha + \eta_t \frac{S_t}{S} a_t \right) \left(\frac{1}{1+\epsilon_\alpha \gamma_\alpha} \right)$$

④ $$C_{L_\alpha} = a (1+\gamma_\alpha) + \eta_t \frac{S_t}{S} a_t (1-\epsilon_\alpha)$$

[illegible]

Static Stability - Continued

- Neutral Point:

From ④ : $\eta_t \frac{S_t}{S} a_t (1-\epsilon_\alpha) = C_{L_\alpha} - a(1+\gamma_\alpha)$

note also that $V_H = \frac{S_t l_t}{S\bar{c}} = \frac{S_t}{S}(h_{ac_t} - h_{cg})$

From ② : $C_{M_\alpha} = (h_{cg} - h_{ac_w})(1+\gamma_\alpha)a - \eta_t \left[\frac{S_t}{S}(h_{ac_t} - h_{cg})\right](1-\epsilon_\alpha)a_t$

$= (h_{cg} - h_{ac_w})(1+\gamma_\alpha)a - (h_{ac_t} - h_{cg})\left[C_{L_\alpha} - a(1+\gamma_\alpha)\right]$

at Neutral Point, $C_{M_\alpha} = 0$ and $h_{NP} = h_{cg}$ $\Rightarrow$

$$0 = (h_{NP} - h_{ac_w})(1+\gamma_\alpha)a - (h_{ac_t} - h_{NP})\left[C_{L_\alpha} - a(1+\gamma_\alpha)\right]$$

$$h_{NP} = \frac{h_{ac_w}(1+\gamma_\alpha)a + h_{ac_t}\left[C_{L_\alpha} - (1+\gamma_\alpha)a\right]}{C_{L_\alpha}}$$

⑤

$$h_{NP} = \frac{h_{ac_w} + h_{ac_t}\left[\frac{C_{L_\alpha}}{(1+\gamma_\alpha)a} - 1\right]}{\frac{C_{L_\alpha}}{(1+\gamma_\alpha)a}}, \text{ and } \frac{C_{L_\alpha}}{(1+\gamma_\alpha)a} = 1 + \eta_t \frac{S_t}{S} \frac{a_t(1-\epsilon_\alpha)}{a(1+\gamma_\alpha)}$$

- Static Margin & C.G. Placement

$S.M. \equiv h_{NP} - h_{cg}$

$\Rightarrow$ $h_{cg} = -S.M. + h_{NP}$

⑥

$$h_{cg} = -S.M. + \frac{h_{ac_w} + h_{ac_t}\left[\eta_t \frac{S_t}{S} \frac{a_t(1-\epsilon_\alpha)}{a(1+\gamma_\alpha)}\right]}{1 + \eta_t \frac{S_t}{S} \frac{a_t(1-\epsilon_\alpha)}{a(1+\gamma_\alpha)}}$$

To determine C.G. Placement require:

h_{ac_w}, h_{ac_t}, $\bar{c}$, $S.M.$, S, S_t, η_t, $\frac{dC_{L_w}}{d\alpha}$, $\frac{dC_{L_t}}{d\alpha}$

and $\frac{d\epsilon}{d\alpha}$ and $\frac{d\gamma}{d\alpha}$

Static Stability - continued

- With fuselage,

$$C_{M_0} = C_{Mac_w} + C_{Mac_t}\,\eta_t\,\frac{S_t}{S}\,\frac{C_t}{\bar{c}} + i_t\left[\eta_t V_H a_t - (h_{cg}-h_{ac_w})\gamma_\alpha a\right]\left(\frac{1}{1+\epsilon_\alpha\gamma_\alpha}\right) + C_{M_{0_f}}$$

$$C_{M_\alpha} = (h_{cg}-h_{ac_w})(1+\gamma_\alpha)a - \eta_t V_H (1-\epsilon_\alpha) a_t + C_{M_{\alpha_f}}$$

Assume fuselage does negligible lift (small, or else)

$$h_{NP} = \frac{h_{ac_w} + h_{ac_t}\left[\eta_t\,\frac{S_t}{S}\,\frac{a_t(1-\epsilon_\alpha)}{a(1+\gamma_\alpha)}\right] - \frac{C_{M_{\alpha_f}}}{(1+\gamma_\alpha)a}}{1 + \eta_t\,\frac{S_t}{S}\,\frac{a_t(1-\epsilon_\alpha)}{a(1+\gamma_\alpha)}}$$

- With drag,

$$C_{D_w} = C_{D_{0_w}} + k_w C_{L_w}^2 = C_{D_{0_w}} + k_w a^2\left[\alpha(1+\gamma_\alpha) - i_t\left(\frac{\gamma_\alpha}{1+\epsilon_\alpha\gamma_\alpha}\right)\right]^2$$

$$C_{D_{w_{\alpha=0}}} = C_{D_{0_w}} - k_w a^2 i_t^2\left(\frac{\gamma_\alpha}{1+\epsilon_\alpha\gamma_\alpha}\right)^2$$

$$C_{D_{w_\alpha}} = \frac{dC_{D_w}}{d\alpha} = 2k_w C_{L_w}\frac{dC_{L_w}}{d\alpha} = 2k_w a^2\alpha_w$$
$$= 2k_w a^2\left[\alpha(1+\gamma_\alpha) - i_t\left(\frac{\gamma_\alpha}{1+\epsilon_\alpha\gamma_\alpha}\right)\right]$$

$$C_{D_t} = C_{D_{0_t}} + k_t C_{L_t}^2 = C_{D_{0_t}} + k_t a_t^2\left[\alpha(1-\epsilon_\alpha) - i_t\left(\frac{1}{1+\epsilon_\alpha\gamma_\alpha}\right)\right]$$

$$C_{D_{t_{\alpha=0}}} = C_{D_{0_t}} - k_t a_t^2 i_t^2\left(\frac{1}{1+\epsilon_\alpha\gamma_\alpha}\right)^2$$

$$C_{D_{t_\alpha}} = 2k_t a_t^2\alpha_t$$
$$= 2k_t a_t^2\left[\alpha(1-\epsilon_\alpha) - i_t\left(\frac{1}{1+\epsilon_\alpha\gamma_\alpha}\right)\right]$$

$$C_{M_0} = C_{M_{0\ w/o\ Drag}} - C_{D_{w_{\alpha=0}}}\left(\frac{\bar{x}_{cg}}{\bar{c}}\right) + \eta_t\,\frac{S_t}{S}\,C_{D_{t_{\alpha=0}}}\left(\frac{\bar{x}_{ac_t}-\bar{x}_{cg}}{\bar{c}}\right)$$

$$\boxed{\begin{aligned} C_{M_0} &= \left(C_{Mac_w} - C_{D_{0_w}}\frac{\bar{x}_{cg}}{\bar{c}}\right) + \left(C_{Mac_t}\frac{C_t}{\bar{c}} + C_{D_{0_t}}\frac{\bar{x}_{ac_t}-\bar{x}_{cg}}{\bar{c}}\right)\eta_t\,\frac{S_t}{S} + C_{M_{0_f}} \\ &\quad + i_t\left[\eta_t V_H a_t - (h_{cg}-h_{ac_w})\gamma_\alpha a\right]\left(\frac{1}{1+\epsilon_\alpha\gamma_\alpha}\right) \\ &\quad - i_t^2\left[\eta_t\,\frac{S_t}{S}\,\frac{\bar{x}_{ac_t}-\bar{x}_{cg}}{\bar{c}}\,k_t a^2 - \frac{\bar{x}_{cg}}{\bar{c}}\,k_w a^2\gamma_\alpha^2\right]\left(\frac{1}{1+\epsilon_\alpha\gamma_\alpha}\right)^2 \end{aligned}}$$

Appendix D: Performance

D.1 TK Solver Iteration Program

Input	Quantity	Output	Units	Descriptions
28	V		ft/s	Velocity
.9167	Dprop		ft	Diameter of Propeller
9.65	S		ft^2	wing area
5.47	W		lbs	Weight
	q	.932176	lb/ft^2	Dynamic pressure
	Cl	.60808193		Coefficient of Lift
	Cd	.05357498		Coefficient of Drag
	D	.48193363	lbs	Drag
	Preq	18.294683	W	Power Required
	ROC		ft/s	Rate of Climb
	LoD	11.350111		L/D
.9	Batcap		Ah	Battery Capacity
	Flttim	654.35475	s	Endurance
	Range	18321.933	ft	Range
	Nm	8826.4036	RPM	Motor RPM
2.21	grat			gear ratio
	Np	3993.8478		Propeller RPM
	J	.45887092		Advance ratio
	Cp	.04083763		Power coefficient
	Pmout	26.461511	W	Motor Pwr Output
6	Ia		Amps	Armature current
9.6	Va		Volts	Actual voltage
	etap	.7277574		Propeller Efficiency
	Pavail	18.294683	W	Power Available
.000792	kv		V/RPM	
1.084	kt		In-oz/A	
.12	Ra		Ohms	Motor Resistance
.084	Rbat		Ohms	Battery Resistance
.95	etag			Gear Efficiency

D.2 Program Rules

q=.5*.002378*V^2
Cl=W/(q*S)
Cd=.049579-.018186*Cl+.040714*Cl^2
D=Cd*q*S
Preq=D*V*1.35575
ROC=(Pavail-Preq)*.7376/W
LoD=Cl/Cd
Flttim=Batcap/Ia*3600
Range=V*Flttim
Np=Nm/grat
J=V/(Np/60*Dprop)
Cp=.017701+.13974*J-.19465*J^2
Pmout=((Cp*.000001835*(Np/60)^3*(Dprop*12)^5)/etag)*.0070612
Ia=((Pmout/.0070612)/(Nm*6.2832/60)+1.313)/kt
etap=2.171-22.652*J+114.25*J^2-264.82*J^3+296.63*J^4-131.24*J^5
Nm=(Va-Ia*(Ra+Rbat))/kv
Pavail=Pmout*etag*etap

takeoff.f

```
      1  c       Takeoff Performance Program
      2  c       written by Dr. S. Batill
      3  c
      4          program main
      5  c
      6          dimension ct(20), cp(20), adv(20)
      7          real j,kt,kv,mass,mu,lift,mrps,mrpm,mrpmn
      8          character*25 filename,casettl
      9  c
     10          ikey=5
     11          imon=6
     12          iprnt=9
     13          write(imon,105)
     14    105   format("   input data file name")
     15          read(ikey,*)filename
     16          open(1,file=filename)
     17          read(1,*)casettl
     18          write(iprnt,*)"case - ",casettl
     19          write(iprnt,*)"case - "
     20          read(1,*)wgt
     21          write(iprnt,*)"wgt =",wgt
     22          write(imon,*)"wgt =",wgt
     23          read(1,*)sref
     24          write(iprnt,*)"sref =",sref
     25          write(imon,*)"sref =",sref
     26          read(1,*)rho
     27          write(iprnt,*)"rho =",rho
     28          write(imon,*)"rho =",rho
     29          read(1,*)clto
     30          write(iprnt,*)"clto =",clto
     31          write(imon,*)"clto =",clto
     32          read(1,*)cdto
     33          write(iprnt,*)"cdto =",cdto
     34          write(imon,*)"cdto =",cdto
     35          read(1,*)clmax
     36          write(iprnt,*)"clmax =",clmax
     37          write(imon,*)"clmax =",clmax
     38          read(1,*)smax
     39          write(iprnt,*)"smax =",smax
     40          write(imon,*)"smax =",smax
     41          read(1,*)mu
     42          write(iprnt,*)"mu =",mu
     43          write(imon,*)"mu =",mu
     44          read(1,*)dia
     45          write(iprnt,*)"dia =",dia
     46          write(imon,*)"dia =",dia
     47          read(1,*)bvolts
     48          write(iprnt,*)"bvolts =",bvolts
     49          write(imon,*)"bvolts =",bvolts
     50          read(1,*)kt
     51          write(iprnt,*)"kt =",kt
     52          write(imon,*)"kt =",kt
     53          read(1,*)kv
     54          write(iprnt,*)"kv =",kv
     55          write(imon,*)"kv =",kv
     56          read(1,*)rarm
     57          write(iprnt,*)"rarm =",rarm
     58          write(imon,*)"rarm =",rarm
     59          read(1,*)rbat
     60          write(iprnt,*)"rbat =",rbat
     61          write(imon,*)"rbat =",rbat
     62          read(1,*)fusamp
     63          write(iprnt,*)"fusamp =",fusamp
     64          write(imon,*)"fusamp =",fusamp
```

takeoff.f

```
      read(1,*)gearat
      write(iprnt,*)"gearat =",gearat
      write(imon,*)"gearat =",gearat
      read(1,*)dt
      write(iprnt,*)"dt =",dt
      write(imon,*)"dt =",dt
      read(1,*)tmax
      write(iprnt,*)"tmax =",tmax
      write(imon,*)"tmax =",tmax
      read(1,*)nj
      write(iprnt,*)"nj =",nj
      write(imon,*)"nj =",nj
c
      write(imon,*)
      write(imon,*)"j     ct     cp"
      do 5 i=1,nj
      read(1,*)adv(i),ct(i),cp(i)
      write(iprnt,*)adv(i),ct(i),cp(i)
      write(imon,*)adv(i),ct(i),cp(i)
    5 continue
      close(1)
c
c     begin calculation
c
      pi=3.14159
      dia4=dia**4
      dia5=dia**5
      mass=wgt/32.174
      rtot=rarm+rbat
      ampmax=bvolts/(2.*rtot)
      pomax=((kt*bvolts**2)/(4.*rtot*kv))*2.*pi
      pomxhp=pomax*1.578e-7
      pomxwt=pomxhp/1.341e-3
      fac1=bvolts/(2.*rtot)
      fac2=(bvolts/rtot)**2
      batlos=0.
      time=0.
      icount=0.
      v=0.
      s=0.
      vto=sqrt(2.*wgt/(rho*sref*clmax))*1.2
      write(iprnt,*)"v takeoff =",vto
      write(imon,*)"v takeoff =",vto
      write(iprnt,*)"max current draw(amp) =",ampmax
      write(imon,*)"max current draw(amp) =",ampmax
      write(iprnt,*)"max motor power(hp) =",pomxhp
      write(imon,*)"max motor power(hp) =",pomxhp
      write(iprnt,*)"max motor power(watts) =",pomxwt
      write(imon,*)"max motor power(watts) =",pomxwt
      amps=0.
      mrpm=(bvolts-ampmax*rtot)/kv
   10 continue
      icount=icount+1
c
c     estimate the motor speed
c
      iter=0
   15 continue
      mrps=mrpm/60
      iter=iter+1
c     write(imon,*)"iteration - ",iter,"motor rps-",mrps
      prps=mrps/gearat
      j=v/(prps*dia)
      call prop(j,ctp,cpp,ct,cp,adv,nj)
```

takeoff.f

```
      c        write(imon,*)j,ctp,cpp
      c        write(imon,*)cpp,rho,prps,dia5
               pmot=cpp*rho*prps**3*dia5*1.152e4
      c        write(imon,*)"prop power req in-ox/min ",pmot
      c        write(imon,*)"prop power req (wts) = ",pmot*1.341e-3/1.578e-7
               if(pmot .ge. pomax)go to 1001
               amps=fac1-.5*sqrt(fac2-4.*pmot*kv/(rtot*kt*2.*pi))
      c        write(imon,*)"iteration -",iter,"motor amps -",amps
               mrpmn=(bvolts-amps*rtot)/kv
               dmrpm=abs(mrpm-mrpmn)
               mrpm=mrpm+(mrpmn-mrpm)*.5
               if(iter .gt. 100) go to 999
               if(dmrpm .gt. 20) go to 15
               if(amps .gt. fusamp) go to 1004
               prps=mrpm/(60.*gearat)
               thrust=ctp*rho*prps**2*dia4
               drag=.5*rho*v**2*sref*cdto
               lift=.5*rho*v**2*sref*clto
               frict=mu*(wgt-lift)
               if(thrust .lt. frict)go to 1005
      c        write(imon,*)thrust,drag,frict,mass
               accel=(thrust-drag-frict)/mass
               if(icount .eq. 1)then
               write(iprnt,*)"static thrust =",thrust
               write(imon,*)"static thrust =",thrust
               write(iprnt,*)"static current draw(amps) =",amps
               write(imon,*)"static current draw(amps) =",amps
               write(iprnt,*)"max motor power(watts) =",prps
               write(imon,*)"static prop rps =",prps
               endif
      c
      c        simple itegration
      c
               delv=accel*dt
               ds=v*dt
               dbat=dt*amps/3600.
               v=v+delv
               s=s+ds
               batlos=batlos+dbat
               time=time+dt
               write(iprnt,*)icount,time,v,s,batlos,accel,amps
      c        wirte(imon,*)icount,prps,thrust,drag,fictlift,accel,pmot,amps,j
      c        write(imon,*)"time=",time,v,s,batlos
               if(s .gt. smax)go to 1002
               if(time .gt. tmax)go to 1003
               if(v .lt. vto)go to 10
               write(imon,*)
               write(imon,*)
               write(iprnt,*)icount
               write(iprnt,*)"vtake off =",vto
               write(imon,*)"time for run(sec) =",time
               write(imon,*)"v at to (ft/sec) =",v
               write(imon,*)"distance(ft) =",s
               batlos=batlos*1000.
               write(imon,*)"battery drain(mahs) =",batlos
               write(imon,*)"advance ratio at to =",j
               write(imon,*)"thrust(lb) at to =",thrust
               write(imon,*)"lift(lb) at to(before rotation) = ",lift
               write(imon,*)"drag(lb) at to(before rotation) = ",drag
               write(imon,*)"friction(lb) at to(before rotation) =",frict
               write(imon,*)"current draw at to(amps) =",amps
               stop
        999    write(iprnt,*)"motor speed calculation did not converge"
               write(imon,*)"motor speed calculation did not converge"
```

takeoff.f

```
      stop
 1001 write(iprnt,*)"power req exceeded max allowable"
      write(imon,*)"power req exceeded max allowable"
      write(iprnt,*)"pomax(in-oz/min) =",pomax
      write(imon,*)"pomax(in-oz/min) =",pomax
      write(iprnt,*)"pmot(in-oz/min) =",pmot
      write(imon,*)"pmot(in-oz/min) =",pmot
      stop
 1002 write(iprnt,*)"distance exceeded max allowable"
      write(imon,*)"distance exceeded max allowable"
      stop
 1003 write(iprnt,*)"time exceeded max allowable"
      write(imon,*)"time exceeded max allowable"
      stop
 1004 write(iprnt,*)"fuse current exceeded max allowable"
      write(imon,*)"fuse current exceeded max allowable"
      stop
 1005 write(iprnt,*)"friction exceeds static thrust"
      write(imon,*)"friction exceeds static thrust"
      stop
      end
c
c
      subroutine prop(j,ctp,cpp,ct,cp,adv,np)
      dimension ct(20),cp(20),adv(20)
      real j
      i=0
  10  i=i+1
      if((j .ge. adv(i)) .and. (j .le. adv(i+1))) go to 11
      if(i .eq. np+1) go to 999
      go to 10
  11  ctp=ct(i)+((ct(i+1)-ct(i))/(adv(i+1)-adv(i)))*(j-adv(i))
      cpp=cp(i)+((cp(i+1)-cp(i))/(adv(i+1)-adv(i)))*(j-adv(i))
      return
 999  write(imon,*)"interpolation error with propeller data"
      pause 2
      end
```

output

```
 1
 2
 3          Takeoff Performance Program Input and Output Files
 4
 5          wgt =    5.47000
 6          sref =    9.65000
 7          rho =    2.37800E-03
 8          clto =   0.800000
 9          cdto =    6.11000E-02
10          clmax =    1.50000
11          smax =    300.000
12          mu =   0.200000
13          dia =   0.916700
14          bvolts =    14.4000
15          kt =    1.08400
16          kv =    7.92000E-04
17          rarm =   0.120000
18          rbat =    8.40000E-02
19          fusamp =    20.0000
20          gearat =    2.21000
21          dt =    5.00000E-02
22          tmax =    40.0000
23          nj =  12
24
25          j               ct               cp
26          0.              0.105500         1.77000E-02
27          0.200000        9.30000E-02      3.60000E-02
28          0.260000        9.00000E-02      4.30000E-02
29          0.320000        8.30000E-02      4.30000E-02
30          0.380000        7.50000E-02      4.30000E-02
31          0.440000        6.60000E-02      4.10000E-02
32          0.500000        5.70000E-02      3.90000E-02
33          0.560000        4.60000E-02      3.40000E-02
34          0.620000        3.50000E-02      2.90000E-02
35          0.680000        2.30000E-02      2.30000E-02
36          0.740000        1.00000E-02      1.50000E-02
37          10.00000        0.               -100.0000
38
39          v takeoff =    21.3931
40          max current draw(amp) =    35.2941
41          max motor power(hp) =   0.344846
42          max motor power(watts) =    257.156
43          static thrust =    2.82692
44          static current draw(amps) =    5.53894
45          static prop rps =    126.319
46
47
48          time for run(sec) =    2.35000
49          v at to (ft/sec) =    21.7761
50          distance(ft) =    25.3833
51          battery drain(mahs) =    5.05844
52          advance ratio at to =   0.196672
53          thrust(lb) at to =    2.18423
54          lift(lb) at to(before rotation) =     4.16603
55          drag(lb) at to(before rotation) =    0.318180
56          friction(lb) at to(before rotation) =   0.260795
57          current draw at to(amps) =    9.79273
```

Geometry Calculations

St	Input	Name	Output	Unit	Comment
	8	dieff		deg	effective dihedral (based on Sw)
	1	bratio			ratio of tail to wing span
	1	cratio			ratio of tail to wing chord
	.12	fratio			ratio of flap to (total) tail chord
	67	Lf		in	fuselage length
	5	Lnose		in	length of nose cone
	0	xwle		ft	x position of wing leading edge
	1.5	hrud		ft	height of the rudder
	0	delxtip		ft	
	6	delztip		in	
	9.65	Sw		ft^2	wing area
	9.65	bw		ft	span of the wing
		cw	1	ft	chord of the wing
	0				
		semiSw	4.8977454	ft^2	semi area of the wing (linair)
		semibw	4.8977454	ft	semi span of the wing (linair)
		sweepw	18.167352	deg	sweep of the wing
		diw	9.8873798	deg	dihedral of the wing
		xwc4	.25	ft	x position of wing c/4
		ywc4	0	ft	y position of wing c/4
		zwc4	0	ft	z position of wing c/4
	20	npanel			number of panels (wing & nonmovable ta
		St	9.65	ft^2	tail area
		bt	9.65	ft	span of the tail
		ct	1	ft	chord of the tail
		ctt	.88	ft	chord of non-moving tail (linair)
		xtle	50	in	x position of tail leading edge
		semiSt	4.2483047	ft^2	semi area of the tail
		semibt	4.827619	ft	semi span of the tail
		sweept	-18.16735	deg	sweep of the tail
		dit	-1.88738	deg	dihedral of the tail
		xtc4	4.3866666	ft	x position of the tail c/4
		ytc4	0	ft	y position of the tail c/4
		ztc4	1.5	ft	z position of the tail c/4
	-1.62	inct		deg	
		ypanel	.24125	ft	width of a panel
		cf	.12	ft	chord of the flap
		semiSf	.28965714	ft^2	semi area of the flap
		semibf	2.4138095	ft	semi span of the flap
		sweepf	-18.16735	deg	sweep of the flap
		dif	-1.88738	deg	dihedral of the flap
		xfc4	5.0766666	ft	x position of the flap c/4
		yfc4	0	ft	y position of the flap c/4
		zfc4	1.5195067	ft	z position of the flap c/4
	0	delf		deg	
	10	tpanel			number of panels on the flap
		semiSe	.28965714	ft^2	semi area of the elevator
		semibe	2.4138095	ft	semi span of the elevator
		sweepe	-18.16735	deg	sweep of the elevator
		die	-1.88738	deg	dihedral of the elevator
		xl	4.285	ft	(use this in linair)
		yl	2.4125	ft	(use this in linair)
		LAzec4	1.4400509		

St	Input	Name	Output	Unit	Comment
		incf	-1.62	deg	
		epanel	10		number of panels on the outboard flap
		xec4	4.3240564	ft	x position of the elevator c/4
		yec4	2.2934808	ft	y position of the elevator c/4
		zec4	1.4400078	ft	z position of the elevator c/4
		x2	.79166666	ft	
		xttipc4	2.8333213	ft	
		yttipc4	4.825	ft	
		zttipc4	1.3418503	ft	
		vhwlet	.75127218	ft	
		wletyc4	4.825	ft	
		wletxc4	1.5333369	ft	
		wletzc4	.69074777	ft	
		xwtipc4	1.8333333	ft	x position of the wing tip c/4sweep of
		vh	.54325397		
		wlsema	.40744048		
		wlsemb	.54325397		
		wletswe	63.395812	deg	
		xwletc4	2.0208333		
		ywtipc4	4.825	ft	y position of the wing tip c/4
		zwtipc4	.8410022	ft	z position of the wing tip c/4

Geometry Equations - 1

$ Rule

```
* dieff       = diw + dit*St/Sw
* sweepw      = -sweept
* tan(sweepw) = (xtle - (xwle + cw))/2 / (bw/2)
* Lf - Lnose  = (xtle + ct) - xwle

* xwc4     = xwle + cw/4
* ywc4     = 0
* zwc4     = 0
* Sw       = cw * bw
* semibw   = (bw/2)/cos(diw)
* semiSw   = semibw*cw
* xwtipc4  = xwc4 + bw/2*tan(sweepw)*bratio
* ywtipc4  = bw/2*bratio
* zwtipc4  = ywtipc4*tan(diw)

* bt        = bw*bratio
* ct        = cw*cratio
* St        = bt*ct
* ctt       = ct*(1-fratio)
* xtle      = (xwtipc4 + 0.75*cw) - tan(sweept)*bt/2 + delxtip
* xtc4      = xtle + ctt/4
* ytc4      = 0
* ztc4      = hrud
* tan(dit)  = ((zwtipc4+delztip)-ztc4)/(bt/2)
* semibt    = (bt/2)/cos(dit)
* semiSt    = semibt*ctt

* ypanel = (bw/2)/npanel
* cf     = ct*fratio
* semibf = ypanel*tpanel/cos(dit)
* semiSf = semibf*cf
* dif    = dit
* sweepf = sweept
* xfc4   = xtle + ctt + cf/4
* yfc4   = 0
* zfc4   = ztc4-.75*ctt*sin(inct)-.5*cf*sin(delf/2)-.25*cf*sin(inct)
* incf=inct+delf

* semibe = semibt-semibf
* semiSe = semibe*cf
* die    = dif
* sweepe = sweepf
* abs(sin(sweepe)) = (xfc4-xec4)/semibf
* abs(tan(sweepe)) = (xfc4-x1)/y1
* abs(cos(sweepe)) = (yec4-yfc4)/semibf
* y1 = ypanel*tpanel
* sin(die)         = (zec4-zfc4)/semibf
* epanel = npanel - tpanel
* LAzec4=ztc4-.25*cf*sin(inct)-.75*ctt*sin(inct)+tpanel*ypanel*sin(die)

* x2 = xfc4 - x1



* xttipc4=xtc4-.25*ctt*cos(inct)+yttipc4*tan(sweept)+.25*(ctt+cf)*cos(inct)
* yttipc4=ywtipc4
* zttipc4=1.5+.25*ctt*sin(inct)+yttipc4*tan(dit)-.25*(ctt+cf)*sin(inct)
```

S Rule
* vhwlet=1.5*(zttipc4-zwtipc4)
* tan(wletswe)=(xttipc4-xwtipc4)/(zttipc4-zwtipc4)
* wletxc4=xwtipc4-.2*vhwlet*tan(wletswe)
* wletyc4=ywtipc4
* wletzc4=zwtipc4-.2*vhwlet
* vh=zttipc4-zwtipc4-.75*(cw+ct)*sin(inct)
* wlsema=.75*vh
* wlsemb=vh
* xwletc4=xwtipc4+.1875

No tail incidence, xref = 0, 20 panels

	hcg				Sweepw	Dihed.w	hc4w	zc4w/cw	Sweept	Dihed.t	hc4t	zc4w/cw			
	0.00				18.1674	9.8874	0.2500	0.0000	-18.167	-1.8874	4.4167	1.5000			
					0.3171	0.1726			-0.3171	-0.0329					
		Total			Wing				Tail				L/D		
Config. No	Alpha	CL	CD	CM	CL	CD	CM	Xacw	CL	CD	CM	Xact	Total	Wing	Tail
Wing108	0	0.0000	0.02447	0.0224	0.0000	0.01232	0.0052	1.0416	0.0000	0.01215	0.0173	3.6176	0.00	0.00	0.00
	2	0.2861	0.02363	-0.5923	0.1698	0.01192	-0.1687	1.0222	0.1163	0.01171	-0.4236	3.7885	12.11	14.25	9.93
	4	0.5709	0.02865	-1.2144	0.3388	0.01520	-0.3443	1.0348	0.2320	0.01345	-0.8701	3.8334	19.93	22.29	17.25
	6	0.8535	0 03941	-1.8411	0.5065	0.02208	-0.5208	1.0467	0.3470	0.01732	-1.3202	3.8768	21.66	22.94	20.03
	8	1.1332	0.05569	-2.4694	0.6724	0.03244	-0.6975	1.0581	0.4608	0.02324	-1.7719	3.9181	20.35	20.73	19.83
	10	1.4092	0 07724	-3.0968	0.8360	0.04611	-0.8736	1.0690	0.5732	0.03112	-2.2231	3.9572	18.24	18.13	18.42
	12	1.6807	0 10374	-3.7202	0.9968	0.06289	-1 0483	1.0795	0.6839	0.04084	-2.6719	3.9939	16.20	15.85	16.75
	14	1.9469	0.13483	-4.3370	1.1544	0.08256	-1.2209	1.0895	0.7925	0.05227	-3.1161	4.0283	14.44	13.98	15.16
	CLa =	.140722		CLa =	.083476			CLa =	.057246						
Wing108a	0	0.0000	0.0245	0.0224	0.0000	0.01232	0.0052	1.0416	0.0000	0.01215	0.0173	3.6176	0.00	0.00	0.00
wing & tail	2	0.3242	0.0227	-0.7569	0.1614	0.01143	-0.1597	1.0185	0.1628	0.01125	-0.5971	3.7673	14.29	14.12	14.47
independa	4	0.6476	0 0259	-1.5479	0.3224	0.01304	-0.3269	1.0310	0.3252	0.01282	-1.2210	3.8112	25.04	24.72	25.37
	6	0.9693	0.0340	-2.3472	0.4825	0.01711	-0.4957	1.0424	0.4868	0.01684	-1.8515	3.8531	28.55	28.20	28.91
	8	1.2887	0.0468	-3.1513	0.6414	0.02359	-0.6653	1.0530	0.6473	0.02323	-2.4860	3.8923	27.52	27.19	27.87
	10	1.6050	0.0643	-3.9566	0.7987	0.03236	-0.8350	1.0630	0.8063	0.03192	-3.1216	3.9289	24.97	24.68	25.26
	12	1.9175	0.0861	-4.7597	0.9541	0.04333	-1.0041	1.0722	0.9634	0.04280	-3.7556	3.9628	22.26	22.02	22.51
	14	2 2256	0.1121	-5.5569	1.1072	0.05635	-1 1717	1.0807	1.1184	0.05575	-4.3852	3.9938	19.85	19.65	20.06
	CLa =	160320		CLa =	.079780			CLa =	.080540						

Results:	dg/da =	.046331						
	de/da =	.289220						
	CLaw =	.079780						
	CLat =	.080540						
	Xacw =	1.04158	to	1.0895	Δ =	0.5749	inches	
	Xact =	3.61755	to	4.0283	Δ =	4.9287	inches	
Tail Incidence:	For	Xacw/cw =	1.0520					
(from Tksolver)		Xact/cw =	3.8900					
	Cruise at:	alphacr =	6.9987	deg				
		it =	4.6302	deg				
		Xcg/cw =	2.0065					
		Xnp/cw =	2.2065					

Interference Coefficient Calculations

Page E-10

St	Input	Name	Output	Unit	Comment
	9.65	Sw		ft^2	
	1	cw		ft	
	.07978	a		1/deg	
	-.24	CMacw			
	1.052	hacw			
	.046331	dgda			
	9.65	St		ft^2	
	1	ct		ft	
	.08054	at		1/deg	
	-.24	CMact			
	3.89	hact			
	.28922	deda			
	0	CMof			
	0	CMaf			
	.6	CLcr			
	.2	SM			
	1	ETAt			
		alphacr	6.998674	deg	
		it	4.6301682	deg	
		hcg	2.0065045		
		hnp	2.2065045		
		CMo1	-.48		
		CMo	.19697419		
		CMa	-.0281445	1/deg	
		CLo	-.384871		
		CLa	.14072251	1/deg	
		VH	1.8834955		

S Rule

```
* CMo1 = CMacw + CMact*ETAt*St/Sw*ct/cw + CMof
* CMo  = CMo1 + it*(ETAt*VH*at-(hcg-hacw)*dgda*a)/(1+deda*dgda)
* CMa  = (hcg-hacw)*(1+dgda)*a - ETAt*VH*(1-deda)*at + CMaf

* CLo = - it*(ETAt*St/Sw*at + a*dgda)/(1+deda*dgda)
* CLa = a*(1+dgda) + ETAt*St/Sw*at*(1-deda)

* hnp = (hacw + hact*(CLa/(1+dgda)/a-1) - CMaf/(1+dgda)/a) / (CLa/(1+dgda)/a)
* hcg = hnp - SM

* VH  = St/Sw * (hact-hcg)/cw

* CMo + CMa*alphacr = 0
* CLcr = CLo + CLa*alphacr
```

Appendix F: Primary Deliverables

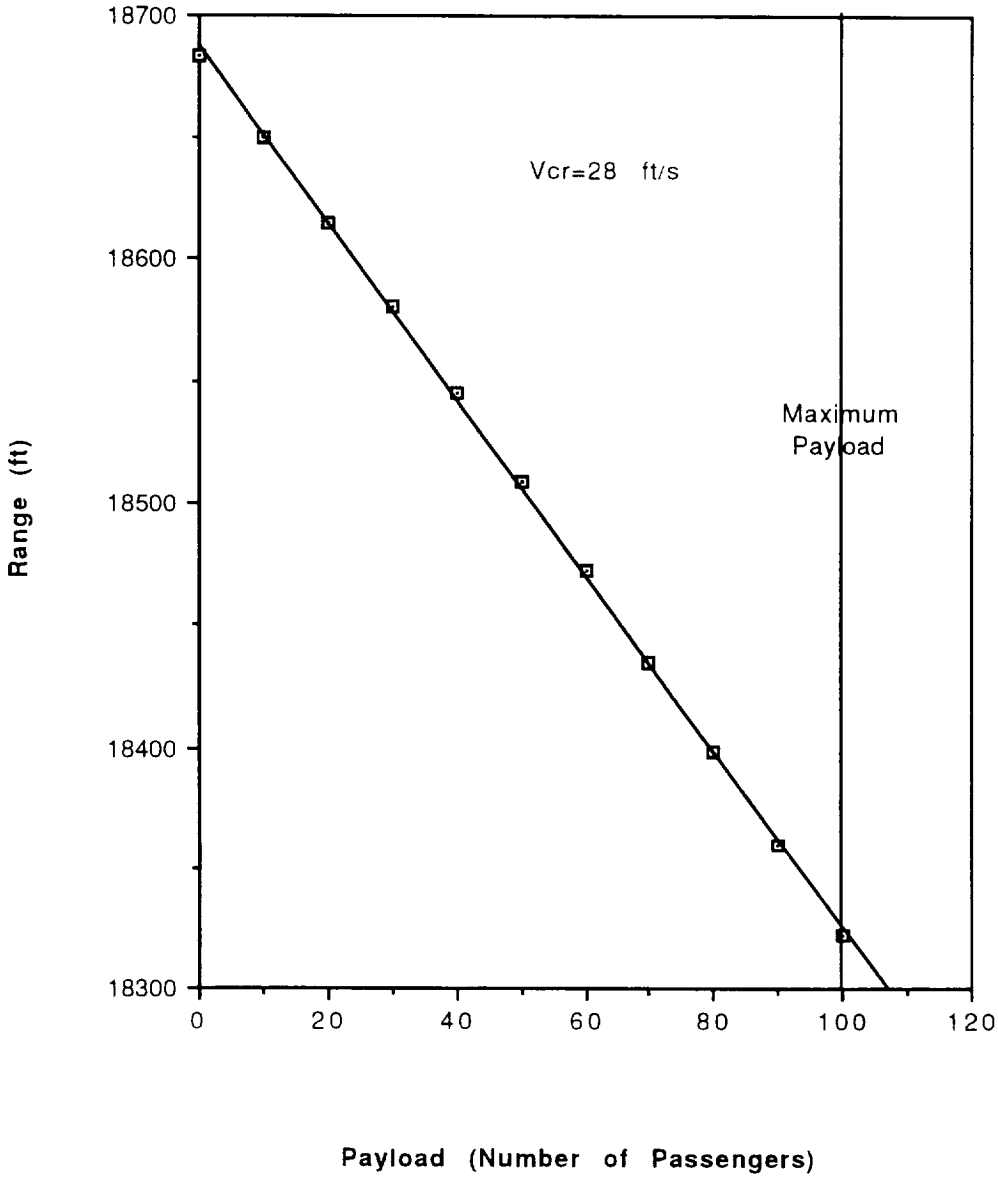

Figure F.1 Range-Payload Diagram

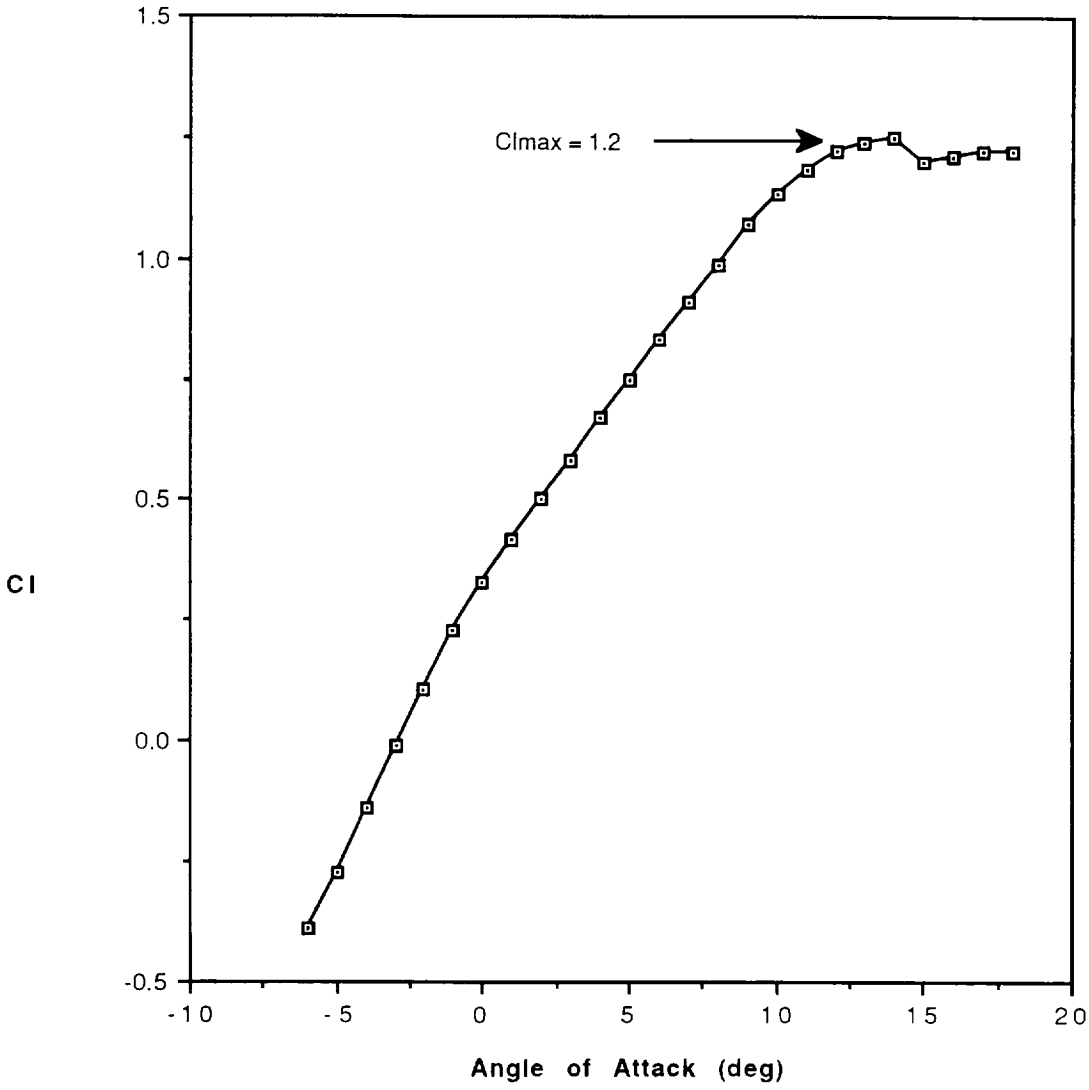

Figure F.2.1 Lift Curve of the Clark-Y

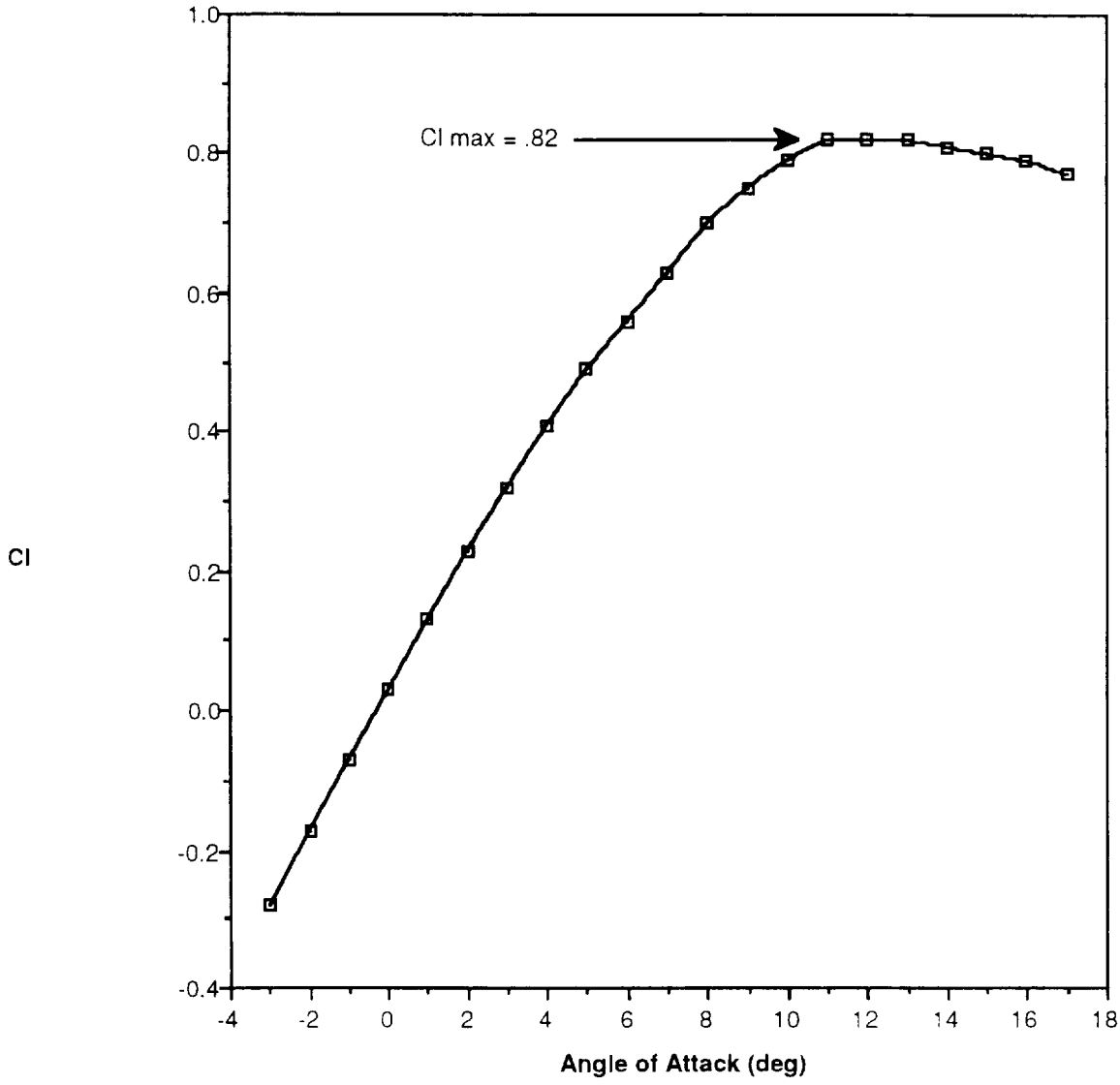

Figure F.2.2 Lift Curve of the NACA 0012

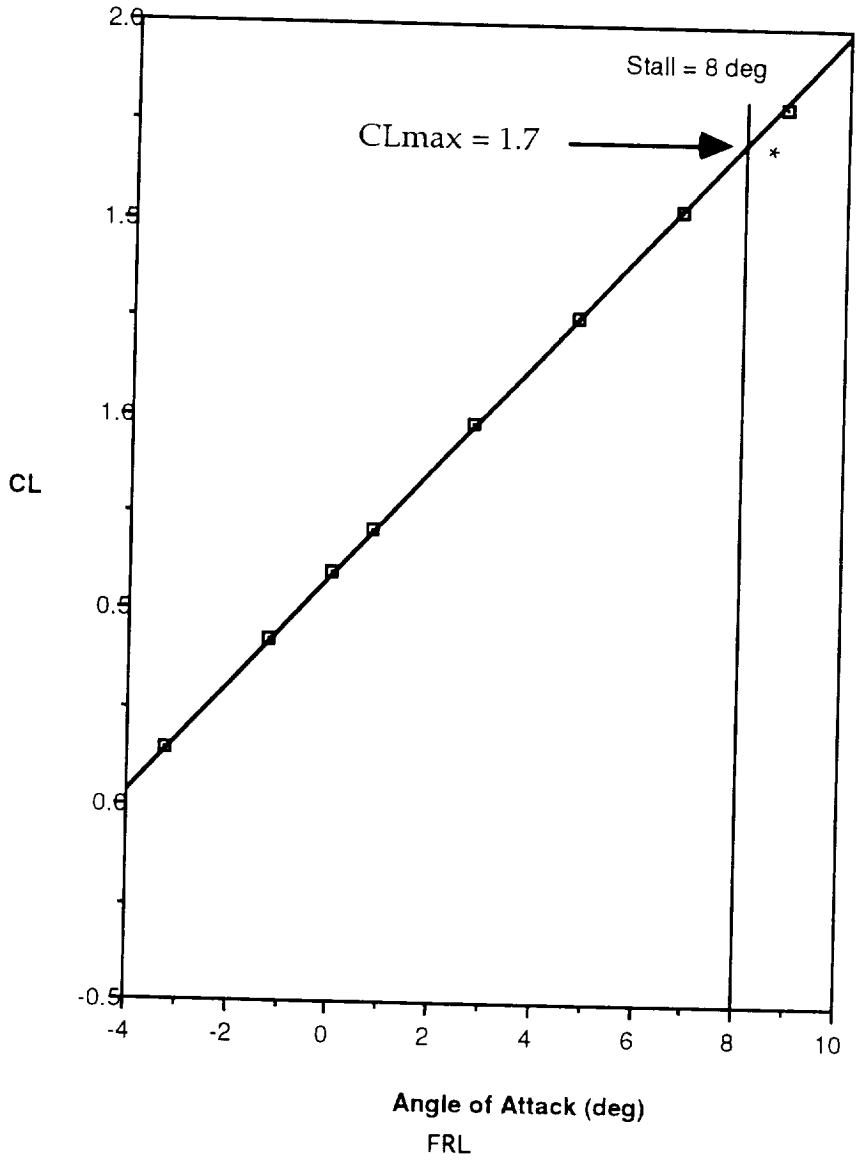

Figure F.3 Lift Curve of the Aircraft

*At this point, the section $C_{l\,max}$ of the wing excedes $C_{l\,max}$ of the Clark -Y. The wing is assumed to be stalled.

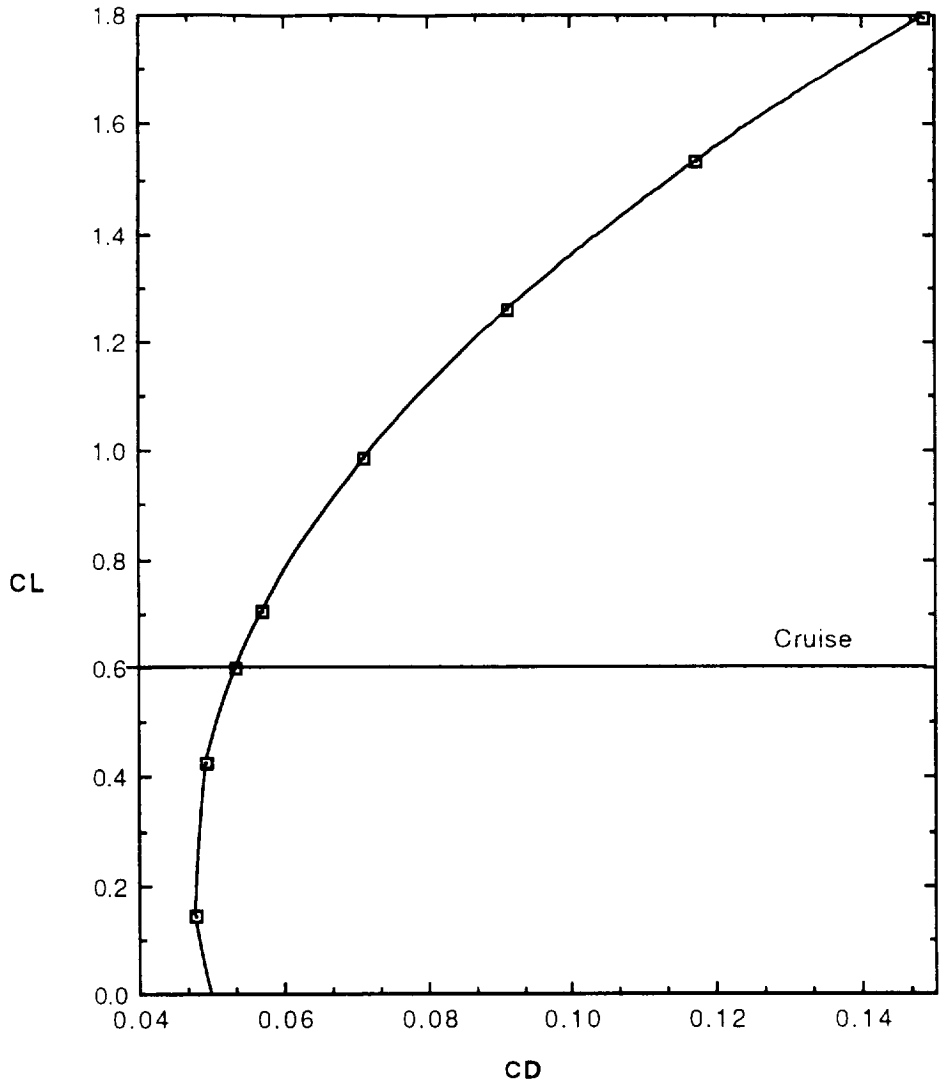

Figure F.4.1 Drag Polar of the Aircraft

Component	$C_{D\pi}$	A_π	% of C_{D_0} total
Fuselage	0.82	0.148	30
Front Landing Gear	0.59	0.016	8.6
Rear Landing Gear	0.20	0.012	1.0
Vertical Tail	0.008	0.400	7.4
			$C_{D_0} = 0.014$
	Wing and Tail	$C_{D_0} = 0.023$	53%

C_{D_0} total = 1.15*(0.014+0.023) = 0.043

Table F.4.2 Component Breakdown of Drag

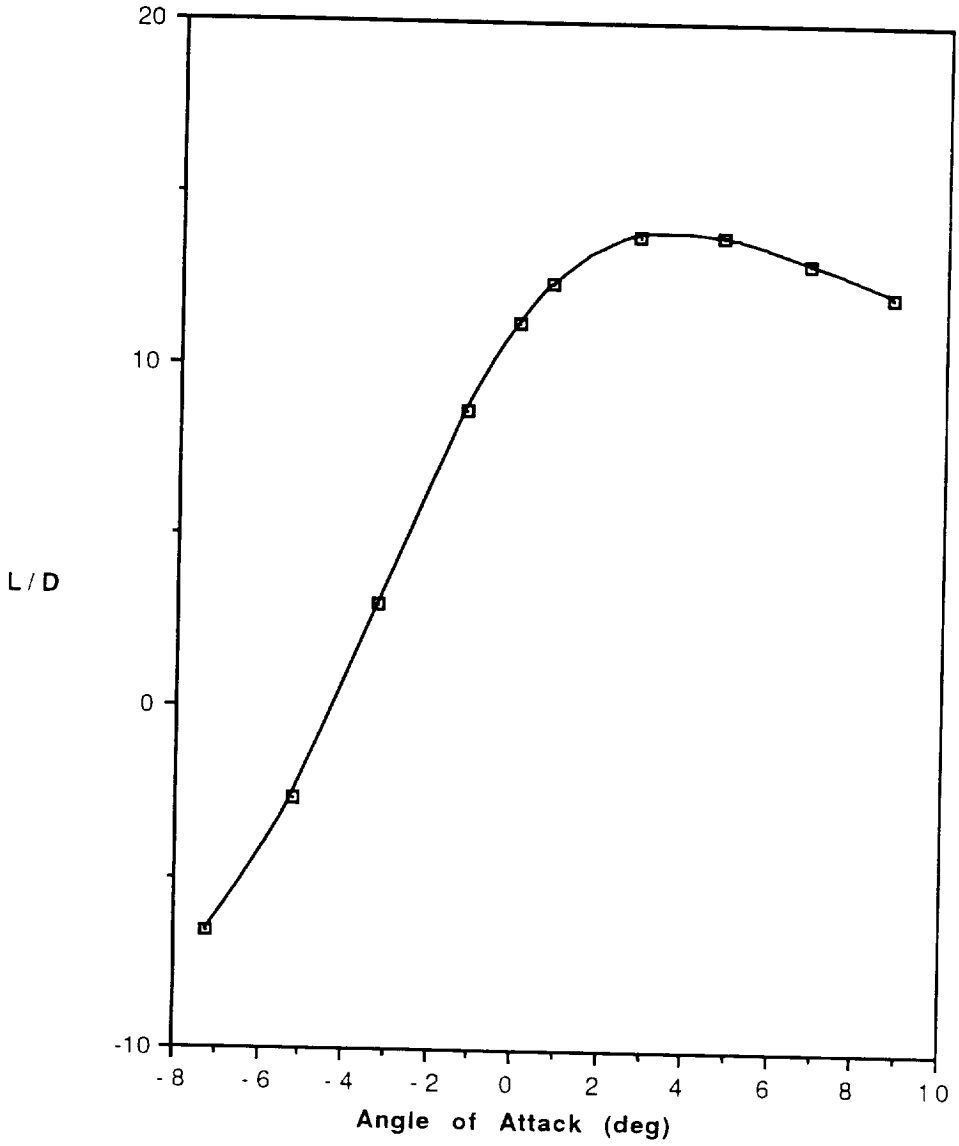

Figure F.5 L/D Curve for the Complete Aircraft

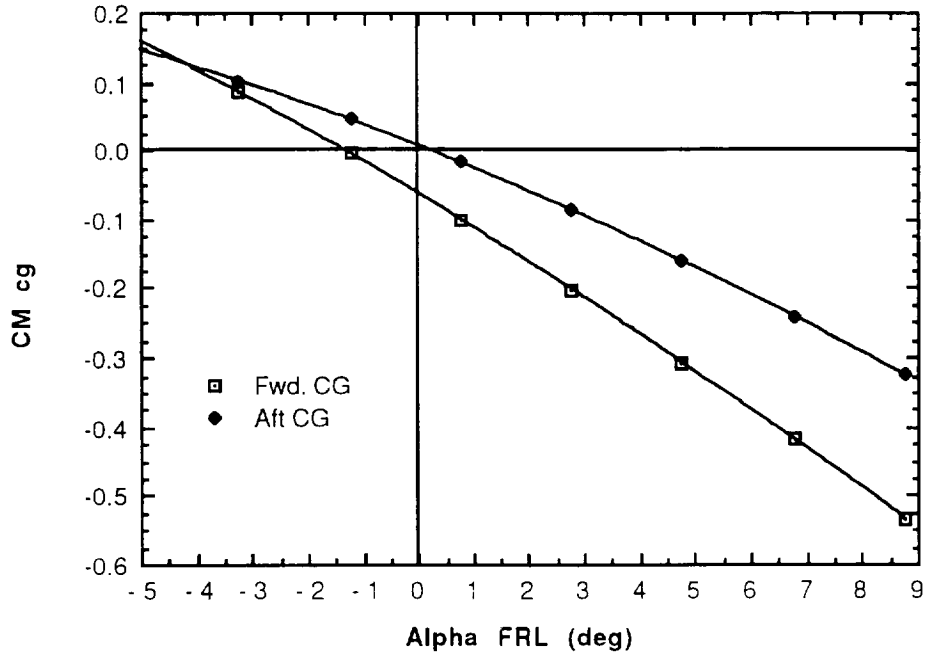

Figure F.6 Coefficient of Moment vs Alpha for Most Forward and Aft C.G.

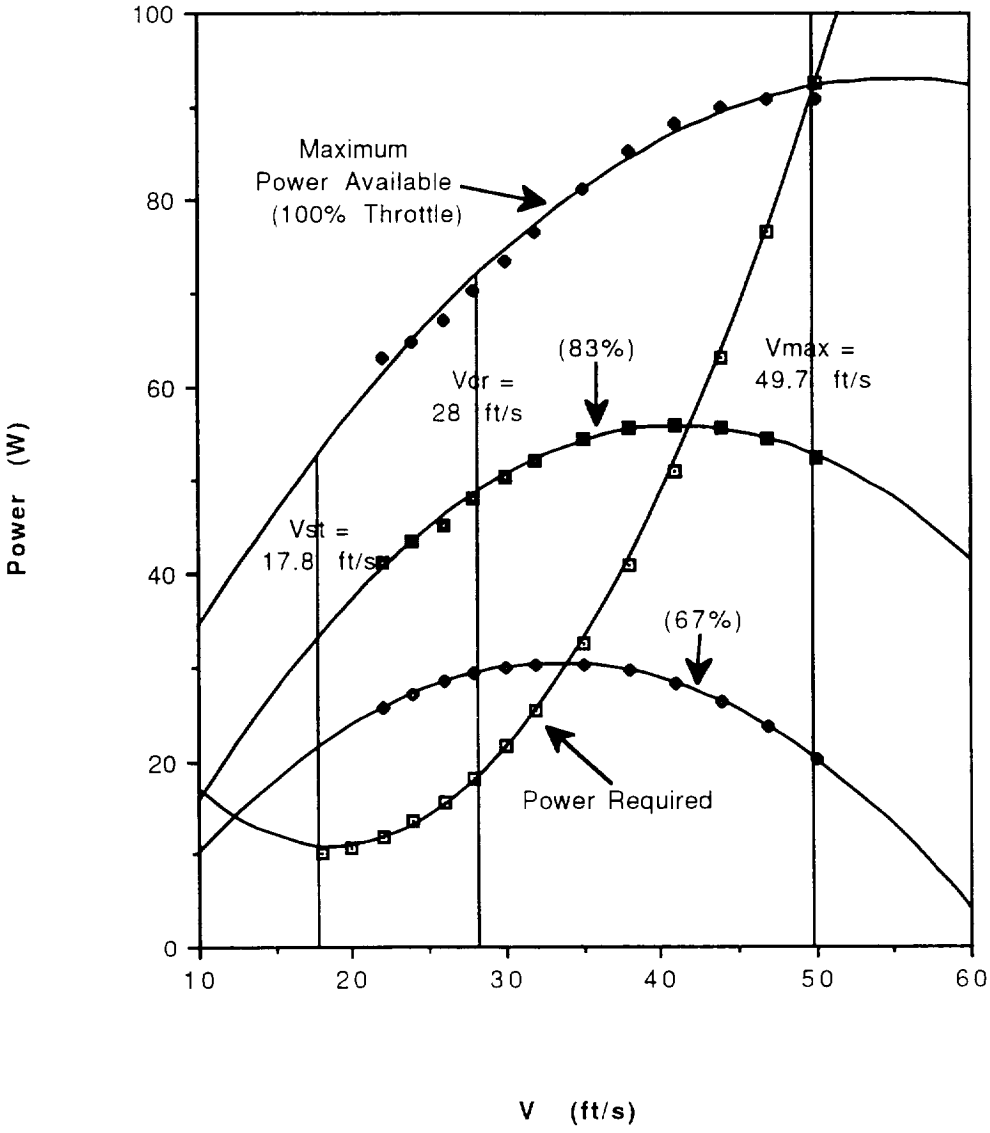

Figure F.7 Power Available and Power Required versus Flight Speed

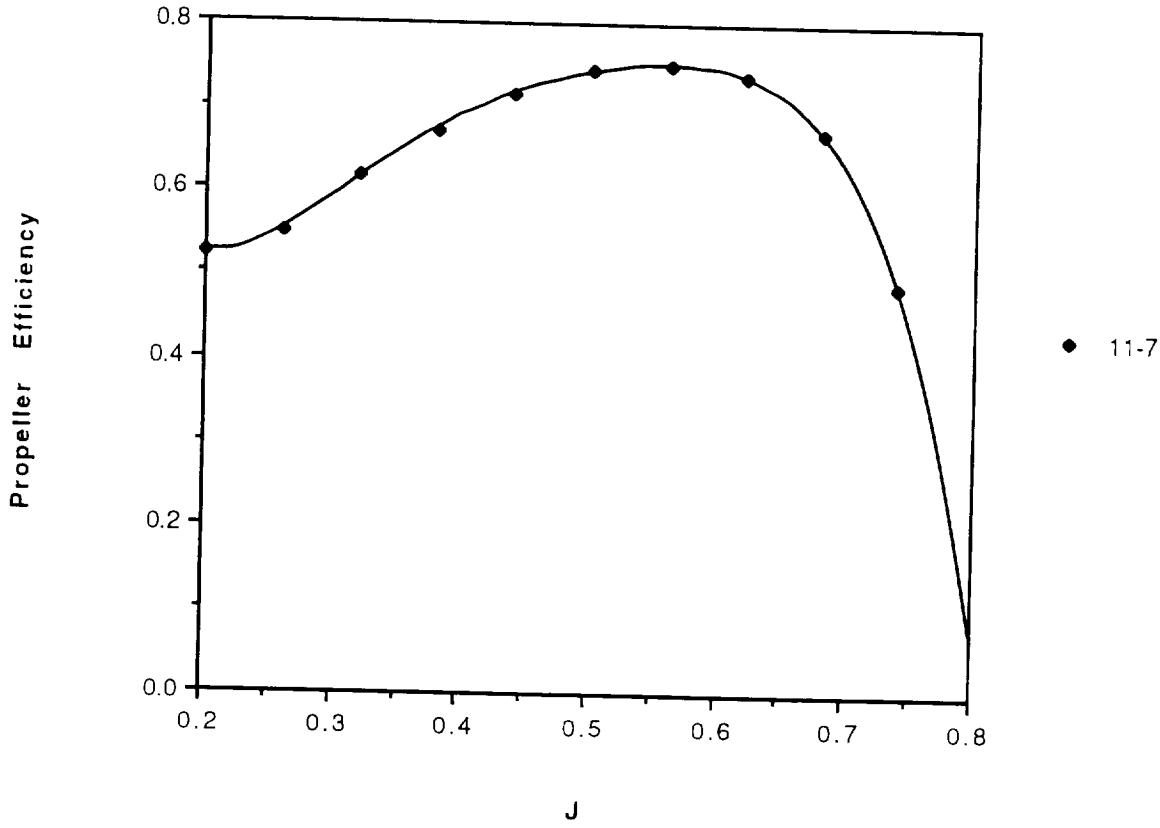

Figure F.8 Propeller Efficiency vs Advance Ratio (J)

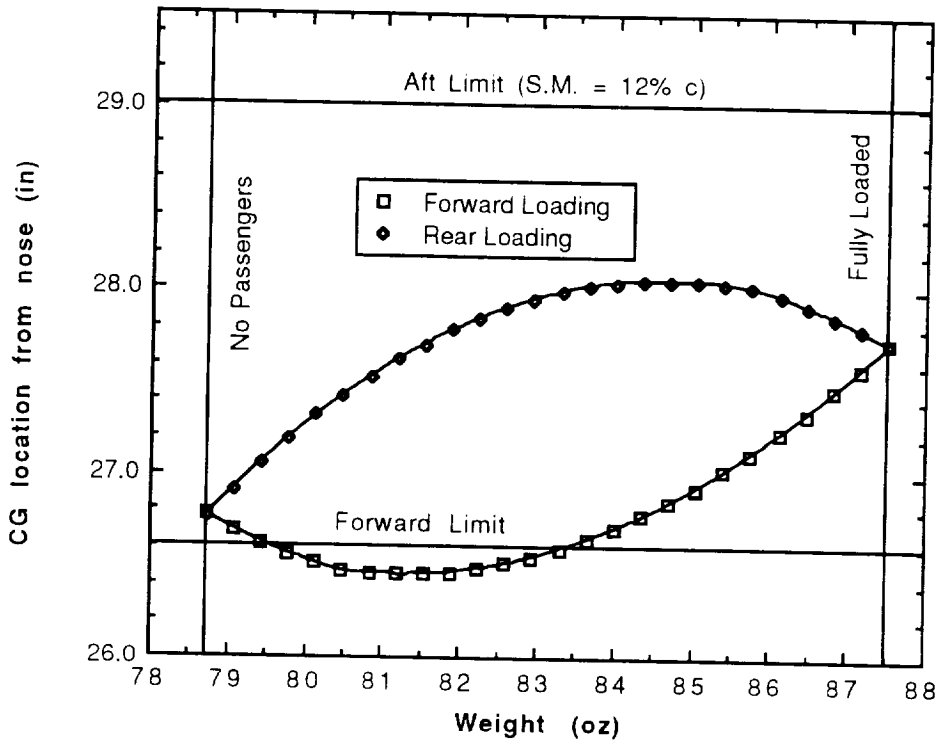

Figure F.9 Weight Balance Diagram

Component		c.g. (in)		Weight (oz)		
	X-loc	Y-loc	Z-loc			
propeller	0	0	2	0.614		
engine	2	0	1.25	11.05		
fuselage	33.5	2.25	1.25	10		
wings	20.5	33.25	6.3	13		
tail (v)	60	0	10.25	3		
tail (h)	51.5	33.25	17	13		
front gear	25.5	5	-5	4.67		
rear gear	62	0	-2	2.33		
avionics tray	17.5	2.25	1.5	20.56		
front passeng.	11.13	2.25	1.25	1.45	W_{full}	W_{emp}
rear passeng.	40.88	2.25	1.25	7.79	5.47 lbs	4.89 lbs
	Fully Loaded				Empty	
Xcg	Ycg		Zcg	Xcg	Ycg	Zcg
27.8 in	0 in		4.3 in	26.8in	0 in	4.7 in
c.g travel=0.99 in						

Table F.10 Component Weights and C.G., and Travel of Aircraft C.G.

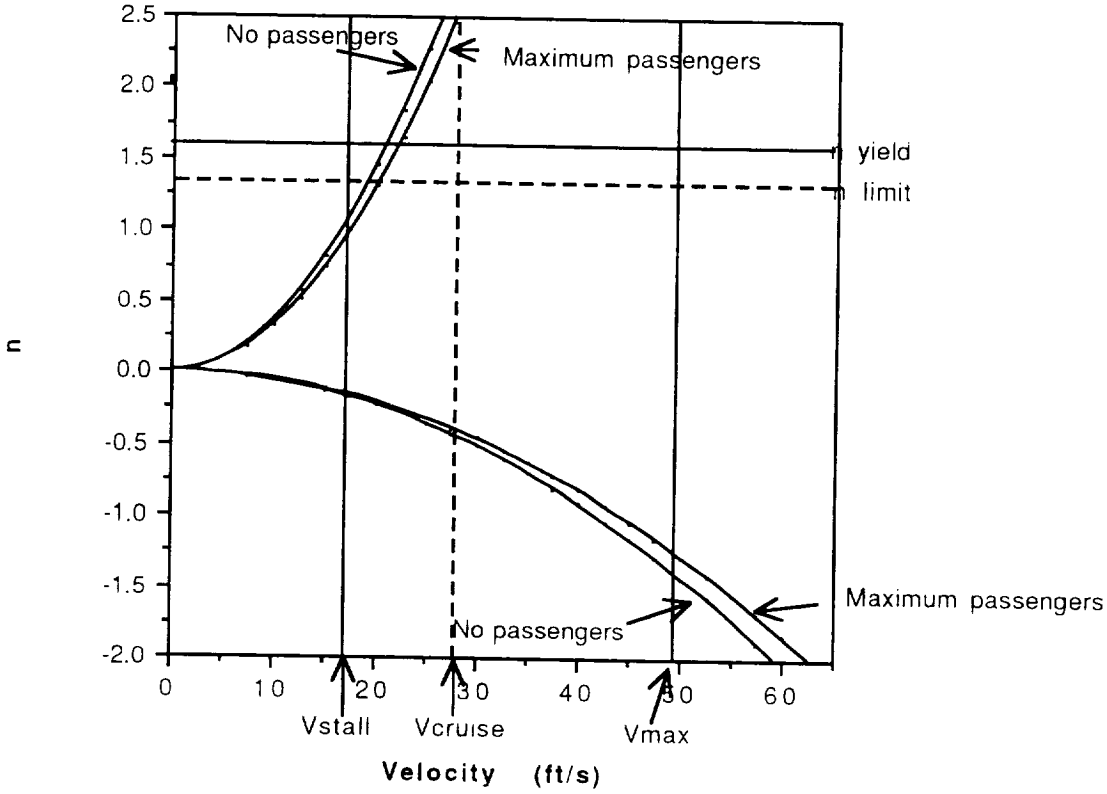

Figure F.11 V-n Diagram

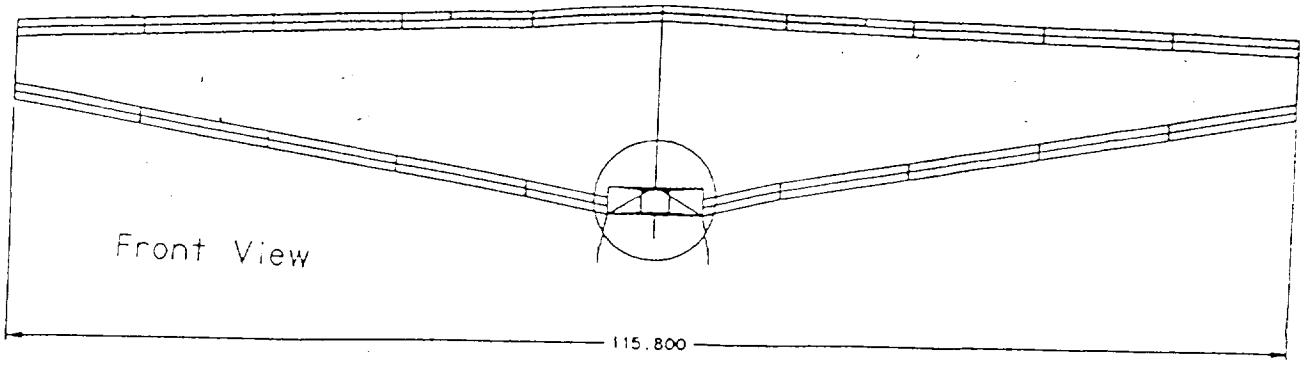

Dimensions in inches

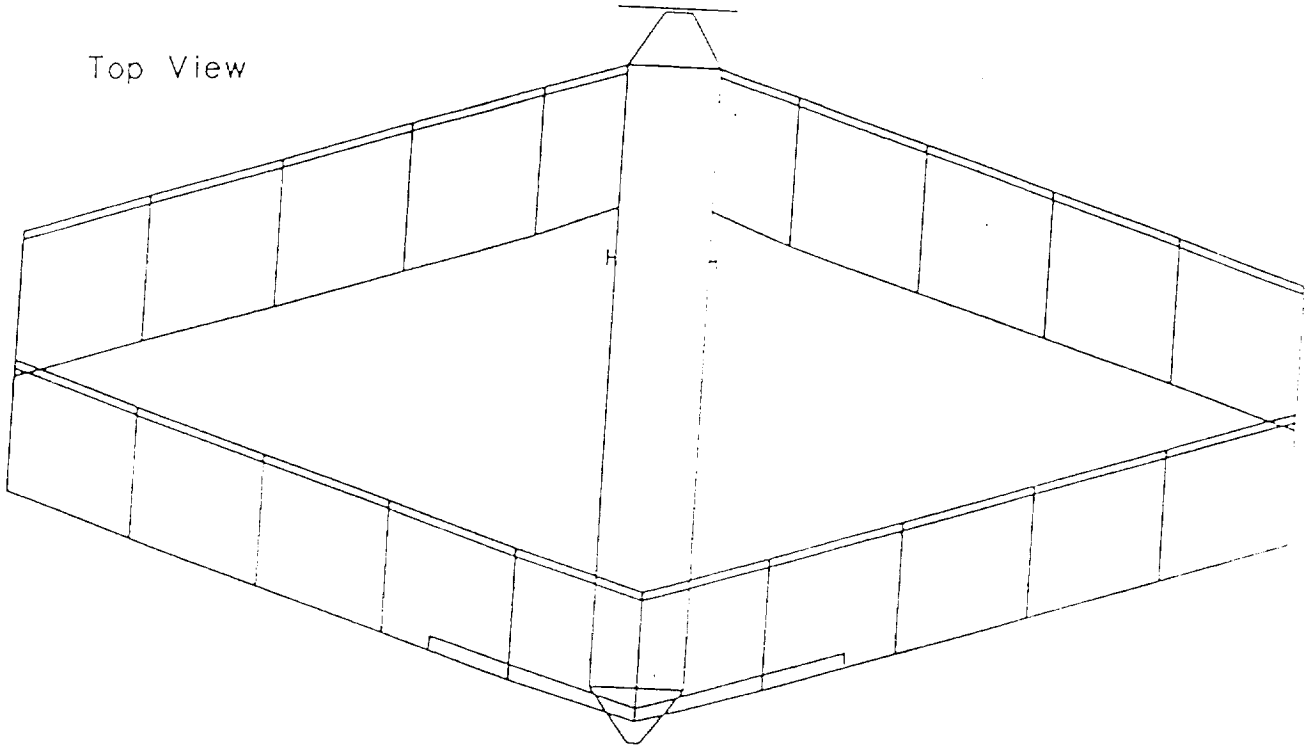

Side View

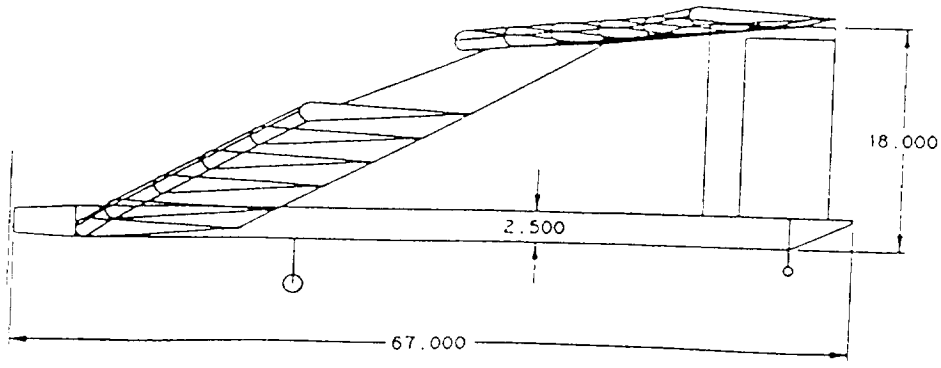

Dimensions in inches

Internal Layout

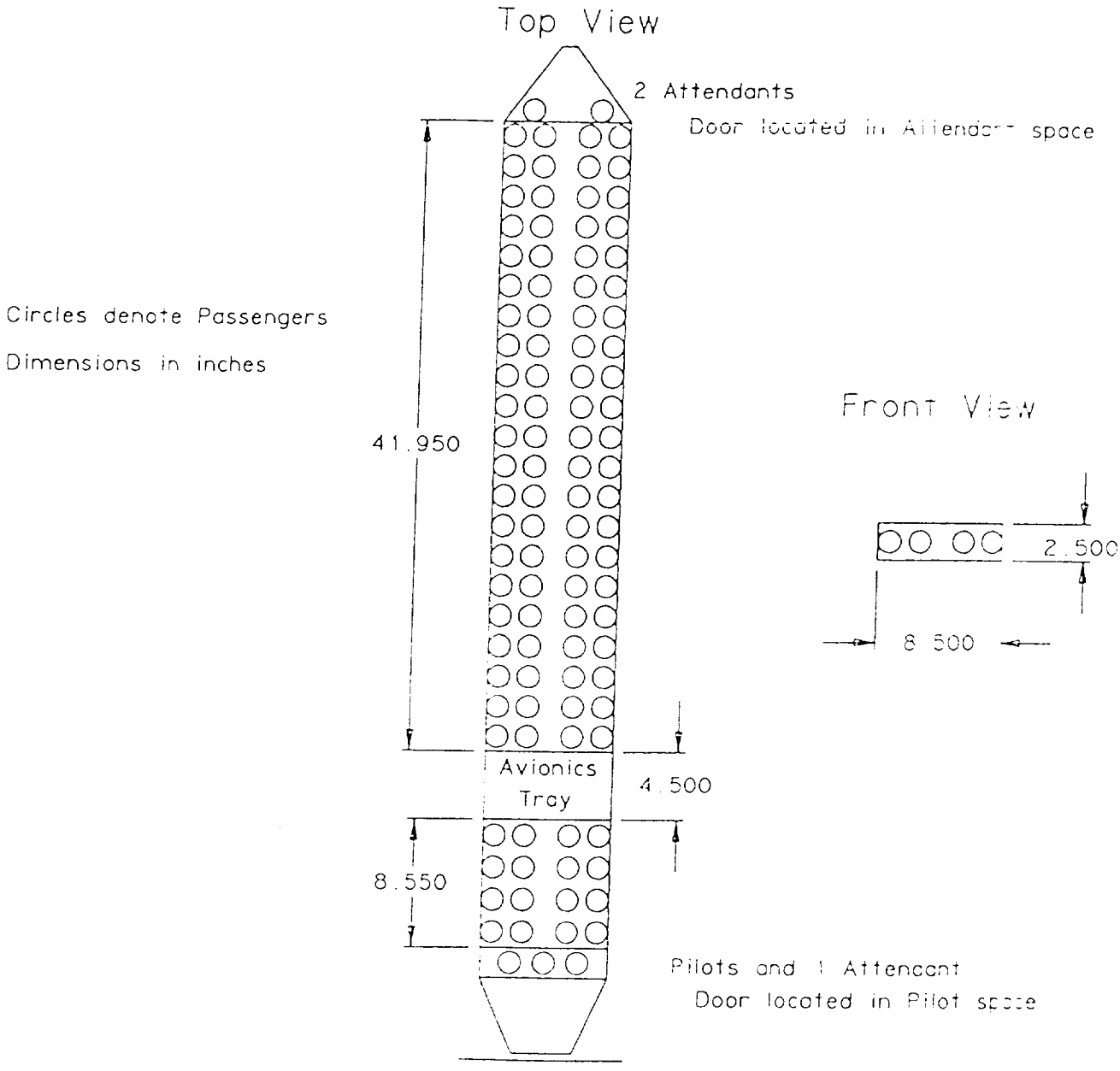

Appendix G: References

4.1 Miley, S.J. "A Catalog of Low Reynolds Number Airfoil Data For Wind Turbine Applications," Texas A&M University, 1982

4.2 Jensen, Daniel. "A Drag Prediction Methodology for Low Reynolds Number Flight Vehicles," University of Notre Dame, Indiana, February 1990.

4.3 Nelson, Robert. "Subsonic Drag Breakdown Method," AE 348 Flight Mechanics Lecture Notes, University of Notre Dame, 1992.

4.4 Horner, Sighard. Fluid Dynamic Drag. (Chapter 9). New York: Published by Author, 1958.

4.5 Koo, Ilan. "LinAir: A Nonplanar, Multiple Lifting Surface Aerodynamics Program," Stanford: Desktop Aerodynamics, 1987-1989.

5.1 Young, Barry N.. Propeller Performance Program for Apple IIe. Hessert Center.

7.1 Nelson, R. C.. Flight Stability and Automatic Control. New York: McGraw-Hill, Inc., 1989.

7.2 Lennon, A. G.. R/C Model Airplane Design. Wisconsin: Motorbooks International, 1986.

7.3 Wolkovitch, J. "The Joined Wing: An Overview," J. Aircraft, pp. 161-178, March 1986.

8.1 Anderson, John D. Introduction to Flight. New York: McGraw-Hill, Inc., 1985.

9.1 Lennon, A. G.. R/C Model Airplane Design, Motorbooks International, Wisconsin, 1986.

A.1 Lennon, A.G.. R/C Model Airplane Design. Wisconsin: Motorbooks International, 1986.

A.2 Wolkovitch, J. "The Joined Wing: An Overview," J. Aircraft, March 1986. pp. 161-178.

C.1 McCormick, B. W.. Aerodynamics, Aeronautics, and Flight Mechanics. New York: John Wiley & Sons, 1979.

C.2 Nelson, R. C.. Flight Stability and Automatic Control. New York: McGraw-Hill, Inc., 1989.

Appendix H: Construction Plans

Construction of the *Diamondback* is to begin immediately following the completion of the Final Draft Proposal and the delivery of the manufacturing materials, and will begin with the simultaneous construction of the major components of the aircraft. The fuselage, wing and tail will be simultaneously, yet individually, constructed. Mass production techniques will be employed in the manufacturing of the wing and tail ribs and riblets. Measures such as the design of a rectangular fuselage, wing and tail make these mass production techniques possible and reduce complications in the manufacturing process. The purpose of these techniques is to reduce the labor costs of the *Diamondback*..

H.1 Major Assemblies

H.1.1 Fuselage

The fuselage will consist mainly of spruce and balsa. The longerons will be made of spruce sticks with dimensions of .25 inches x .25 inches. The supporting elements of the fuselage structure (cross-pieces) will be made of balsa sticks with dimensions of .25 inches by .25 inches. These cross-pieces will be placed every 3.5 inches along the top, bottom and sides of the fuselage. Additional supporting elements will be placed diagonally between the longerons and the cross-pieces. These diagonals will be made of balsa sticks with dimensions of .25 inches x .125 inches. These supporting elements will help the fuselage maintain its shape and prevent folding.

The first task in constructing the fuselage will be to build the port and starboard panels. These will be identical and can therefore be built using the same plans. These will then be joined by the bottom structure of the fuselage. The top of the fuselage will be added later once the placement of the passengers and the avionics for the correct center of gravity location has been determined. Once the sides and bottom of the fuselage have been built, the additional bracing

for the landing gear, the wing carry-through structure and the firewall/engine mount will be added. Flooring will be added later to allow access to the entire fuselage during the remainder of the construction process.

H.1.2 Main Wing

The wing will be constructed entirely of spruce and balsa. The spar caps will be made of spruce sticks with dimensions of .25 inches x .125 inches. The ribs and riblets will be cut from .125 inch thick balsa sheets. Finally, the shear webs will also be cut from .125 inch balsa sheets (Figure H.1). The ribs and riblets will be placed at 4 inch intervals and will be cored out wherever possible to reduce the overall wing weight. The two halves of the wing will be constructed individually so that they can be removed for transportation to the test facility.

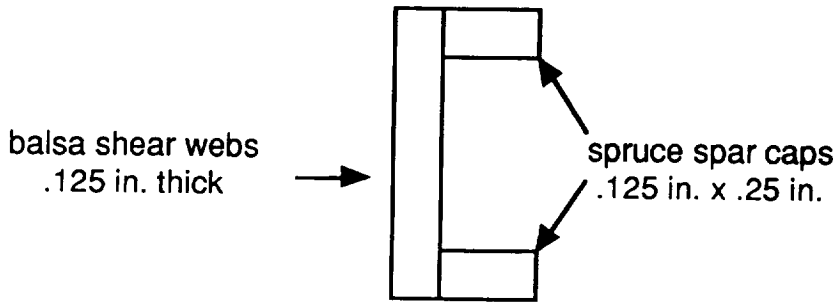

Figure H.1

The two wing halves will be attached to the fuselage using a bayonet-style design. The wing box structure will extend into the fuselage where it will be fastened to the carry-through structure with a dowel rod.

H.1.3 Horizontal Tail

Due to the similarity of the wing and the horizontal tail, the tail will be constructed in the same manner as the wing. The two halves of the tail will also be seperate and removable for transportation.

H.1.4 Vertical Tail

The vertical tail will be constructed entirely of spruce and balsa. Main spars will be placed at the leading edge and at the .25c locations. The .25c spar will be the main load-carrying member of the vertical tail since the horizontal tail will be attached to the vertical tail at this location. These main spars will be constructed using spruce while the supporting elements and the rudder will be made of balsa with dimensions of .25 inches x .25 inches and .25 inches x .125 inches. These spars will extend down into the fuselage so that the vertical tail can be firmly joined to the fuselage.

H.2 Assembly

Once the major components have been constructed, the passengers and the avionics can be placed to set the center of gravity at the location set by stability and control requirements (28.7 inches from nose). The vertical tail can then be joined to the fuselage. This joint will be permanent (the vertical tail is not removable). Once the firewall and landing gear mounts have been built, the motor and the landing gear can be installed. The four main lifting surfaces (2 wings, 2 tails) are all designed to be removable to facilitate transportation.

H.3 Complete Parts Count

Fuselage			
6	spruce	1/4 x 1/4 x 48	longerons
7	balsa	1/4 x 1/4 x 36	cross pieces
12	balsa	1/4 x 1/8 x 36	cross pieces and diagonals
1	plywood	1/8 x 4 x 6	firewall and gear mounts
Wing			
8	spruce	1/4 x 1/8 x 36	spar caps
4	balsa	1/2 x 1/2 x 36	leading edges
4	balsa	1 x 1/4 x 36	trailing edges

7	balsa	1/8 x 6 x 36	ribs, riblets, shear webs
Horizontal Tail			
8	spruce	1/4 x 1/8 x 36	spar caps
4	balsa	1/2 x 1/2 x 36	leading edges
4	balsa	1 x 1/4 x 36	trailing edges
7	balsa	1/8 x 6 x 36	ribs, riblets, shear webs
Vertical Tail			
1	spruce	1/2 x 1/2 x 36	.25c spar
1	spruce	1/4 x 1/4 x 36	leading edge spar
1	spruce	1/2 x 1/4 x 36	cross pieces
3	balsa	1/4 x 1/4 x 36	rudder, cross pieces
2	balsa	1/4 x 1/8 x 36	diagonals

Appendix I: Technology Demonstrator

I.1 Weights and Center of Gravity

The final weights for the technology demonstrator along with the final design requirements are shown in Table I.1.

	Technology Demonstrator	Final DesignRequirement
Wing	15.2 oz	13.0 oz
Empennage	19.0 oz	16.0 oz
Landing Gear	5.9 oz	6.4 oz
Battery Pack/ Avionics	27.0 oz	20.5 oz
Fuselage/ Joints	17.3 oz	10.0 oz
Propulsion	11.7 oz	11.7 oz
Passengers/ Crew	0.0 oz	9.2 oz
Total Weight	**6.0 lbs**	**5.4 lbs**

Table I.1 Configuration Weights and Final Design Weights

As seen from Table I.1, the technology demonstrator weighs 0.6 lbs more than the final design requirements. The increase in total weight was due an underestimation of the monokote weight, the weight of the joints, and the weight of the battery pack. Because of the large surface area of the horizontal tail, the amount of monokote on the technology demonstrator was significantly greater than any other previous design, which led to the estimation

error. In order to carry the loads of the wing-tail structure, the wing carry-through structure and tail joints needed more material than was estimated in the final design requirements. Lastly, the battery pack weighs more in the technology demonstrator due to the unavailability of the size of batteries that were requested.

Because of the large total weight of the technology demonstrator, it was feared that the the enormous time and effort that was invested in the construction would be for naught. Because of this and the fact that the *Diamondback* presented a new technology, upper management requested that the demonstrator be flown without the weight of passengers and crew, which allowed the total final weight to remain near the design weight.

The location of the center of gravity of the technology demonstrator was at x=27.8 inches, which is exact location that was dictated in the final design requirement. This accurate placement was accomplished by moving the avionics tray forward until the center of gravity was located exactly at 27.8 inches.

I.2 Manufacturing and Cost Detail

A major concern of the *Diamondback* was the time to manufacture and the material costs. Although all attempts were made to hasten the construction time and lower materials cost, the raw materials of the technology demonstrator cost $234.13 and the total amount of labor hours was 271 hours. The breakdown of raw materials cost is shown in Table I.2.

Material	Cost
Monokote	$60
Glue	$15
Landing Gear	$12

Propeller	$7
Servo rods	$5
Velcro/ horns/ attachments	$30
Mail order wood	$40
Rest of wood	$70

Table I.2 Raw Material Cost

As can be seen from Table I.2, the main reason for the large cost of the raw materials is due to the increase in monokote and wood costs associated with the large joined-wing design. Furthermore, there was a cost increase due to the fact that a large portion of wood had to be delivered through the mail, with the associated delivery costs.

The 271 labor hours that were invested in the technology demonstrator were significantly more than the estimated 150 labor hours. One reason for this increase in construction time was due to the fact that the *Diamondback* required two full-size wing structures, each with dihedral and sweep. Furthermore, much of the design was not finalized until the manufacturing of the particular component was started. Because it was difficult to visualize many of the joints and the wing carry-through structure, the construction of the *Diamondback* was started before the completion of the final manufacturing plans.

The total cost of the technology demonstrator was based on raw materials cost, labor hours, machining costs, and waste removal costs. The waste costs of the *Diamondback* were high due to the fact that the manufacturing plans changed several times during the actual construction. The materials that were actually used were used very efficiently, helping to minimize the overall waste.

However, certain materials were purchased and cut, but were never used. This resulted in a major increase in the amount of waste of the *Diamondback*. The actual weight of the *Diamondback* is within 12% of the preliminary estimated weight. This fact also serves to show the efficiency in the construction of the *Diamondback*.